An Evolutionary Approach to Physics-based Modelling of Piezoelectric Actuators

Narges Miri

School of Mechanical Engineering

The University of Adelaide

South Australia 5005

Supervisors:

Dr. Lei Chen

Dr. Morteza Mohammadzaheri

This thesis is submitted in fulfilment of the requirements for the degree of Master of Philosophy on 3rd October 2014

Abstract

The objective of this research is to improve physics-based models of piezoelectric actuators through developing a global parameter identification method for the models and introducing a new high performance model. Piezoelectric actuators produce nano-metre scale displacements making them the dominant actuators in nanopositioning applications. In nanopositioning, the control of actuators' displacement requires highly accurate displacement sensors. The sensors are expensive and difficult, if not impossible, to use. Therefore, the models are employed to estimate the displacement of piezoelectric actuators, using the voltage across them, without any displacement sensors. Accordingly, several mathematical models have been developed to estimate the displacement of piezoelectric actuators. However, due to the nonlinear behaviour of the actuators, the models cannot capture their behaviour precisely. Therefore, developing a model to simulate the nonlinear behaviour of the actuator would constitute an important contribution to the development of high precision sensorless nanopositioning systems. Models can also be used in control system design.

To model piezoelectric actuators, this research utilises physics-based models that have a small number of parameters compared with standard black box models of piezoelectric actuators minimising the computation efforts in real-time applications. In this thesis, the physics-based models are enhanced by dealing with two main diagnosed weaknesses of these models: (1) the lack of a global parameter identification method and, (2) the relatively low accuracy of the models due to their inadequate mathematical structure.

The method for identifying the parameters of the physics-based models is one of the main challenges for these models. In general, the parameters of physics-based models are determined by non-optimal *ad-hoc* methods. Hence, this research adopts a standard, optimal and global (*non-ad-hoc*) method to identify the parameters of the nonlinear models of the piezoelectric actuators.

Another challenge for the physics-based models of piezoelectric actuators is the relatively low accuracy of the models compared with the black box models, partially arising from the rather simple mathematical structure and a small number of parameters of these models. Therefore, improving the model structure will increase the model accuracy. To address this matter, complementary terms/inputs are added to a physics-base model constructing an enhanced structure for the model. The new model doubles the estimation accuracy of the original model

and results in accuracies comparable with those of the best reported models of piezoelectric actuators.

The proposed ideas are substantiated to increase the applicability and accuracy of the models of piezoelectric actuators. From the range of physics-based models, the Voigt model is a particular focus for this research. The Voigt model can capture the rate-dependent and nonlinear behaviour of piezoelectric actuators. Furthermore, this model has been reported to be adequate for a broad excitation frequency range (1-1000) *Hz*. However, the proposed ideas are easily extendable to other physics-based models of piezoelectric actuators.

Statement of Originality / Declaration by author

I certify that this work contains no material which has been accepted for the award of any other degree or diploma in any university or other tertiary institution and, to the best of my knowledge and belief, contains no material previously published or written by another person, except where due reference has been made in the text. In addition, I certify that no part of this work will, in the future, be used in a submission for any other degree or diploma in any university or other tertiary institution without the prior approval of the University of Adelaide and where applicable, any partner institution responsible for the joint-award of this degree.

I give consent to this copy of my thesis when deposited in the University Library, being made available for loan and photocopying, subject to the provisions of the Copyright Act 1968.

The author acknowledges that copyright of published works contained within this thesis resides with the copyright holder(s) of those works.

I also give permission for the digital version of my thesis to be made available on the web, via the University's digital research repository, the Library catalogue and also through web search engines, unless permission has been granted by the University to restrict access for a period of time.

Signed……Date……

NOTE:

This page is intentionally left blank.

Acknowledgements

It is a great pleasure to acknowledge the many people who have made this thesis possible.

Firstly, I would like to thank my supervisors Dr Lei Chen and Dr Morteza Mohammadzaheri, who have been a supportive supervisory team. Without their advice and feedback, technically and otherwise, I would not have completed my thesis.

I would also like to thank Dr Steven Grainger and Dr Mohsen Bazghaleh for providing experimental data. And, I would like to thank Miss Alison Jane-Hunter and Dr Peter Trudinger who helped with the editing of my thesis.

I am grateful to all the academic faculty and staff at the School of Mechanical Engineering. In particular, they gave me this opportunity to study among Engineers while I have a Science background. I should also express my sincere gratitude to Professors Colin Hansen, Bassam Dally and Associate Professor Anthony Zander, for their friendly conversations and support, especially in my early months in the School of Mechanical Engineering.

I would like to thank all my friends in the School of Mechanical Engineering who have supported me emotionally and scientifically. They made my time pleasant here.

I would like to thank my family members, parents and siblings, who have always encouraged me and believed in me.

NOTE:

This page is intentionally left blank.

Contents

NOTE:

This page is intentionally left blank.

List of Figures:

NOTE:

This page is intentionally left blank.

List of Tables:

NOTE:

This page is intentionally left blank.

Nomenclature

Abbreviations

ANN	Artificial neural network
NARMAX	Nonlinear autoregressive moving average with exogenous inputs
AFM	Atomic force microscope
PZT	Lead zirconate titanate
PI	Parandtl-Ishlinski
sgn	Sign
exp	Exponential
SQP	Sequential quadratic programming
OSP	One step prediction
GA	Genetic algorithm
MAC	Minimum of absolute change
Max	Maximum value
Min	Minimum value
MAX	Maximum of absolute error
MAE	Mean of absolute error

Symbol

E	Electric field
T	Stress vector
S	Strain vector
D	Electrical induction

s^E	Mechanical flexibility
ε^T	Electrical permittivity
d	Piezoelectric coefficient
B	External magnetic field
$y(t)$	Piezoelectric displacement
$\mu(\alpha', \beta')$	Preisach density function
α', β'	Voltage representations in the Preisach model
$y_{\max}$	Local maximum of the piezoelectric displacement
$y_{\min}$	Local minimum of the piezoelectric displacement
y_{ext}	Local extremum of the piezoelectric displacement
$V_{\max}$	Local maximum of the piezoelectric voltage
$V_{\min}$	Local minimum of the piezoelectric voltage
V_{ext}	Local extremum of the piezoelectric voltage
$H(i)$	Backlash (play) operator
i	Width of the backlash operator
ω	Slope of the backlash operator
r	Half-width of the input voltage
y_0	Initial displacement of piezoelectric actuator
j	Number of backlash operators/widths
μ	Friction coefficient
N	Normal force
k	Spring stiffness

b	Spring damping coefficient
F	External force (reaction force)
w_i	Saturation force
g_1, g_2	Hysteresis slopes
α, λ, β	Sigmoid parameters
F_c	Initial applied force
n	Number of elements
A_{th}	Theoretical hysteresis loop areas
A_{hyst}	Experimental hysteresis loop areas
l	Number of estimations
m	Number of bits
p_b	Parameter (gene) value
p_{min}	Minimum value of each parameter (gene)
p_{max}	Maximum value of each parameter (gene)
T_1	Internal length of the piezoelectric stack
T_2	External length of the piezoelectric stack
W_1	Internal width of the piezoelectric stack
W_2	External width of the piezoelectric stack
H	Height of the piezoelectric stack
L	Length of the lead wire
t_s	Sampling time
r_y	Output order
θ	Parameter vector

$\varphi(t)$	Regression vector
A	Voltage amplitude
f	Voltage frequency

Chapter 1 - Introduction

Piezoelectric material is one of the *smart* materials which couples electrical voltage and mechanical force. If an electrical voltage is applied to a piezoelectric material which is in contact with an object, it will apply a force to the object; thus, the piezoelectric material plays the role of an actuator. Fine displacements of piezoelectric actuators in the range of (10^{-6}-100) μm makes them suitable for various areas such as nanopositioning (Karam, 1999) that is, the technology of manipulating materials at nano/micro metre scale (Adriaens et al., 2000, Salapaka et al., 2002). Figure 1.1 (a) shows a typical piezoelectric actuator in a nanopositioning application. In nanopositioning, in order to control the displacement of piezoelectric actuators accurately, feedback control systems are employed, wherein the actuator displacements are measured by a highly accurate displacement sensor. A typical feedback control system including a piezoelectric actuator and sensor is shown in Figure 1.1 (b). However, the application of the sensor is limited by its high expense and practical constraints including implementation, calibration and, insufficient resolution and bandwidth (Croft et al., 2000). Accordingly, to eliminate sensors from nanopositioning systems, several models have been developed to model the piezoelectric actuators using voltage across them (Bhikkaji et al., 2007, Mohammadzaheri et al., 2013).

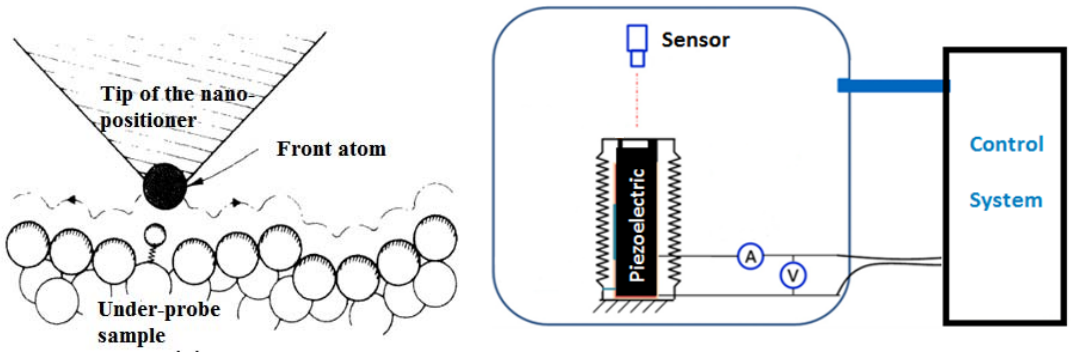

(a) (b)

Figure 1.1: A typical piezoelectric actuator in (a) a nanopositioning application (Binnig et al., 1986) and (b) a feedback control system.

The modelling of piezoelectric actuators is a challenging task as piezoelectric actuators have a highly nonlinear behaviour. A model that can accurately capture this behaviour is a sufficient model (Chen and Tan, 2008). Hence, improving the model is significant to utilise it in the control system in order to develop the positioning precision of the actuator in the system. In other words, to design a feedback controller appropriately, a precise mathematical model is necessary (Adriaens et al., 2000).

This chapter introduces current models of piezoelectric actuators, the research motivation, gap statement and thesis overview including thesis contribution, methodology and structure. At the end of the chapter, the publications from the thesis are summarised.

1.1. Present Models of Piezoelectric Actuators

In most research fields, the system models are constructed through either empirical observations or physical considerations (Richter et al., 2001). However in the case of nanopositioning systems, the nonlinear behaviour of piezoelectric actuators incurs a challenging task for the modelling. The models explaining the behaviour of piezoelectric actuators are presented through three types of mathematical models: (1) the finite element, (2) the black box and (3) physics-based models.

The finite element technique divides the whole domain into small subdomain elements to model the system. This technique can be applied to complex geometries and dissimilar material properties and it can capture local defects. Through this technique, the behaviour of piezoelectric actuators has been explained using a multilayer approach (DeVoe and Pisano, 1997, Wang and Cross, 1999). However, the finite element technique is not appropriate for real-time control because it does not guarantee response at most working frequencies of the actuators (Ramtekkar, 2009, Han et al., 1999, Soderkvist, 1997).

Black box models have standard mathematical structures and are created based on data mapping (Mohammadzaheri et al., 2012b). Both the mathematical structure and parameters of these models are identified based on the system input, output and transferred features without any knowledge about the internal behaviour of the system. A typical black box model is illustrated in Figure 1.2. Some examples of black box models include Artificial

Neural Networks (ANN), including perceptrons (Mohammadzaheri et al., 2012b), neuro-fuzzy networks (Mohammadzaheri et al., 2012b), radial basis networks (Xie et al., 2009b) and Nonlinear AutoRegressive Moving Average with eXogenous inputs (NARMAX) (Deng and Tan, 2009). These models usually have a considerable number of parameters and the role of each parameter in the system's behaviour is unclear. The large number of parameters increases the computational efforts to run and tune the model.

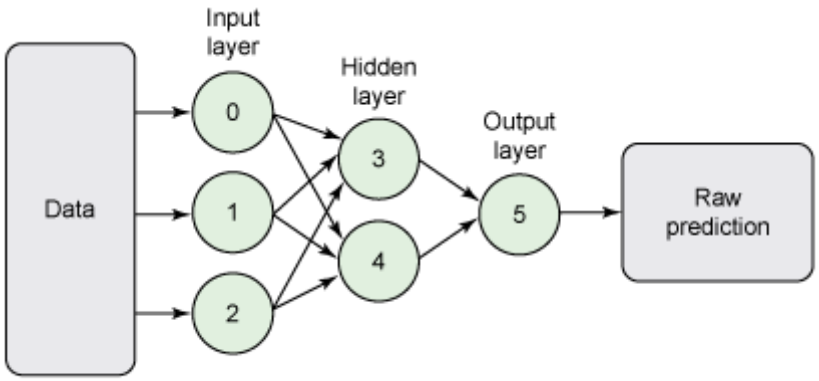

Figure 1.2: A typical black box model.

A few physics-based models, inspired by physical phenomena, have been introduced to estimate the displacement of piezoelectric actuators. Physics-based models are superior to black box models in terms of offering 'physically interpretable' and small numbers of parameters. Small numbers of parameters reduces the computation requirement for running the models and increases the potential use for real-time feedback control. Accordingly, through physics-based models, the static behaviour of piezoelectric actuators has been modelled by Weinberg using energy modelling (Weinberg, 1999). Furthermore, a few lumped-parameter models have been commercialised such as 20-Sim and Lab Amesim (Boukari et al., 2011, Ryou and Oldham, 2012). However, these products are valid around the functioning point based on the IEEE standard (Meeker, 1996). In (1987), the IEEE published a standard to model piezoelectric actuators through physics-based models (Meeker, 1996). These models, estimate only the linear behaviour of piezoelectric actuators occurring at electric field frequencies of zero/constant (Sirohi and Chopra, 2000). Moreover, physics-based models have been developed to model the nonlinear behaviour of piezoelectric actuators (Goldfarb and Celanovic, 1997, Sitti et al., 2001, Weinberg, 1999).

The most well-known physics-based models include the Preisach (Farsangi and Saidi, 2012), Prandtl-Ishlinskii (Hassani and Tjahjowidodo, 2011), Maxwell-Slip (Quant et al., 2009), Duhem (Hui et al., 2011) and Voigt (Yeh et al., 2008) models.

This thesis is focused on the improvement of physics-based models of piezoelectric actuators for sensorless or model-based control purposes.

1.2. Motivation and Gap Statement

Piezoelectric actuators have pervasive applications in different areas such as tactile displays (Pasquero and Hayward, 2003), minimally invasive surgery end effectors (Shimada et al., 2000), precision micromanipulators, vibration controllers and crawling robots (Kermani et al., 2002). In particular, the high precision positioning capability of piezoelectric actuators has been employed in Scanning Probe Microscopes (SPM), like Atomic Force Microscopes (AFM) collecting the nano-scale information of the under-probe surface (Salapaka et al., 2002, Binnig et al., 1986). The AFM is commonly employed in scanning different surfaces such as organic/biological layers, polymer and crystal surfaces and materials that are sensitive to radiation (Eaton and West, 2010). Overall, in nanopositioning, there is a piezoelectric actuator displaced in nano-metre scale and a sensor measures its displacements but, the sensors are expensive and/or their application is limited by practical constraints, e.g. non-accessible installation or difficult calibration (Boukari, 2010). To remove the sensors, researchers and engineers were pushed to estimate the actuator displacement through different models (Aphale et al., 2007, Fairbairn et al., 2011, Ronkanen et al., 2011). As piezoelectric actuators have a nonlinear behaviour, a sufficient model can accurately capture this behaviour and can be employed as a controller (Bhikkaji et al., 2007, Mohammadzaheri et al., 2013). Accordingly, improving the models of piezoelectric actuators has high potential benefits in nanopositioning and has thus been a subject of much interest in various nanotechnology applications. Thus, this thesis improves physics-based models of piezoelectric actuators from two primary perspectives: parameter identification and model structure.

The main challenge for physics-based models is how to identify the parameters of the governing equation of the model. It is diagnosed that these models suffer from *ad-hoc*,

tedious and non-optimal parameter identification methods. Many of the reported parameter identification strategies in the literature, e.g. Maxwell-Slip, Parandtl-Ishlinski, need the data collected immediately after a relatively long relaxation which might be difficult in practice, especially for working actuators.

Another significant research gap is a lower model accuracy compared with black box models which benefit from universal approximators. This loss in the accuracy is partially due to inadequacy of mathematical structure for these models.

To deal with the challenge of parameter identification, a standard, optimal and global parameter identification method is introduced. Furthermore, to improve the model accuracy, the structure of a well-known model will be modified by introducing complementary terms to the model.

Having reviewed the literature, this thesis identifies and presents the following gaps in physics-based models of piezoelectric actuators:

1- A systematic and comparative study has not been conducted on different features of physics-based models of piezoelectric actuators such as the frequency range of performance and invertibility.
2- A global, standard and optimal method of parameter identification has not been ascertained for physics-based models of piezoelectric actuators.
3- The reported accuracies for physics-based models are rather low compared with the best accuracies reported for black box models benefiting from mathematical structures in the form of universal approximators. This may be influenced by insufficiently proper mathematical structures or insufficient model inputs.

1.3. Thesis Overview

1.3.1. Thesis Contribution

This thesis deals with physics-based models of piezoelectric actuators to improve the models. The primary contributions of the project would be as follows:

1- To establish a novel global (*non-ad-hoc)* method of parameter identification for physics-based models of piezoelectric actuators, independent of the model, as detailed in Chapter 4.
2- To improve the accuracy of a well-known physics-based model through performing an innovative modification in the model structure and model inputs. The superiority of the proposed model is clearly shown experimentally, as detailed in Chapter 5.

The aforementioned contributions increase the applicability of physics-based models of piezoelectric actuators. The following aims will enable the achievement of the contributions described above:

1- Identifying the parameters of a physics-based model by a genetic algorithm which is a global optimisation algorithm.

2- Investigating the influence of different approaches, for model error estimation, on the model accuracy.

3- Improving the model structure based on the model input: adding complementary terms including extrema of the voltage/displacement to improve the model accuracy.

4- Assessing the enhanced model and comparing the model's performance with conventional models of piezoelectric actuators.

1.3.2. Methodology

To fulfil the aims and contributions of the project, the experimental data will be utilised. These data have been collected from the Robotic Laboratory at the University of Adelaide. Then, the Voigt model, a well-established physics-based model, will be employed to model a piezoelectric stack actuator. Moreover, a genetic algorithm is employed to identify the model parameters.

Subsequently, the structure of the Voigt model is improved by adding two complementary terms, inspired by the Preisach model, including extrema of the voltage/displacement as the model input.

The estimated displacements are compared with experimental displacements. The model error is defined as the average of absolute discrepancy for the model output and the system or real output. The small value of the model error is a sign of the high accuracy of the model. All stages to be completed are summarised as:

- Discretisation for the Voigt model
- Sampling time selection
- Parameter identification for the discrete Voigt model using the experimental data
    a) Model error calculation
    b) Model error minimisation as parameter identification
    c) Model validation
- Adding complementary terms
- Parameter identification for the new model
    a) Model error calculation
    b) Model error minimisation as parameter identification
    c) Model validation
- Selecting the most appropriate structure

1.3.3. Thesis Structure

This thesis opens by introducing the thesis scene. Then, the body of the thesis will be presented in six chapters:

Chapter 1) Introduction:

- Chapter 1 introduces a 'big picture' of the thesis including motivation, gap statement and thesis overview.

Chapter 2) Piezoelectric Actuators:

- Chapter 2 starts with the characteristics of piezoelectric materials. Then, the behaviour of piezoelectric actuators and challenges for their modelling are presented.

Chapter 3) Physics-based Models of Piezoelectric Actuators:

- Chapter 3 follows on from chapter 2 by modelling piezoelectric actuators through physics-based models. The models are constructed analogous with either magnetic or mechanical systems. The material in Chapters 2 and 3 was presented in a conference paper [C1].

Chapter 4) Innovative Parameter Identification Method for Physics-based Models:

- Chapter 4 discusses different approaches to estimate the model error for physics-based models of piezoelectric actuators. It demonstrates the experimental setup for the piezoelectric actuator in the control system. Then, a global method of parameter identification defines the parameters of a model. The materials in this chapter were presented in a conference paper [C2] and journal paper [J2].

Chapter 5) Structural Enhancement for Physics-based Models:

- Chapter 5 follows on from other chapters by proposing a new model for piezoelectric actuators. It introduces an enhanced form for the Voigt model, inspired by another physics-based model, to increase the model accuracy. To identify the model parameters, this chapter applies the introduced parameter identification method in Chapter 4. The concepts of this chapter were presented in a journal paper [J1].

The thesis is concluded in Chapter 6, with a discussion followed by suggestions for future research opportunities in the modelling of piezoelectric actuators.

1.4. Publications

1.4.1. Journal Papers

[J1] *An Enhanced physics-based model to estimate the displacements of piezoelectric actuators*

N. Miri, M. Mohammadzaheri, L. Chen

Journal of Intelligent Material Systems and Structures, Submitted date: 11/08/2013, Published date: 11/08/2014.

[J2] *An Evolutionary Approach to Physics-based Modelling of Piezoelectric Actuators, Supported by a Critical Review and Experimental Results*

N. Miri, M. Mohammadzaheri, L. Chen

International Journal of Intelligent Systems Technologies and Applications, Submitted date: 11/06/2014.

1.4.2. Conference Proceedings

[C1] *A Comparative Study of Different Physics-based Approaches to Modelling of Smart Piezoelectric Actuators*

N. Miri, M. Mohammadzaheri, L. Chen

IEEE/ASME International Conference on Advanced Intelligent Mechatronics (AIM),

Wollongong, Australia, (9-12) July 2013.

[C2] *Physics-Based Modelling of a Piezoelectric Actuator Using Genetic Algorithm*

N. Miri, M. Mohammadzaheri, L. Chen, S. Grainger, M. Bazghaleh

IEEE Symposium on Industrial Electronics and Applications (ISIEA 2013),

Kuching, Malaysia, (22-25) September 2013.

NOTE:

This page is intentionally left blank.

Chapter 2 - Piezoelectric Actuators

Piezoelectric materials can convert electrical energy into mechanical energy in the form of displacement. This chapter opens by presenting characteristics of piezoelectric materials. Then, the behaviour of piezoelectric materials in interaction with electrical voltage and/or mechanical force is addressed. Finally, the modelling challenges for piezoelectric actuators are presented.

2.1. Piezoelectricity

Piezoelectric material is a *smart* material. It is called *smart* because the material is able to respond to external variations (e.g. loads) and internal changes (e.g. damage) (Chopra, 2002). It can couple electrical voltage and mechanical force. These materials are made of crystals (e.g. quartz), ferroelectric polycrystalline ceramic substances, piezoceramics (e.g. barium titanate ($BaTio_3$)) and lead zirconate titanate (PZT) (Izyumskaya et al., 2007): the PZT is widely acceptable piezoelectric material (Minase et al., 2010). A typical PZT unit cell is illustrated in Figure 2.1.

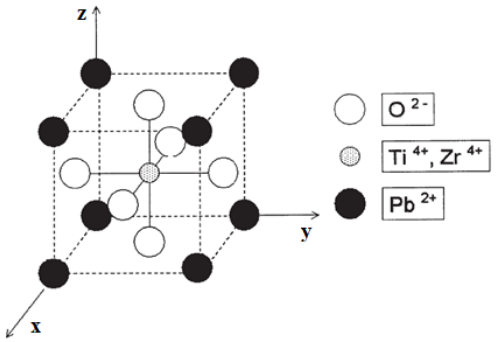

Figure 2.1: A typical PZT unit cell (Sirohi and Chopra, 2000).

The interaction of mechanical and electrical quantities in piezoelectric materials was discovered in the 1880s, as the first experiment on a piezoelectric material was performed by

the Curie brothers on quartz, SiO_2 (Minase et al., 2010). Subsequently, it was discovered that piezoelectric materials are deformed by applying an electrical field (Chopra, 2002). The modality of the material charge distribution explains this characteristic of piezoelectric materials. Charge distribution in materials is either symmetrical or non-symmetrical. As Figure 2.2 (a) demonstrates, in the symmetrical charge distribution, the applied mechanical force does not mutate the combination of gravity centres, whereas in the non-symmetrical charge distribution, the gravity centre is altered under the applied mechanical force, as Figure 2.2 (b) demonstrates. The piezoelectric material has a non-symmetrical charge distribution. Therefore this innate feature of piezoelectric materials results in generating an electric voltage across the material, when a mechanical force is applied to the material. Conversely, the material is displaced, when an electric voltage is applied.

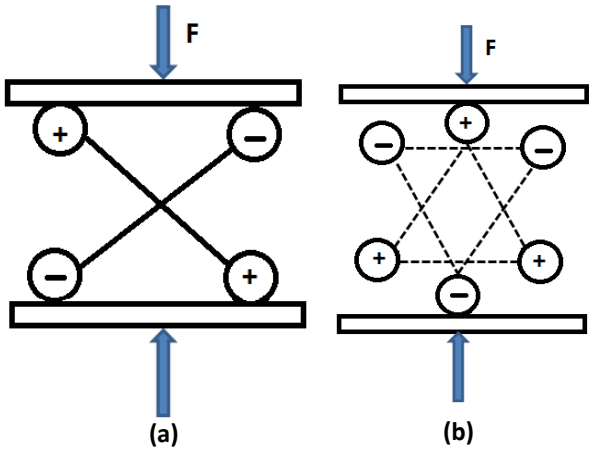

Figure 2.2: (a) Symmetrical and (b) non-symmetrical charge distribution of a material.

2.2. Piezoelectric Stack Actuator

Piezoelectric actuators are fabricated in different configurations such as piezoceramic thin flat patches (Halim and Reza Moheimani, 2003), piezoelectric stacks (Mohammadzaheri et al., 2012b), piezoelectric tubes (Mohammadzaheri et al., 2012c) and piezoelectric strips embedded into a polymer matrix (Irschik et al., 2010). The piezoelectric stack actuators are the most widely spread actuators used for small displacements on the normal to the top and bottom of the actuator surfaces (Chopra, 2002).

In order to fabricate a piezoelectric stack actuator, piezoelectric wafers are added together. The wafers have a thickness in the range (100-300) μm and two stack silver alloys are put on both sides of each wafer to be used as electrodes. The stacks should be prepared prior to being combined. The preparation involves a process called poling. In the poling process, a strong electrical current and a high temperature are applied to the piezoelectric stacks to align material dipoles in the direction of the external field. Initially, randomly oriented dipoles are aligned in the direction of the electrical field (dipole axes). At the end of the process, the temperature and electrical field are quickly reduced to 'fix' the dipoles in the aligned state (Shayegan et al., 2003). However, some domains switch their alignments by time, causing the nonlinear behaviour of piezoelectric actuators (Kim et al., 2010, Sakata et al., 1996). Finally, several layers of wafer and stack are assembled together to complete the fabrication process. The stacks are mechanically in series and electrically in parallel. This arrangement generates large forces and small displacements for the actuator (Chopra, 2002, Adriaens et al., 2000). A typical piezoelectric stack actuator is shown in Figure 2.3.

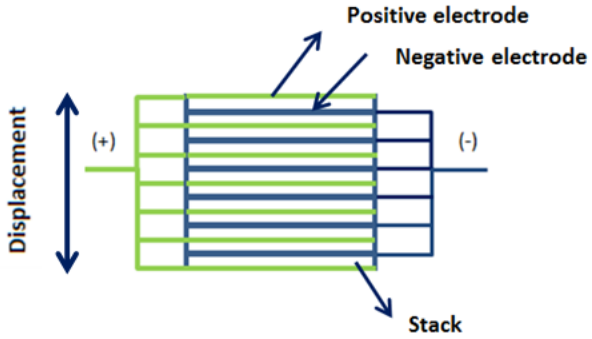

Figure 2.3: A typical piezoelectric stack actuator.

2.3. Challenges to Model Piezoelectric Actuators

Different models have been designed to estimate the displacement of piezoelectric actuators using the voltage across the actuators (Blackwood and Ealey, 1993, Lee, 1990, Bazghaleh et al., 2013).

In (1987), an American National Standard described the behaviour of piezoelectric actuators in the IEEE Standard on Piezoelectricity (Meeker, 1996). This well-known publication was based on two linear constitutive relations originally introduced by Woldemar Voigt, a German physicist in (1910) (Vasanthanathan and Raamachandran, 2008). Through these relations, a tensorial notation of two kinds of variables, mechanical (T, S) and electrical (E, D) variables, were used to describe the behaviour of piezoelectric materials. If electrical variables (E, D) are converted to mechanical variables (T, S), the piezoelectric material is an actuator and, inversely, it is a sensor (Tadigadapa and Mateti, 2009). Accordingly, the coupled electromechanical constitutive relations for piezoelectric actuators/sensors are written as:

$$\begin{aligned} S &= [s^E].T + [d]^t.E \\ D &= [d].T + [\varepsilon^T].E \end{aligned} \quad , \tag{2.1}$$

where E, T, S and D are the electric field, stress vector, strain vector and electrical induction, respectively (Vasanthanathan and Raamachandran, 2008). As long as we deal with piezoelectric actuators, (E, D) are the inputs and (S, T) are the outputs. s^E and ε^T are mechanical flexibility and electrical permittivity matrices, respectively, E and T indices show that the electrical field (E) and mechanical stress (T) are either constant or zero. Furthermore, d is the piezoelectric coefficient that couples the mechanical domain to the electrical domain. The parameters of Eq. (2.1) are determined by considering the boundary conditions and material symmetry (Sirohi and Chopra, 2000). This equation is useful to estimate the piezoelectric displacement when the actuator has an almost linear behaviour (Sirohi and Chopra, 2000). The equation fails to model the nonlinear behaviour of piezoelectric actuators occuring when the strain increases to more than 0.2% (Adriaens et al., 2000, Tzou and Tseng, 1990, Hegewald et al., 2008). The nonlinear aspect for the performance of piezoelectric actuators comes about from a combination of two phenomena: hysteresis and creep (Liaw and Shirinzadeh, 2011).

Hysteresis: Hysteresis is regarded as having different system outputs for identical system inputs, the outputs depend on the input history (Yeh et al., 2008). This phenomenon is a complex nonlinear behaviour observed in ferromagnetism, ferroelectricity, plasticity and superconductivity (Yu et al., 2002). It causes energy loss and nonlinearity in the voltage-displacement relation of piezoelectric actuators (Han et al., 1999). Hysteresis is assumed to be rate(frequency)-dependent by many researchers (Yeh et al., 2008, Boukari et al., 2011, Al Janaideh et al., 2008). As Figure 2.4 shows, one distinctive loop is obtained for each

excitation frequency. Moreover according to this figure, when the excitation frequency increases, the system input-output (presented as the hysteresis loop in the literature) becomes shorter, wider and rotates clockwise. However, the hysteresis is not differentiable from other phenomena, i.e. the vibration and creep, so the rate dependency of the presented loops may be due to other phenomena. The hysteresis effect significantly reduces the precision of piezoelectric actuators in relatively long range positioning applications (Croft et al., 2000).

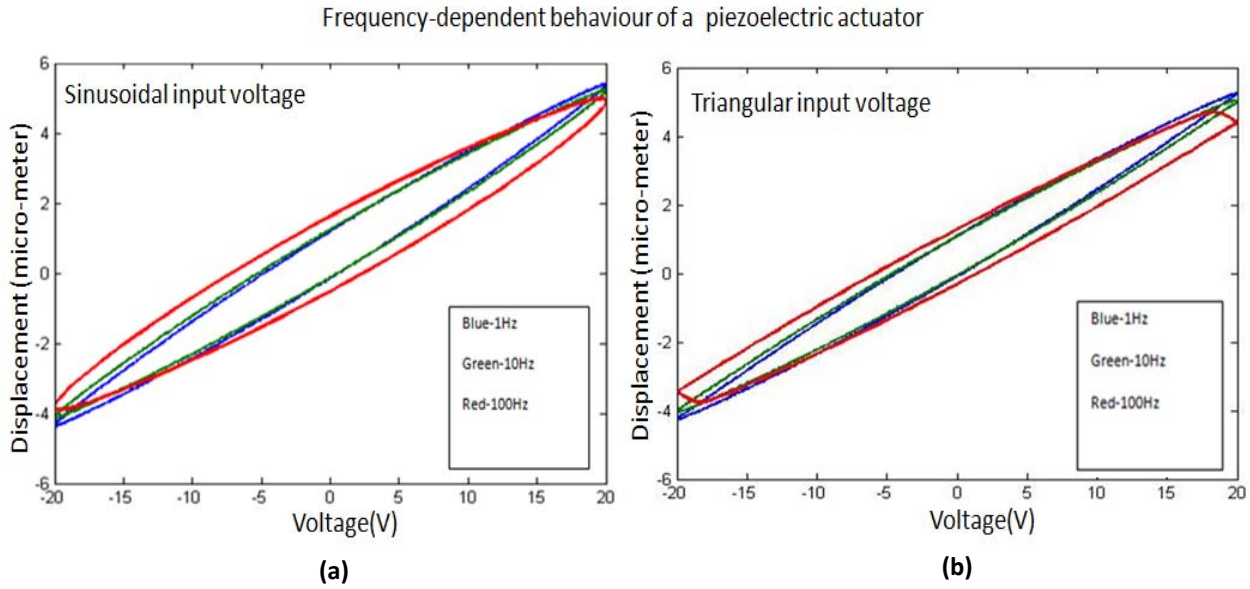

Figure 2.4: The displacement of a piezoelectric actuator vs voltage for a) a sinusoidal and b) a triangular input voltage at three different excitation frequencies.

Creep: Creep is a behaviour of piezoelectric actuators causing error in long operations (Jung and Gweon, 2000, Guillon et al., 2004). It is the decrease of the displacement of piezoelectric actuators over time for a constant applied electrical field (Yeh et al., 2008). The physical reason behind the creep phenomenon is switching process in microscopic domains of the piezoelectric materials (Zhou and Kamlah, 2006, Sakata et al., 1996). When positioning is performed over a period of time, the creep phenomenon becomes more critical (Croft et al., 2000). A creep pattern is shown in Figure 2.5 and, the curves' thickness in Figure 2.4 indicates the presence of the creep phenomenon in the behaviour of piezoelectric actuators.

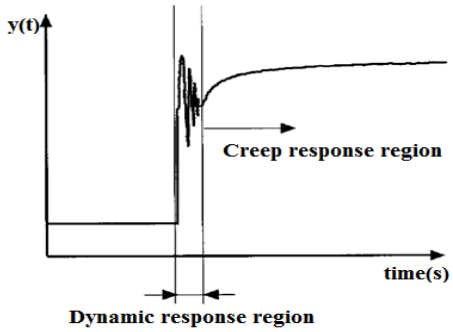

Figure 2.5: A creep pattern for a piezoelectric actuator. A dynamic response region is upon applying an electrical field followed by a creep region (Jung and Gweon, 2000).

Structural vibration: In addition to the hysteresis and creep, the structural vibration causes the loss of positioning precision in piezoelectric actuators (Baz and Poh, 1988). The structural vibration is a frequency dependent phenomenon influenced by physical characteristics of the actuator such as mass, stiffness and damping. The structural vibration is more significant close to resonance frequencies of the actuators (Hagood and von Flotow, 1991, Yeh et al., 2008). Typically the operating bandwidth, sampling rate, of piezoelectric actuators should be 10 to 100 times less than the first resonant vibrational frequency of the actuator to minimise the structural vibration (Croft et al., 2000, Huber et al., 1997, Abramovitch et al., 2007). One approach to increase the bandwidth is to use a piezoelectric actuator with fast dynamic response, i.e. with large resonant vibrational frequency. This can be fulfilled by exploiting a small actuator and/or an alternate configuration for the actuator (Croft et al., 2000).

Figure 2.4 illustrates the nonlinear behaviour of a piezoelectric stack actuator associated with the three phenomena. Such plots are normally assumed as hysteresis loops in the literature and they are used as an evidence for rate-dependency of the hysteresis. However, the rate-dependency of these plots may be influenced by the structural vibration. To achieve a precise nanopositioning, all the three effects should be compensated for through the control system. As the three different phenomena cannot be differentiated, the author has found no experimental evidence proving the rate-dependency of the hysteresis phenomenon. However as a general rule, at high-input magnitudes and frequencies, respectively, the hysteresis and vibration effects are large and, for long-run operation of the nanopositioning system, the creep effect is significant.

A nonlinear rate-dependent model can capture the nonlinear behaviour of piezoelectric actuators by considering all training data sets. Accordingly, in model-based control techniques for nanopositioning applications, if the model accuracy improves, a significant enhancement is demonstrated in positioning speed and precision (Croft et al., 2000).

2.4. Summary

At the beginning of this chapter, important characteristics of piezoelectric materials were presented. Then, it was explained how the material is prepared to be used as an actuator. Finally, dominant challenges to model piezoelectric actuators were addressed.

Overall in this chapter, the most important features of piezoelectric materials, actuators and challenges for their modelling were introduced. It provides background for the research carried out in this thesis.

NOTE:

This page is intentionally left blank.

Chapter 3 - Physics-based Models of Piezoelectric Actuators

The models constructed by non-formal analogies with physical phenomena are called physics-based models. Physics-based models of piezoelectric actuators are made based on an analogy between the behaviour of piezoelectric actuators and magnetic/mechanical systems. The parameters of these models are physically interpretable, at the same time; they do not use any physical properties of the system. Apart from application in sensorless and model-based control systems, due to the physical nature of physics-based models, the accordance between model predictions and experimental results may provide insight into the underlying actuation mechanisms of piezoelectric materials (Chen and Tan, 2008). In this chapter, the most well-known physics-based models of piezoelectric actuators are presented and their important characteristics are discussed.

3.1. Models Analogous with Magnetic Systems

Magnetostrictive materials are composed of *Weiss* domains seeking to align themselves in the direction of the external magnetic field B, as shown in Figure 3.1. These domains have a tendency to rotate in the direction of the external magnetic field (Fontana, 1995). Hence, during magnetisation process, the external magnetic field and demagnetising field of each domain are superposed (Della Torre et al., 1990). However, when the external field is removed, the domains revert partially, as illustrated in Figure 3.1 (c). This innate feature of these materials results in their nonlinear behaviour (Della Torre et al., 1990).

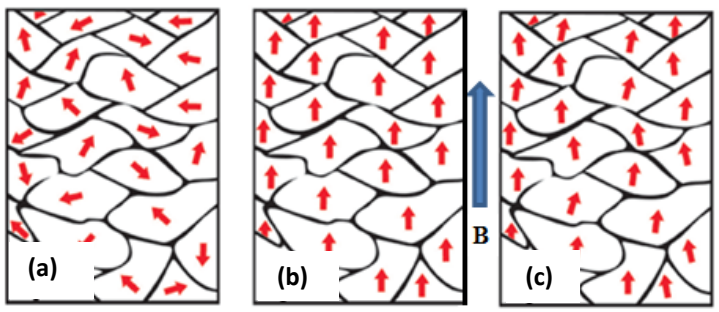

Figure 3.1: Magnetostrictive materials in (a) no external magnetic field, (b) a strong external magnetic field and c) the removed magnetic field.

In this section, physics-based models of piezoelectric actuators, inspired by the nonlinear behaviour of magnetostrictive materials in an external field, are explained. The most well-known models of this category are explained, i.e. the Preisach (Mayergoyz, 1991) and Prandtl-Ishlinskii (Al Janaideh et al., 2011) models, and some important features of each are discussed.

3.1.1. Preisach Model

The Preisach model was introduced in the early 1930s to model the hysteresis behaviour of ferromagnetic materials placed in a magnetic field, as the model input-output represented the applied elements of the magnetic field-magnetisation, respectively (Hegewald et al., 2008). This model explains the nonlinear behaviour of ferromagnetic materials by dividing it into small microscopic domains. Each domain is characterised by two magnetic fields: external and internal fields (Robert et al., 2001). As shown in Figure 3.2, in the case of piezoelectric actuator, the input-output is the applied electric voltage-displacement demonstrating a nonlinear behaviour similar to the ferromagnetic materials (Hegewald et al., 2008). This similarity resulted in introducing the Preisach model for piezoelectric actuators (Wolf et al., 2011, Zelinka et al., 1987). According to the Preisach model, if a varying voltage is applied to a piezoelectric actuator, the piezoelectric displacement *y* is estimated by:

$$y(t) = \iint_{\beta' \geq \alpha'} \mu(\alpha', \beta') d\alpha' d\beta', \tag{3.1}$$

where the vertical and horizontal axes, α' and β', both represent the input voltage, $\mu(\alpha', \beta')$ is the Preisach density function and different presentations have been offered for it (Zelinka et al., 1987, Mohammadzaheri, 2011, Robert et al., 2001).

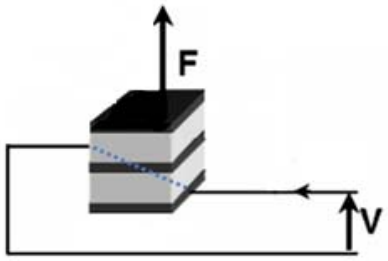

Figure 3.2: Applied voltage to a piezoelectric actuator.

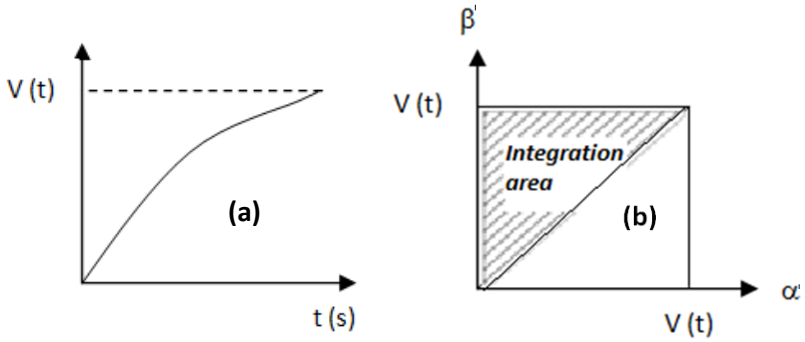

Figure 3.3: (a) A varying input voltage (*V*) applied to a piezoelectric actuator and, (b) the corresponding integration area for Eq. (3.1).

Figure 3.3 shows a varying input voltage applied to a piezoelectric actuator and the corresponding integration area for Eq. (3.1). In the Preisach model, for the input voltage behaviour (ascending/descending), Eq. (3.1) is converted to the following equations:

Ascending: $$y(t) = \iint_{S(0 \to V_{\min})} \mu(\alpha', \beta') d\alpha' d\beta' + \iint_{S(V_{\min} \to V)} \mu(\alpha', \beta') d\alpha' d\beta' , \tag{3.2}$$

Descending: $$y(t) = \iint_{S(0 \to V_{\max})} \mu(\alpha', \beta') d\alpha' d\beta' - \iint_{S(V_{\max} \to V)} \mu(\alpha', \beta') d\alpha' d\beta' , \tag{3.3}$$

where S is the integration area known as the Preisach plane. Consequently, Eq. (3.2) and Eq. (3.3) could be rewritten as:

Ascending $$y(t) = y_{\min} + \iint_{S(V_{\min} \to V)} \mu(\alpha', \beta') d\alpha' d\beta' , \tag{3.4}$$

Descending $$y(t) = y_{\max} - \iint_{S(V_{\max} \to V)} \mu(\alpha', \beta') d\alpha' d\beta' , \tag{3.5}$$

where $y_{\max}$ is the last local maximum when descending and $y_{\min}$ is the last local minimum when ascending (Zhang et al., 2009). According to the Preisach model, Eq. (3.4) and Eq. (3.5) show that the current input *V*, the last extremum of the input $[V_{ext} = (V_{\min}) \text{ or } (V_{\max})]$ and its corresponding output $[y_{ext} = (y_{\min}) \text{ or } (y_{\max})]$ are used to estimate the current output $y(t)$ (Miri et al., 2013a).

The Preisach model is rate(frequency)-independent. To compensate for this, some modifications such as introducing a rate-dependent density function have been devised (Wolf et al., 2011). Furthermore, the classical Preisach model is not reversible for control purposes and it may fail to model large experimental areas (Mayergoyz and Friedman, 1988).

3.1.2. Parandtl-Ishlinski Model

The Parandtl-Ishlinski (PI) model is a subclass of the Preisach model, originally designed for ferromagnetic materials (Hassani and Tjahjowidodo, 2011). The PI model identifies the model parameters more easily than the Preisach model (Hassani and Tjahjowidodo, 2011, Ang et al., 2007). It estimates the piezoelectric displacement by:

$$y(i) = \omega H(i), \tag{3.6}$$

where $y(i)$, $H(i)$, i and ω are the model output (displacement), backlash operator (play operator), width of the backlash operator and slope of the backlash operator, respectively.

The PI model is formed by a number of backlash operators $H(i)$ where a backlash operator is defined as:

$$H(i) = \max\{V(i) - r, \min[V(i) + r, H(i-1)]\}, \tag{3.7}$$

where $V(i)$ and r are the input voltage and half-width, respectively, and the value of r is between *0* and the maximum input voltage $V(i)$ (Wang et al., 2011, Deng et al., 2011). A typical backlash operator is shown in Figure 3.4.

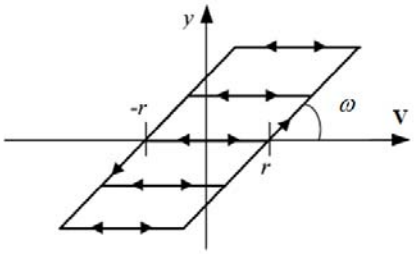

Figure 3.4: A typical hysteresis operator of the Parandtl-Ishlinski model (Ang et al., 2007).

The initial condition for the backlash operator is:

$$H(0) = \max\{V(0) - r, \min[V(0) + r, y_0]\}, \tag{3.8}$$

where y_0 is the initial displacement and it equals zero, if the starting point is from the rest state. In a PI model, different backlash operators $H_j(i)$ with different slopes ω_j and widths r are added together to model the complex behaviour of the piezoelectric actuator:

$$y(i) = \vec{\omega} \vec{H}(i) = \sum_{j=1}^{N} \omega_j H_j(i), \tag{3.9}$$

where j is the number of backlash operators/widths (Wang et al., 2011).

The PI model is rather simple and can be analytically inverted. This model cannot capture the rate(frequency)-dependent behaviour of the system (Al Janaideh et al., 2008). Moreover, it is able to estimate the displacement of piezoelectric actuators at an excitation frequency range of [0.1-500] *Hz* (Wang et al., 2011).

3.2. Models Analogous with Mechanical Systems

In force interaction with viscoelastic materials, there is an elastic force proportional with displacement and a viscose force proportional with velocity (Adhikari and Woodhouse, 2001). This behaviour is very similar to the behaviour of mechanical systems consisting of springs-dampers. Hence, the governing equations of the mechanical systems were suggested for the viscoelastic materials. Moreover, a remarkable similarity between the behaviour of the

nonlinear viscoelastic systems and piezoelectric actuators resulted in introducing a non-formal analogical model for piezoelectric actuators (Richter et al., 2001). Hence, in this section, the main analogical models of piezoelectric actuators inspired by the mechanical systems are explained and important features for each model are discussed. These models include the Maxwell-Slip (Quant et al., 2009), Duhem (Xie et al., 2009b) and Voigt (Yeh et al., 2008) models.

3.2.1. Maxwell-Slip Model

The Maxwell-Slip model was initially suggested by Goldfarb and Celanovik in (1997) to model piezoelectric actuators. This model is based on a theory first formulated by James Maxwell in the mid-1800s to model friction phenomena (Goldfarb and Celanovic, 1997). The original friction model employs ideal massless springs and friction elements so as the springs are used for energy storage and Columb friction elements for rate-independent dissipation (Goldfarb and Celanovic, 1997). Consequently, the Maxwell-Slip model consists of a parallel connection of various elementary friction models, each with the same structure but a different set of parameters (Swevers et al., 2000).

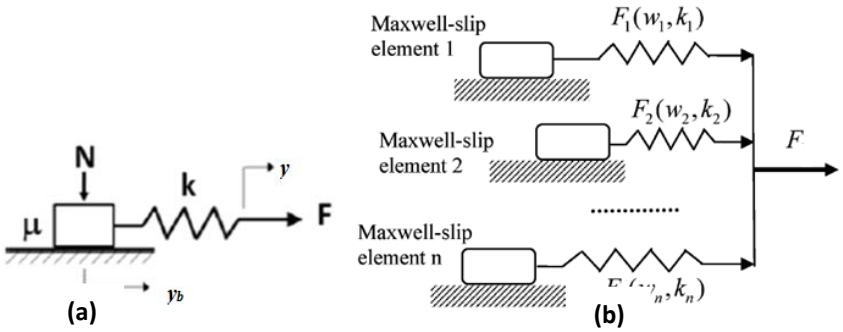

Figure 3.5: (a) A single and (b) multiple elasto-slide element(s) of the Maxwell-Slip model (Vo-Minh et al., 2011).

Figure 3.5 demonstrates element(s) of the Maxwell-Slip model wherein μ, N, y, y_b, k and F are, respectively, the friction coefficient, normal force acting on the block, block position after exerting the external force, current position of the block, linear spring stiffness and the

external force (reaction force) (Goldfarb and Celanovic, 1997, Yeh et al., 2008). In the friction model, to define friction between two contacting surfaces, two regimes are distinguished: pre-sliding and sliding (Swevers et al., 2000). In the pre-sliding regime, the external force F is a function of the displacement rather than the velocity, the element will behave like a spring with certain stiffness. (Lampaert et al., 2003). The sliding regime occurs if the element keeps displacing until only the smooth contacts remain at the maximum force. The maximum force is called saturation force w_i (Vo-Minh et al., 2011). Hence, each element is defined by two parameters: stiffness and saturation force, as shown in Figure 3.6.

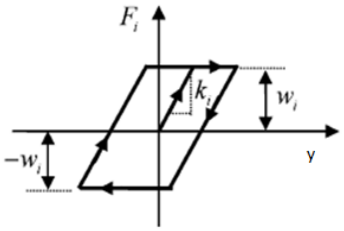

Figure 3.6: A schematic of the Maxwell-Slip model (Vo-Minh et al., 2011).

The Maxwell-Slip model consists of '*n*' number(s) of such elements in parallel. The model accuracy increases with an increase in the number of elements. Considering $w_i = \mu_i N_i$, the friction force for each element is:

$$F_i = \begin{cases} k_i(y_i - y_{bi}) & \text{if } k_i(y_i - y_{bi}) < w_i \\ w_i \operatorname{sgn}(\dot{y}_i) \quad \text{and} \quad y_{bi} = y_i - \dfrac{w_i}{k_i}\operatorname{sgn}(\dot{y}_i) & \text{if } k_i(y_i - y_{bi}) < w_i \end{cases}, \tag{3.10}$$

where $i \in [1, n]$.

By analogy, the same structure is employed to model piezoelectric actuators. In this analogy, the voltage across the actuator and the actuator displacement play the role of the external force (F in Eq. (3.10)) and displacement y , respectively and, experimental voltage-displacement data are used to determine the model parameters.

This model is quasi rate(frequency)-dependent; the accuracy of this model decreases when the excitation frequency of the actuator increases. Moreover, the accuracy of the Maxwell-Slip model decreases for long-run operation of the system due to the creep phenomenon (Vo-Minh

et al., 2011). Moreover, this model is reversible for control purposes (Georgiou and Ben Mrad, 2006).

3.2.2. Duhem Model

The Duhem model is a dynamic friction model described by Duhem in (1897) distinguishing pre-sliding and sliding regimes (Hui et al., 2011, Padthe et al., 2008). The Duhem model is a first-order differential equation from which a number of other models have been derived, e.g. the Dahl (Dahl, 1977), Coleman-Hodgdon (Coleman and Hodgdon, 1987), Bouc-Wen (Wen, 1976, JinHyoung and Bernstein, 2005) and Jiles-Atherton (Ozer and Royston, 2001, Hodgdon, 1988, Huang and Lin, 2008) models.

The Duhem model for piezoelectric actuators is often presented by the nonlinear differential equation:

$$\frac{dy}{dV} = \begin{cases} g_1(V(t), y(t)) & \dot{V} \geq 0 \\ g_2(V(t), y(t)) & \dot{V} \leq 0 \end{cases}, \tag{3.11}$$

where y is the displacement of the piezoelectric actuator and V is the voltage across the actuator. In this equation when the piezoelectric input rate $\dot{V}(t)$ increases, the hysteresis slope is g_1 and when it decreases, the hysteresis slope is g_2 (see Section 2.3 for the hysteresis definition). The Duhem model is also presented by an alternative notation:

$$\begin{aligned} &\frac{dy}{dt} = \alpha \left| \frac{dV(t)}{dt} \right| \left[f(V) - y \right] + \frac{dy}{dt} g(V) \Rightarrow \\ &\begin{cases} \dfrac{dy_u}{dt} = \alpha \dfrac{dV(t)}{dt} \left[f(V) - y_u \right] + \dfrac{dy}{dt} g(V) & \dot{V} \geq 0 \\ \dfrac{dy_d}{dt} = -\alpha \dfrac{dV(t)}{dt} \left[f(V) - y_d \right] + \dfrac{dy}{dt} g(V) & \dot{V} \leq 0 \end{cases} \end{aligned} \tag{3.12}$$

where the indices of u and d represent the upward and downward curve of the displacement-voltage plot, respectively (Hui et al., 2011). In this model, α is a constant number and, $f(V)$ and $g(V)$ are functions of input voltage.

The Duhem model cannot capture the frequency dependent behaviours of the system (Oh and Bernstein, 2004, Xie et al., 2009a) and it is reversible for control purposes (Sprekels, 1996).

3.2.3. Voigt Model

The Voigt model, also known as the Kelvin-Voigt model, is an analogical model originally designed for viscoelastic systems (Wood et al., 2005). This model consists of a series connection of different elementary friction models; each with the same structure but a different set of parameters. A single element of the Voigt model is illustrated in Figure 3.7.

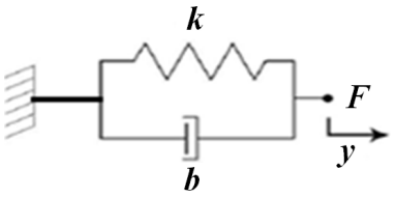

Figure 3.7: A single element of the Voigt model.

The governing equation for a system shown in Figure 3.7 is presented by:

$$b\dot{y} + ky = F \Rightarrow \dot{y} + \frac{ky}{b} = \frac{F}{b}, \tag{3.13}$$

where y is the spring displacement, F is the external force acting on the system and, k and b are the spring stiffness and damping coefficient, respectively.

In a qualitative sense, the behaviour of viscoelastic systems matches the characteristics observed in piezoelectric actuators as it inspires the model employment for piezoelectric actuators (Richter et al., 2001). By analogy, the mechanical parameters of the Voigt model are converted to piezoelectric parameters and, k and F are replaced with $d^{-1}(V)$ and V, respectively, as $d(V)$ and V are considered the piezoelectric coefficient and voltage across the actuator, respectively. Accordingly, the governing equation of the Voigt model for piezoelectric actuators is:

$$\dot{y} + \frac{y}{d(V)\cdot b} = \left(\frac{V}{b}\right)^{P}. \tag{3.14}$$

Note that for the spring-damper system, P is *1* but for the piezoelectric materials, P may find other values. In addition, to avoid complex values for the right-hand side, which are likely to arise from parameter identification, a signum function is introduced to the right-hand side of Eq. (3.14) (Richter et al., 2001). Hence, the Voigt model presents the dynamic displacement of piezoelectric actuators by:

$$\dot{y} + \frac{y}{d(V) \cdot b} = \text{sgn}(V) \cdot (\frac{|V|}{b})^P , \tag{3.15}$$

Boukari et al. (2011) defined $d(V)$ by:

$$d(V) = \frac{\alpha\lambda \exp(-\lambda(V-\beta))}{(1+\exp(-\lambda(V-\beta)))^2}, \tag{3.16}$$

wherein α, λ, β are Sigmoid parameters (Boukari et al., 2011).

The Voigt model can capture the rate(frequency)-dependent behaviour of piezoelectric actuators and is reversible for control purposes. This model can simulate the nonlinear effects of piezoelectric actuators operating over a long period of time and, it performs well at the excitation frequencies above 1 *Hz* and below 400 *Hz* (Boukari et al., 2011).

3.3. Common Challenges for the Model Selection and Identification

In spite of the findings highlighted in previous sections, the fundamental questions remain: 1) how to identify the parameters of physics-based models and, 2) are these models' structures adequate to present the systems' nonlinear behaviour. This section explains the deficiencies of existing parameter identification methods and mathematical structures for each of the aforementioned models. These issues are rarely addressed in the literature and are summarised below.

Preisach model: A decisive task for the Preisach model is to identify the density function μ. Normally, a function dependent on both variables of the Preisach plane *S*, *i.e.* α' and β', is proposed, then in order to find its parameters, a set of reversal (transition) curves should be experimentally found (Mayergoyz, 1986). For example, Kaltenbacher et al. (2007) applied an incremental triangular excitation voltage to the actuator (Kaltenbacher and Kaltenbacher, 2007). Figure 3.8 shows a typical input-output of the system.

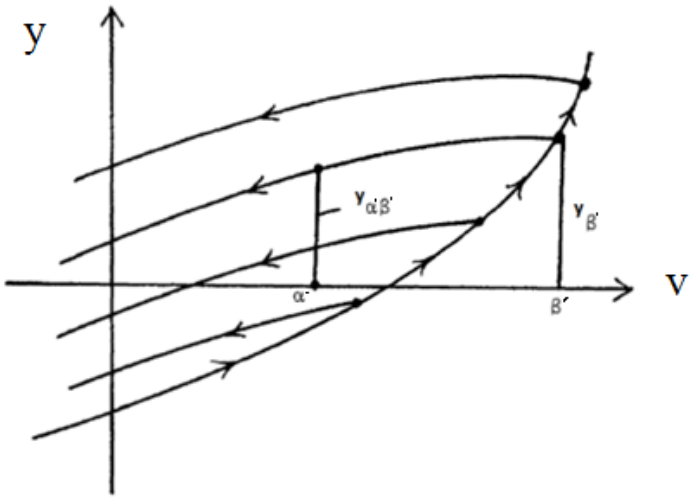

Figure 3.8: Typical first order reversal curves.

In Figure 3.8, the correspondence output values to the inputs of β' and α' are $y_{\beta'}$ and $y_{\alpha'\beta'}$, respectively (Mayergoyz, 1986). Then, to identify the density function, below definition was performed:

$$F(\alpha', \beta') = (y_{\beta'} - y_{\alpha'\beta'})/2 \ . \tag{3.17}$$

Considering the Preisach half plane and geometrical interpretations explained by Mayergoys et al. (1986), Eq. (3.17) was expressed in terms of the density function as:

$$F(\alpha', \beta') = \iint_{S(\alpha', \beta')} \mu(x, z)dxdz = \int_{\alpha'}^{\beta'} (\int_{\alpha'}^{z} \mu(x, z)dx)dz \ . \tag{3.18}$$

Hegawald et al. (2008) identified the density function of each element by considering Eq. (3.17), Eq. (3.18) and symmetrical hysteresis loop, avoiding evaluation of the double integral (Hegewald et al., 2008). Accordingly, the density function was represented as:

$$\mu(x, z) = -\frac{\partial^2 F(\alpha', \beta')}{\partial \alpha' \partial \beta'} . \tag{3.19}$$

Therefore, they identified a density function through using available system input-output data and a least-square approach. However, the hysteresis loop is not necessarily symmetric in practice.

Overall, the main difficulties with the Preisach function are: 1) the error for the density function is amplified, due to the inherited experimental error in $F(\alpha', \beta')$, to perform the differentiation, 2) the need to solve the double integral of Eq. (3.1) to compute the output, 3) a large number of reversal transition inputs should excite the piezoelectric actuator and a large

set of density functions should be identified in order to allocate an appropriate Preisach function. (Kaltenbacher and Kaltenbacher, 2007).

Prandtl-Ishlinskii model: To characterise a Prandtl-Ishlinskii model, the core task is to define the backlash operators. To this purpose, the rising curve of the hysteresis is created by a uniform increasing input signal initiated from a relaxed state. This is a practical restriction for working actuators (Kuhnen, 2003). To define the rising curve, the number, width and slope of backlash operators should be identified. The number of the operators is normally determined by trial and error and the width and slope values of each operator are defined by different optimisation methods (Wang et al., 2011). Jiang et al. (2010) and Wang et al. (2011) identified the operator parameters by reformulating the problem as a recursive least-square fit using experimental data (Jiang et al., 2010, Wang et al., 2011). Kuhnen et al. (2003) used quadratic optimisation to identify the model parameters (Kuhnen, 2003). Two main problems with the PI model are the convex property of the rising curve and symmetric features of the model operator around the centre point, whereas, in practice, the hysteresis loops are non-convex and asymmetric (Jiang et al., 2010). These issues result in the model inaccuracies.

Maxwell-Slip model: In order to identify the parameters of a Maxwell-Slip model, the initial rising curve of the hysteresis should be parameterised (Huang and Lin, 2008). As explained in Section 3.2.1, the curve is divided into '*n*' elements with different slopes and saturation voltages. Therefore, the model parameters are a pair of (k_i , w_i) for each element; *2n* parameters totally. These parameters are determined by different algorithms fitting the experimental data of the initial rising curve to the mathematical model (Quant et al., 2009). The accuracy of the model increases with a larger number of elements, if sufficient set of data are available. The main drawback of this model is the need to start the piezoelectric actuator from a relaxed state, to achieve the initial rising curve, which is difficult in practice. Moreover, to identify the model parameters, many set of experiments should be conducted and parameter identification should be performed for each different signal frequency, magnitude and waveform (Richter et al., 2001, Huang and Lin, 2008).

Duhem model: In order to model piezoelectric actuators using the Duhem model, the model's mathematical structure should meet below conditions:

a) $f(0)$ is monotone increasing, piecewise smooth and $\lim_{V\to\infty} \dot{f}(V)$ is finite .

b) $g(0)$ is piecewise continuous, even and satisfies $\lim_{V\to\infty} g(V) = \lim_{V\to\infty} \dot{f}(V)$.

c) For all $V>0$, $\dot{f}(V) > g(V) > \alpha e^{\alpha V} \int_{V}^{\infty} \left| \dot{f}(\zeta) - g(\zeta) \right| e^{\alpha \zeta} d\zeta$.

If the three conditions are met, with proper selection of $f(V)$ and $g(V)$, the model is ready to be used for piezoelectric actuators (Stepanenko and Su, 1998). However, defining the mathematical structure and parameters of $f(V)$ and $g(V)$ is a challenging task for the Duhem model. These functions have been approximated by different approaches such as *Weierstrass* theory and using polynomial functions (Ying, 1998). Moreover, Stepanenko et al. (1998) have used fuzzy systems to identify the functions (Stepanenko and Su, 1998).

Voigt models: The governing equation of the Voigt model is a first order differential equation, as detailed in Section 3.2.3. Therefore, the structure of this model is simpler than other physics-based models. However, the mechanism of parameter identification for this model is a momentous task. The following are some commonly used *ad-hoc* parameter identification methods for this model:

- Using Multiple Voigt equations: In this method, a staircase odd function of voltage, *f(-V)=-f(V)*, is applied to the actuator and for each step, the displacement is measured as a series arrangement of *n* Voigt units and functions are generated (Yeh et al., 2008, Richter et al., 2001, Wood et al., 2005). The solution of the equations for the total *n* elements is:

$$y = \sum_{i=1}^{n} \frac{F_C}{k_{ci}} \cdot [1 - e^{-\frac{k_{ci}}{b_{ci}} t}], \tag{3.20}$$

where k_{ci} and b_{ci} are respectively, the spring stiffness and damping coefficient of each element and, F_c and n are the initial applied force and number of elements, respectively. F_c was initially identified by considering $b_{ci}=0$ and the actuator as a spring with the stiffness of k_m. Then, k_m was replaced with a series connection of the Voigt elements (Yeh et al., 2008). To identify k_{ci} and b_{ci}, they formed a series with n=20 elements of Eq. (3.20) within a specific timeframe. Finally, they determined the parameters by least-square fit optimisation to minimise the absolute discrepancy for the experimental and estimated displacement through Eq. (3.20).

- Using single Voigt equation: Boukari et al. (2011) used the Voigt model Eq. (3.15) representing one element of the Voigt model. They first identified the Sigmoid parameters of the Eq. (3.16) using experimental data obtained in static condition so as they could calculate

the value of *d(V)* at each voltage. Then, they looked for P and $b$of Eq. (3.15) using the hysteresis loop areas A_{hyst} in two steps:

1- Identifying the mean value of b_{mean} :

- Set d_m: the mean value of *d (V)*,
- $P = 1$,
- Analytical solution of (3.15).
- Determining the experimental and theoretical hysteresis loop areas, A_{hyst} and A_{th}, respectively, at each frequency in the range of [1-400] *Hz*

Note: To define A_{th}, it was known to be proportional to the energy loss. For more detail for the definition, see (Boukari, 2010).

- Set b_{mean} : b minimising the differences between A_{hyst} and A_{th}.

Note: Minimisation was performed using Mathematica function NMinimize.

2- Identifying P and b.

- Setting a table of numbers for P symmetrical around *1*
- Setting a table of numbers for b symmetrical around b_{mean}
- Solving Eq. (3.15) numerically for each couple of (P , b) at each frequency
- Determining the hysteresis loop areas for each couple of (P , b) at each frequency.
- Finding the couple of (P , b) minimising the differences between A_{hyst} and A_{th} (Boukari et al., 2011).

No rendered approaches for parameter identification of the Voigt model are global because of the many approximations and simplifications made during identification algorithm development. In addition, in all suggested methods of parameter identification, a large number of experiments should be conducted at different frequencies and time domains (Richter et al., 2001).

In summary, the strategies to identify the parameters of the physics-based models and their mathematical structures were addressed in this section. It has been identified that although some introduced methods of parameter identification characterise the model as accurate, they are *ad-hoc* to the specific parameter identification problem requiring specific, often difficult to carry out, experiments. These methods are not global, and there is no evidence showing that they are optimal even for their particular case.

A mathematical structure is appropriate/sufficient for this particular research area that has four characteristics: 1- Simplicity, the model should not be complicated; 2- Causality, the model should address cause-effect relationships; 3- Identifiability, the model parameters and structure should be identifiable using available information and; 4- Predictive capability, the model should be valid for reasonable experimental conditions. Finally, the analysis of the identified models may result in proposing to add/eliminate some terms/equations to the model structure to improve the model performance (Donoso-Bravo et al., 2011). For more details about the model structure, see Appendix A.

3.4. Summary

This chapter reviewed the foremost physics-based models of piezoelectric actuators and identified the common strengths and weaknesses of these models. A non-formal analogy of well-known physical phenomena with the behaviour of piezoelectric actuators is used to construct the mathematical structure for physics-based models of piezoelectric actuators. These models are not directly constructed based on physics laws; therefore, the analogy is of limited use in gaining physical insight about the piezoelectric actuator. Instead, the model parameters are normally identified using the experimental data and mathematical methods.

These models are constructed analogous with two physical systems:

- Magnetic systems: Preisach and Parandtl-Ishlinski (PI) models.
- Mechanical systems: Maxwell-Slip, Duhem and Voigt models.

Table 3.1: Summary of the key features of physics-based models.

Model	*Rate-dependency*	*Frequency range of validity (Hz)*	*Reversibility*
Preisach	×	-	×
Parandtl-Ishlinski	×	0.1-500	√
Duhem	×	1-40	√
Maxwell-Slip	Quasi	0-100	√
Voigt	√	1-1000	√

The literature review in this chapter addresses the most important features of each model including rate(frequency)-dependency, reversibility for control purposes and validity range of the excitation frequency. These models' features have been summarised in Table 3.1.

These models suffer from *ad-hoc* and tedious solutions rendered to identify their parameters. As many of the reported parameter identification methods need the information of the very first instances of the actuator operation, after a relatively long relaxation of the actuator, which might be difficult to collect, especially for working actuators. Moreover, improving the sufficiency of the mathematical structure for these models may result in enhancing the models performance.

Overall, this chapter paved the way for identifying the gaps in the physics-based models of piezoelectric actuators and developing strategies through which to improve them.

Chapter 4 – Innovative Parameter Identification Method for Physics-based Models

This chapter introduces an innovative parameter identification method for physics-based models of piezoelectric actuators. The method is then applied to a real problem and the identification of the model parameters. Experimental validation of the model is also addressed in this chapter.

4.1. Parameter Identification

As explained in Chapter 3, all current methods of parameter identification render *ad-hoc* solutions and/or need the data of some special operation areas such as the data collected after a long relaxation of the actuator which are difficult to collect, in practice. Therefore, this thesis introduces a global and optimal method of parameter identification.

In this research, the available recorded experimental input-output (piezoelectric voltage-piezoelectric displacement) data are used to identify the model parameters (Mohammadzaheri et al., 2012b). The model error is defined as the average of absolute discrepancy for the model output and the system output:

$$\text{model error} = \frac{\sum_{k=1}^{l} \left| y_{model}(k) - y_{system}(k) \right|}{l}, \tag{4.1}$$

where l is the number of estimations. The small value of the model error is a sign of the closeness of the model parameters to their correct values. As a result, a 'cost function' or model error exists requiring minimisation through fine-tuning the values of the model parameters. This process is a classical optimisation problem. In other words, the parameter identification problem is converted into an optimisation problem. In system identification problems, to optimise the 'cost function', several numerical algorithms have been developed. These algorithms are divided into two main categories: local and global algorithms.

Local algorithms are fast converging optimisation methods as in ideal conditions, they can converge in one iteration after a small number of basic mathematical operations (Mohammadzaheri et al., 2009). However, the main drawback of these methods is trapping in local minima (Donoso-Bravo et al., 2011). To avoid the trapping, initial parameters are started from several random points extending the search space. Therefore, the initialisation stage is very important in local algorithms and several methods have been proposed to determine the initial conditions. Gradient-based methods are one of the most common algorithms in which the first and second derivative of the cost function are used. Some examples of this method are steepest descent, Gauss-Newton and Levenberg-Marquadt method (Hulhoven et al., 2005). These methods are relatively appropriate for linear unconstrained optimisation. However, to perform nonlinear constrained optimisation, local algorithms such as sequential quadratic programming (SQP) have been devised (Figueiredo et al., 2007). All aforementioned approaches sequentially evaluate the cost function through a call to a time integrator and are relatively unstable (Müller et al., 2002). They are more or less sensitive to the local minima and they may result in wrong convergences (Donoso-Bravo et al., 2011).

Global algorithms, however, are the other search techniques numerically approaching the optimum values of the parameters. Unlike local algorithms, global algorithms do not require the differentiation of the objective function. Global methods aim at finding the best solution to nonlinear parameter identification problems through searching a broad area so they do not trap at local minima at the cost of being computationally demanding. They find the optimum value for each parameter minimising the discrepancy between the outputs of model and actual system (Wolf et al., 2008). The most common global algorithms are grid search, branch and bound, simulated annealing, tabu search, genetic algorithm (GA), differential evolution, colony optimisation and particle swarm optimisation (PSO). The initial idea of these algorithms was inspired by natural/social phenomena such as annealing techniques in metallurgy and animal social behaviour in a group (Chang et al., 2013). GAs are based on evolutionary algorithms inspired by natural evolution including inheritance, mutation, selection and crossover (Coello and Lamont, 2004). Some advantages of GAs are taken below:

- GAs have the ability to avoid the premature convergence due to a parallel search in the population space.

- GAs conduct a fine-tuning of the parameters because they work on encoded versions of the potential optimum values of the parameters (chromosomes), rather the parameters themselves.
- GAs can solve every optimisation problem using cost values, which are obtained from objective functions, without other derivative or auxiliary information. Therefore, these algorithms are highly efficient to solve noisy, stochastic, multi-dimensional, non-differential, and noncontinuous objective functions.
- GAs are a method which is easy to understand and do not demand a broad knowledge of mathematics.
- GAs are easily transferred to existing simulations and models (Gutell and Jansen, 2006).

However, this method has never been employed to minimise the model error of physics-based models of piezoelectric actuators (Sivanandam and Deepa, 2008). In this research, a GA is used for this purpose and MATLAB R2011b is utilised as a computer environment.

4.1.1. Approaches for Modelling Error Estimation

There are two approaches to estimate the model error (Ljung, 1998). In one approach, all the inputs to the model are assumed to be known at a given instant, then the model output at the next instant (step) is estimated, and the output is compared with the real output of the system. The resultant discrepancy is called 'One Step Prediction' (OSP) error (Mohammadzaheri et al., 2012a).

In the second approach for calculating the model error, after the first estimation, previously estimated value(s) of the system output(s) is/are used as the model input(s) (instead of the real values). The model error in this approach is called 'Simulation' error (Mohammadzaheri et al., 2012a).

In dynamic systems, the current values of the system output depend on their previous value(s). However, the previous values are not measured/available to be fed into the model during long-term simulations. Therefore for dynamic systems, previously model outputs are used as the model inputs to estimate the outputs at each instant. This approach is the Simulation approach.

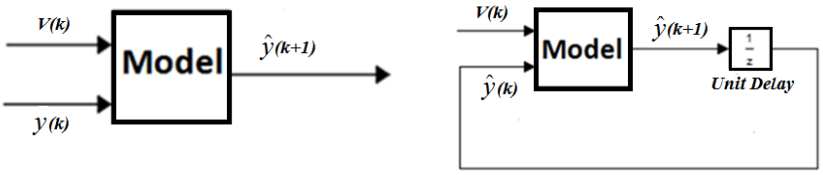

(a) (b)

Figure 4.1: Estimation of the model error through (a) One Step Prediction (OSP) and (b) Simulation approaches.

Let us consider a first order discrete model representing a single-input-single-output (SISO) system:

$$y(k+1) = f\left(V(k), y(k)\right). \tag{4.2}$$

After the initial steps, for the OSP approach, the model output to be used in Eq. (4.1) is calculated as:

$$y_{model}(k+1) = f\left(V(k), y_{real}(k)\right), \tag{4.3}$$

and for the Simulation approach:

$$y_{model}(k+1) = f\left(V(k), y_{model}(k)\right). \tag{4.4}$$

Figure 4.1 illustrates the difference between the OSP and Simulation approaches. The variables with *hat* are estimated values which are different in two approaches as shown in Eq. (4.3) and Eq. (4.4). Generally, both approaches presented by Eq. (4.3) and Eq. (4.4), together with Eq. (4.1), are used to find the model error. The model error is used both for the purpose of modelling, e.g. parameter identification, and model validation. In modelling, the parameters require identification so as to minimise the model error while in model validation, the model error shows the accuracy/validity of the model.

The OSP model error is usually much lower than the Simulation model error due to the error accumulation phenomenon in the Simulation approach. Nevertheless, the OSP approach is not applicable to validate the models of dynamic systems (Mohammadzaheri et al., 2012a). Therefore in this research, the simulation approach is employed to validate a model.

4.1.2. Parameter Identification using Optimisation

In this research, a GA is used for parameter identification through minimising the model error, because it is a global optimisation method. (Haupt and Haupt, 1998). Moreover, the original binary GA is employed in which a binary number is assigned to each parameter so as to minimise the model error as presented in Eq. (4.1). This binary number is called a *gene*. First, a number of *bits* with the value of 0 or 1 are assigned to each gene. The whole set of genes forms a *chromosome*, which is a full set of parameters and a probable solution to the optimisation problem. A number of chromosomes are made and tuned to solve the problem. The whole set of chromosomes is called the *population* and the mechanism for fine-tuning the genes and chromosomes is called *evolution* (Popov, 2005). The algorithm starts from assigning random values to the bits to form the initial population. Subsequently, the model error for each chromosome (set of parameters) is evaluated, then the chromosomes are evolved; that is, they go through a *selection*, *cross over* and *mutation* process (Homaifar et al., 1994, Chipperfield and Fleming, 1995a), and a new population is generated. For more detail about evolution, see Appendix C. This sequence is repeated several times until it is demonstrated that there will be no further improvement through evolution; this happens when the cost function does not decrease through more evolutions. Each time that the evolution is repeated is called *iteration*. After several iterations, the best chromosome amongst the population (with the lowest model error) is selected as the solution.

As a subtle point, a gene with m bits may have a value between 0 and $\sum_{i=0}^{m-1} 2^i$ (equal to $2^m - 1$), where m is the number of bits in a gene. Initially, an arbitrary binary population is created, and then the population is converted to decimal values. These values may fall obviously outside the ranges of some parameters. In order to address this issue, before evaluation of the chromosomes, the real value of each parameter (presented by a gene) is found by mapping the range presented by its associated gene onto its real range. For example, the value of a gene p_b should go through the following mapping to produce its real value at the range of $[p_{min}, p_{max}]$:

$$p = \left(\frac{p_{max} - p_{min}}{\sum_{i=0}^{m-1} 2^i} \right) p_b + p_{min}, \tag{4.5}$$

where p_{min} and p_{max} are the minimum and maximum values of each parameter respectively. According to Eq. (4.5), as the minimum absolute change of p_b is 1, the minimum absolute change (MAC) of each parameter is:

$$\mathrm{MAC} = \frac{p_{max} - p_{min}}{\sum_{i=0}^{m-1} 2^i}. \tag{4.6}$$

Therefore, as the number of bits increases, the minimum absolute change for the parameters decreases, and consequently the global minima are less likely to be missed out by the algorithm. However, the number of bits is problem dependent initially generated by a random value (Cao and Wu, 1999). A schematic of parameter identification by the GA is illustrated in Figure 4.2.

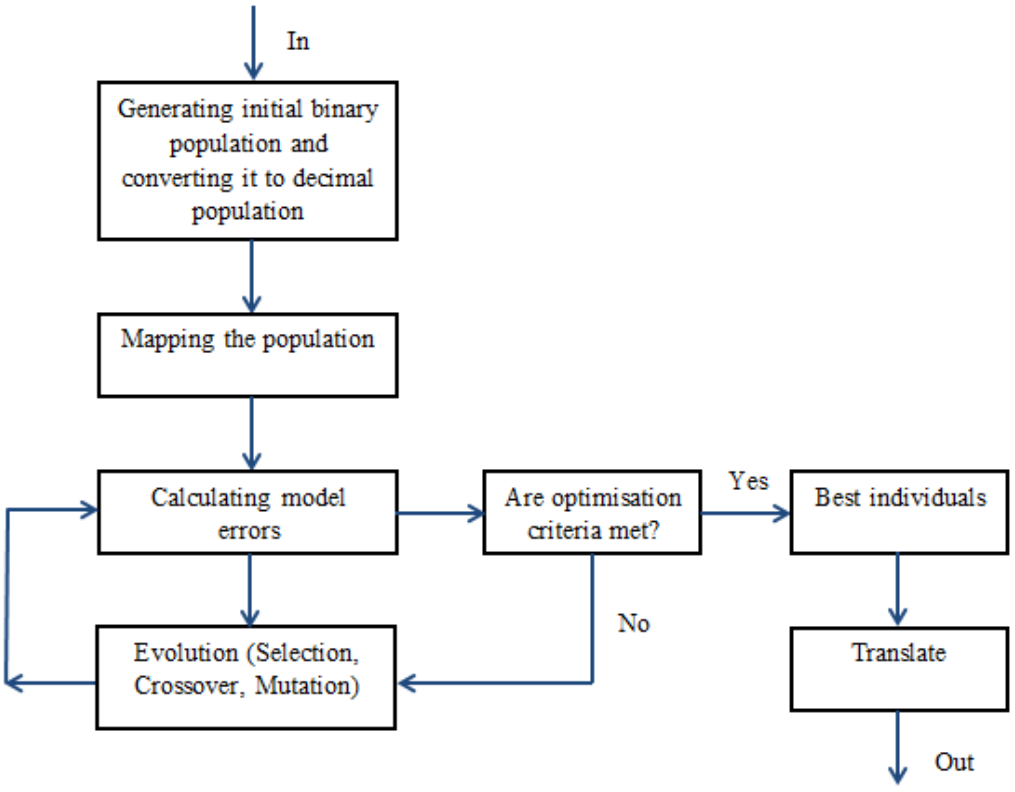

Figure 4.2: A standard procedure of a genetic algorithm.

4.1.3. Over-fitting Phenomenon in System Identification

Over-fitting is a term in learning or system identification used in relation to the identification of a model through a series of input-output data. A model which has been over-fit will

generally have poor predictive performance, exaggerating minor fluctuations of the validation data (Donoso-Bravo et al., 2011). Over-fitting occurs when a model memorises training data rather than learning to generalise from the trend. In parameter identification, first the model error is defined, then the algorithm tunes the model parameters so as to minimise the model error. If this excessive tuning generates a very small model error for the training data but a large error for the validation data, then the over-fitting has occurred (Coca and Billings, 2001). If the minimum validation error happened sooner than the minimum modelling error, then the over-fitting has occurred in parameter identification.

4.2. Solving a Real Problem

4.2.1. Experimental Setup and Data Gathering

An experimental setup was devised to mount the piezoelectric actuator in the control system. The experiments were performed in the Robotics Laboratory of the School of Mechanical Engineering at the University of Adelaide. The setup includes a PC, dSpace (electronic input/output board), voltage amplifier, piezoelectric stack actuator and a sensor. A function is generated in Simulink in a PC and transferred through the dSpace board to a voltage amplifier then, it is applied to the piezoelectric actuator. Finally, the actuator displacement is measured by an optical sensor. The measured signal is then amplified and transferred to the PC through the dSpace board.

DSpace (Electronic Input/Output (I/O) Board): The dSpace (DS1104 R&D Controller Board) connects the computer to the external hardware. A dSpace is shown in Figure 4.3.

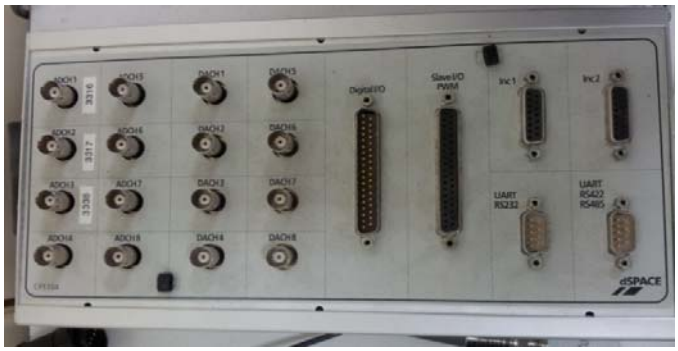

Figure 4.3: An electronic input/output (I/O) board.

Signal Amplifier: The signal amplifier amplifies the signals both before being applied to the actuator and after being received by the sensors. A signal amplifier has been demonstrated in Figure 4.4.

Figure 4.4: A signal amplifier.

Piezoelectric Actuator: The piezoelectric actuator, used for all experiments, is a piezoelectric stack known as Nek AE0505D44H40 which is composed of several ceramic layers developed by the factory of NEC/TOKIN (Micromechatronics, 2013). This piezoelectric stack is smaller than the conventional multilayer piezoelectric stacks, 1/10, leading to a faster scan rate and higher displacement/force at low voltages (Croft et al., 2000, Micromechatronics, 2013). The small size of the piezoelectric stack allows for a wide range of applications from ultra-fine positioning to drive sources such as printer/magnetic head position adjustment, mirror/prism positioning, linear motors and manipulators (Takahashi, 1985, Takahashi, 1989). A multilayer piezoelectric stack is demonstrated in Figure 4.5.

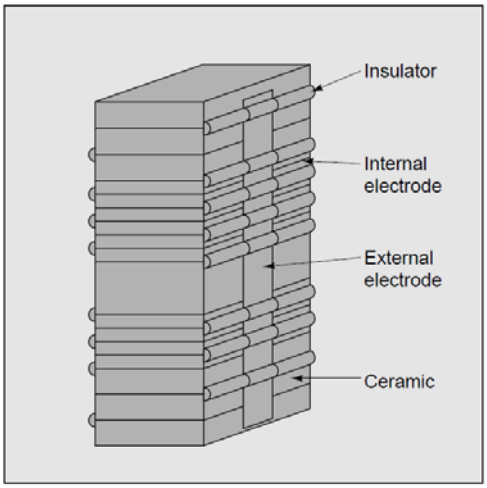

Figure 4.5: Configuration of a multilayer piezoelectric stack (Micromechatronics, 2013).

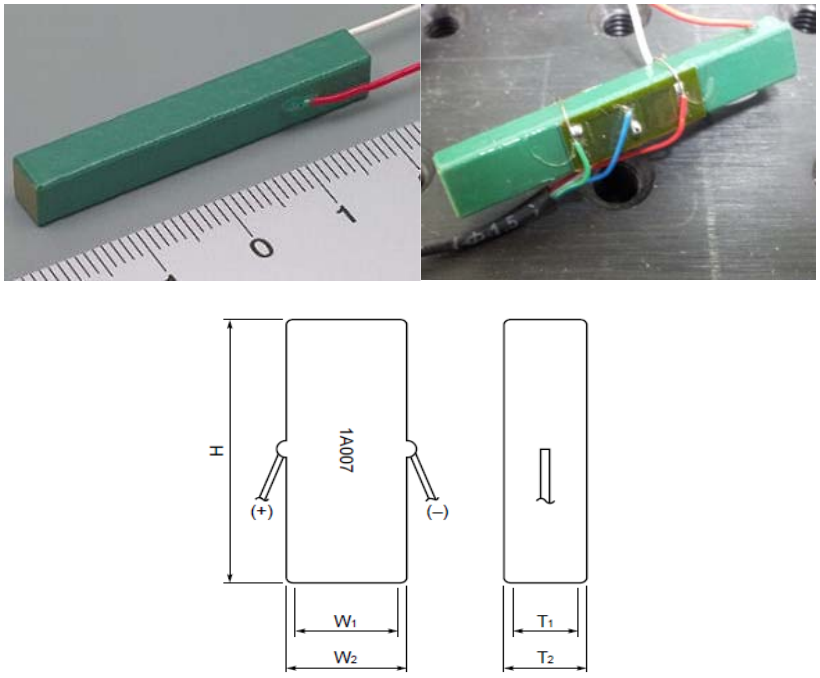

Figure 4.6: Multilayer piezoelectric stacks made by NEC/TOKIN (Micromechatronics, 2013).

In these experiments, the piezoelectric stack is a resin-coated type made at the temperature of 85^0C. Its cross section and length is $5\,mm \times 5\,mm$ and $40\,mm$, respectively. The stack actuator is capable of generating a typical force in the order of 3500 Ncm^{-2} and high speed responses in the order of 10 *kHz*. It has a nominal displacement of 44 μm (Micromechatronics, 2013). The piezoelectric stack is shown in Figure 4.6 and its key characteristics have been summarised in Tables 4.1 and 4.2.

Table 4.1: Standard characteristics of the piezoelectric stack.

Model	*Displacement(μm)*		*Generated force(N)*	*Resonance frequency (kHz)*	*Capacitance (μF)*	*Insulation resistance ($\mu\Omega$) min*	*Overall length (mm)*
	Maximum driving voltage	*Recommended driving voltage*					
AE0505D44H40	42.0 ± 6.6	28.0 ± 6.6	850	34	3.4	5	40

Table 4.2: Outer dimension of the piezoelectric stack. Unit: mm, *l: Length of the lead wire.**

Model	T_1	W_1	H	T_2	W_2	L*
AE0505D44H40	5±0.1	5±0.1	40 ± 0.1	6.5max	6.5max	100

Sensor: An optical sensor is used to measure the displacement of the piezoelectric actuator. A PHILTECH D20 is a fast responding optical sensor ideal to measure relative motions in dynamic applications (PHILTEC, 2013). It measures the actuator displacement using the reflected light from the actuator. The optical sensor and basics of its work are illustrated in Figure 4.7 and the sensor's key features are summarised in Table 4.3.

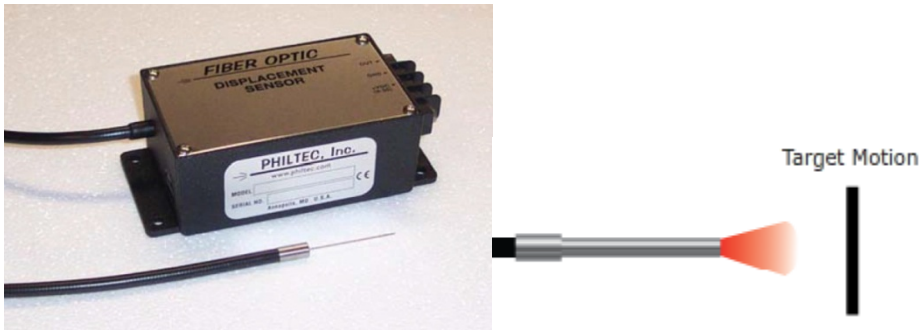

Figure 4.7: Optical sensor and the basics of its work (PHILTEC, 2013).

Table 4.3: Key physical features of the optical sensor.

Model	*Linear range near side(mm)*	*Resolution at 100Hz near side(μm)*	*Linear range far side(mm)*	*Resolution at 100Hz far side(μm)*	*Tip diameter(mm)*	*Total range(mm)*
PHILTECHD20	0.02	0.007	0.25	0.06	0.81	1.3

The excitation voltage, in different experiments, generates sinusoidal and triangular functions of time. For the both functions, three frequencies of 1, 10 and 100 *Hz* were used and the

voltage amplitude was within the range of $\pm 20V$ which are common values in nanopositioning (Wang et al., 2011, Hegewald et al., 2008). Each experiment lasted 2 second. The data gathered through the excitation by the triangular voltage function at a frequency of 10 *Hz* was used for the model validation. The rest of the data was employed for modelling. For more details about the actuator input-output, see Appendix B.

In a system modelling, if the model is trained by the data of different wave form-frequency combinations, e.g. sinusoidal/triangular waves at different frequencies, and it is still valid for the data of any other wave form-frequency combinations (unseen data), the model validity has been demonstrated. This is called cross validation and there is no need to validate the model for every single frequency/magnitude. A great number of works in the modelling of piezoelectric actuators have exploited this strategy (Goldfarb and Celanovic, 1997, Quant et al., 2009, Mohammadzaheri et al., 2012c).

4.2.2. Modelling: Sampling Time and Initial Condition

This section investigates the optimum sampling time for the discrete form of the Voigt model. As explained in Sections 3.1 and 3.2, the Preisach and Duhem models are presented by at least two functions resulting in a relatively high level of complexity to identify their parameters. Moreover, the Maxwell-Slip and Parandtl-Ishlinski model require the data achieved exactly after the relaxed state which are difficult to collect in practice. However, the Voigt model is formed by only five parameters presenting a more straightforward structure. In addition, the literature has shown that this model is reversible and can capture the frequency-dependent behaviour of piezoelectric actuators. It can also offer a wide frequency range of validity (Boukari et al., 2011). Therefore, the Voigt model is employed to model the piezoelectric actuator.

At the first stage, the Voigt model should be discretised. Considering:

$$\dot{y} = \frac{y(k+1) - y(k)}{t_S}, \tag{4.7}$$

and Eq. (3.15), the discrete form of the Voigt model estimating the piezoelectric displacement is:

$$y(k+1) = y(k) + \left(sign(V(k)) \left(\frac{|V(k)|}{b} \right)^{P} - \frac{y(k)}{d(V(k)) \cdot b} \right) \cdot t_S , \tag{4.8}$$

where t_S is the model sampling time. In this case study, the first natural/resonant frequency of the actuator is 34 *kHz* and driving frequencies up to about 1/3×34 *kHz* is possible (Micromechatronics, 2013). Therefore, a dSpace (DS1104 R&D Controller Board) on a PC-compatible computer with a sampling rate of 10 *kHz* was used to generate the digital driving voltage for the actuator, i.e., an experimental sampling rate every $10^{-4}\,s$ (Mohammadzaheri et al., 2012c). In the literature, the range of sampling time for the models of piezoelectric actuator is between $3.3\times10^{-5}\,s$ and $10^{-3}\,s$ (Mohammadzaheri et al., 2012a). To find the optimum sampling time for the current model, the modelling was performed for a few sampling times of larger than $10^{-4}\,s$ and the model error was identified for each of them. Table 4.4 summarises MAEs of the model validation for different sampling times and Figure 4.8 shows these results. Based on these outcomes, a sampling time of 5×10^{-4} s is selected for the model (Miri et al., 2013b).

The OSP model error, explained in Section 4.1.1, and the experimental data, explained in Section 4.2.1, were used during the optimisation/identification process.

Table 4.4: Mean absolute errors (MAEs) of the model simulation for different sampling times.

Sampling time –t_s (s)	10^{-4}	2×10^{-4}	5×10^{-4}	10^{-3}	2×10^{-3}	5×10^{-3}	10^{-2}
MAE(μm)	0.5063	0.6129	0.3811	0.5054	0.6470	0.4777	1.0365

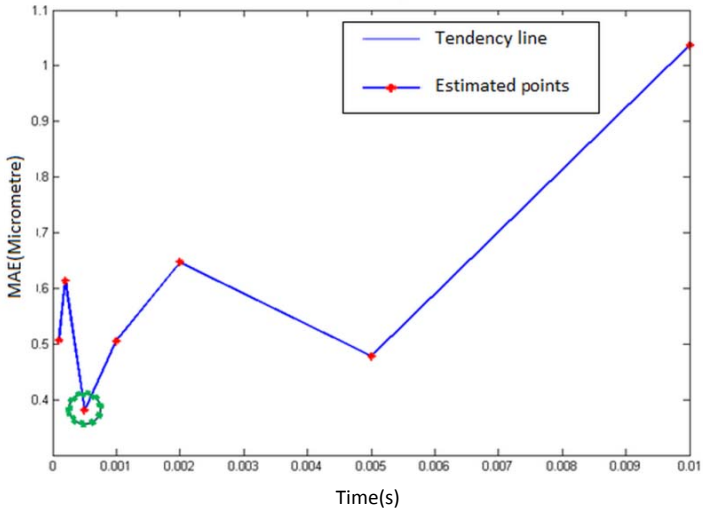

Figure 4.8: Validation errors for different sampling times. The circle refers to the optimum sampling time.

As explained in Section 4.1.2, a range should be defined for each parameter. Considering the literature (Boukari et al., 2011), after trial and error explained in Appendix C, the parameter ranges were defined as seen in Table 4.5. The full ranges and minimum absolute changes for each parameter are listed in this table.

Table 4.5: Parameter ranges and minimum absolute changes (MACs).

Parameters	*Min*	*Max*	*Range*	*MAC*
$\alpha[\mu m]$	100	2500	2400	2.35
$\beta[V]$	200	1000	800	0.78
$\lambda[V^{-1}]$	0.001	0.01	0.009	8.79×10^{-6}
$b[\Omega]$	5000	200000	195000	190.61
P	0.1	1.2	1.1	0.0011

For the model Eq. (4.8), each chromosome has five genes (equal to the number of parameters) and the number of bits for each gene is considered 10. The population is formed by 64 chromosomes. Therefore, each population has 3200 bits.

4.3. Simulation Results and Analysis

The parameters of the model Eq. (4.8) were identified by considering the investigated sampling time in Section 4.2.2. The parameter identification was performed through minimising the model error Eq. (4.1). A set of parameters is the solution when the model error reaches a constant value; meaning that the model error obtains the minimum value through increasing the number of iterations (Miri et al., 2013b).

The model error was obtained through the two approaches detailed in Section 4.1.1, the OSP and Simulation. The identified parameters, which form two models with similar structure, have been listed in Table 4.6.

Table 4.6: Identified model parameters by two different approaches.

Model error approach	*OSP*	*Simulation*
Parameters	$\alpha = 672.434\,\mu m$	$\alpha = 1139.296\,\mu m$
	$\beta = 729.423\,V$	$\beta = 749.755\,V$
	$\lambda = 0.00725\,V^{-1}$	$\lambda = 0.00772\,V^{-1}$
	$b = 95923.754\,\Omega$	$b = 90777.126\,\Omega$
	$P = 0.742$	$P = 0.754$

The parameters of Table 4.6 have physical interpretations and find the equivalent SI units. As explained in Section 3.2.3, α, λ, β construct *d(V)* corresponding to the system piezoelectric capacitance, piezoelectric coefficient. Moreover, *b* corresponds to the piezoelectric losses. *d(V)* and *b* are analogous with the spring and damper of the Voigt unit, respectively (Boukari et al., 2011).

Having identified the model parameters, the model Eq. (4.8) can be readily constructed and validated for other inputs. To assess the predictive quality of the new models, each is validated by 'unseen data' in the identification process. The validation errors of both models are presented in Table 4.7.

Table 4.7: Modelling and validation errors for the models made by two different approaches.

No	*Model error approach*	*OSP*	*Simulation*
	Error indicator	***MAE***	***MAE***
1	***Modelling error value (μm)***	0.3258	0.4993
	Iteration (#)	88th	356th
2	***Model validation error value (μm)***	0.3324	0.3357
	Iteration (#)	185th	360th

According to Table 4.7, the minimum modelling error for the two models happened in the 88th and 356th iteration number, respectively (MAE=0.3258 μm and MAE=0.4993 μm) whereas the minimum validation error for these models occurred in the 185th and 360th iteration number (MAE=0.3324 μm and MAE=0.3357 μm). Therefore, for both approaches, the minimum validation error happened later than the minimum modelling error, as shown in Figures 4.9 and 4.10. Larger iteration number for the 'minimum validation error' than

'minimum modelling error' shows that no over-fitting has occurred in the computations. Hence, the parameter tuning has been performed appropriately.

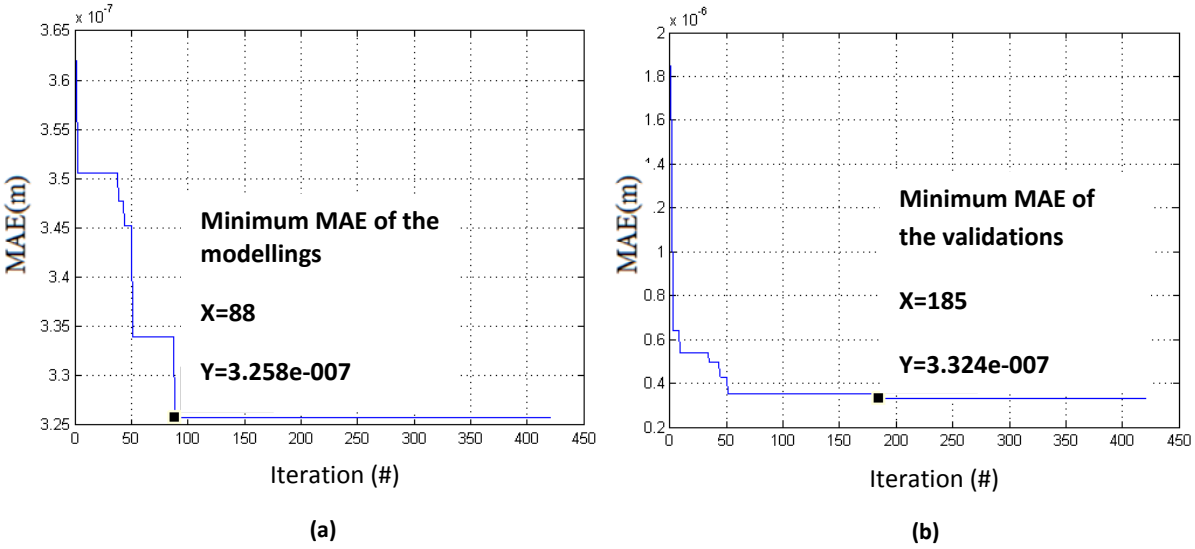

Figure 4.9: MAEs versus iteration for the (a) modelling (OSP approach) and (b) model validation.

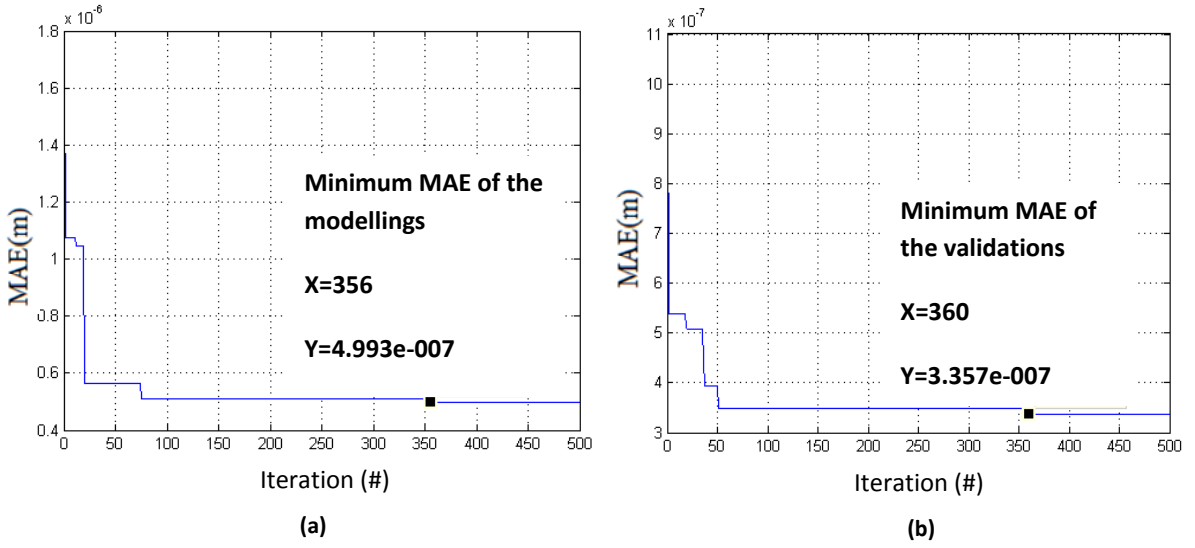

Figure 4.10: MAEs versus iteration for the (a) modelling (Simulation approach) and (b) model validation.

Table 4.8 brings forward two representatives for the model error: the mean of the absolute error (MAE) and the maximum of the absolute error (MAX).

Table 4.8: Validation errors for the models made by two different approaches.

Minimised model error	*OSP*		*Simulation*	
Error Indicator	***MAE***	***MAX***	***MAE***	***MAX***
Error value (μm)	0.3324	0.9937	0.3357	0.9313

As seen in Table 4.8, there is not a meaningful difference between the modelling approaches; both the OSP and Simulation approaches result in models with rather similar accuracies. As the OSP approach is also less computationally demanding, it is recommended for modelling in similar research works.

The estimated displacement by the models identified through both approaches is shown in Figure 4.11. In this figure, the measured and simulated displacements through the model Eq. (4.8) are graphed using bold dashed and solid lines. The error for each model is demonstrated by narrow dashed lines.

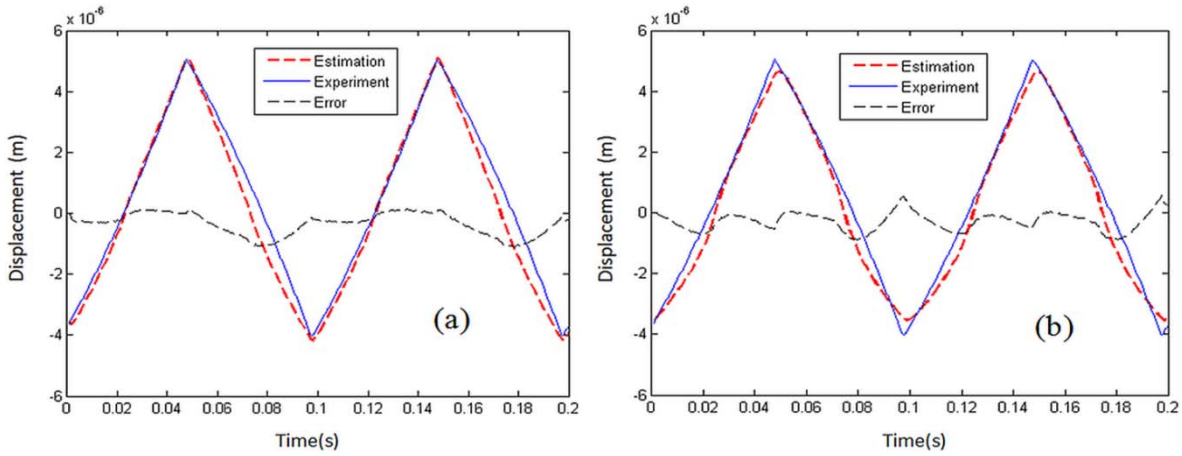

Figure 4.11: Real and estimated displacement values of the piezoelectric actuator made through Eq. (4.8) (Parameter tuning by the GA with minimal model error achieved through the (a) OSP and (b) Simulation approaches.)

4.4. Summary

The central innovation of this chapter was introducing a global method for the most challenging task for physics-based models of piezoelectric actuators: parameter identification. The parameters of physics-based models are normally identified using the experimental data

presenting an *ad-hoc* solution to a particular problem. This task was tackled in this chapter by establishing a standard and global approach based on a GA. In the introduced method, parameter identification was defined as the process of fine-tunning the model parameters so as to minimise the model error. Therefore, the parameter identification problem was converted to an optimisation problem. Two models were made, by minimising the model errors obtained through the 'One-Step-Prediction' and 'Simulation' approaches: both led to rather similar accuracies.

From the range of physics-based models, the Voigt model was opted due to its rather simple structure and small number of parameters compared with other physics-based models, as well as its other reported advantages.

An important factor not raised in this chapter is the model improvement through structural enhancement. In the literature, improving black box models by adding complementary inputs has been shown to increase the model accuracy. Similarly, adopting an enhanced structure for physics-based models may increase the model accuracy. This is investigated in the next chapter.

Overall, this chapter employed a standard, optimal and global algorithm that successfully identified the parameters of a physics-based model.

NOTE:

This page is intentionally left blank.

Chapter 5 - Structural Enhancement for Physics-based Models

In Chapter 5, an enhanced model is presented to model piezoelectric actuators. The enhanced model is the modified Voigt model inspired by the Preisach model. Moreover, the enhanced model has new terms integrating new inputs into the model. The new terms consist of four parameters. All parameters are defined through the global optimisation method introduced in Chapter 4.

5.1. Model Structure

One of the primary challenges for physics-based models of piezoelectric actuators is the rather low accuracy of the models, partially due to inadequate mathematical structure of the models (Sjöberg et al., 1995, Richter et al., 2001). Accordingly, as stated in Section 3.3, introducing new inputs to the model would be a novel approach to improve the model performance (Donoso-Bravo et al., 2011).

5.1.1. Preisach Model

According to Eq. (3.4) and Eq. (3.5) of the Preisach model, the last extremum value of the input [$V_{ext} = (V_{\min})$ or $(V_{\max})$] and its corresponding output [$y_{ext} = (y_{\min})$ or $(y_{\max})$] are used to estimate the current output $y(t)$ of the piezoelectric actuator. Therefore, the original Preisach model can be defined as:

$$y(t) = f\left(V(t), V_{ext}, y_{ext}\right), \tag{5.1}$$

where *ext* stands for the extremum values of either voltage or displacement (Miri et al., 2013a). This means that in the Preisach model, the model input includes the extremum values of the voltage and displacement of the actuator. In summary, the Preisach model inspires the approach of adding complementary inputs, including extremum values of the voltage/displacement, to other models to improve their accuracies.

5.1.2. Modified Black Box Models

The structure of the Preisach model inspired introducing new inputs to black box models. In these models, the extremum values of the system input/output were used as the model inputs (Mohammadzaheri et al., 2012a). There are different categories of these models such as: 1) Preisach-like static models (Yang et al., 2008), 2) Preisach-like dynamic models (Zhang and Xu, 2011) and 3) System identification-based models (Dong et al., 2008).

In the first category, in addition to the voltage, the extremum values of the voltage and displacement are the inputs to the black box model. This approach, inspired by Eq. (5.1), was initially introduced to model the materials' behaviour in magnetic fields (Makaveev et al., 2001, Sixdenier et al., 2008, Makaveev et al., 2002). Then, the approach was employed in black box models to model piezoelectric actuators (Mohammadzaheri et al., 2012b). In the second category, temporal derivatives and the output/input gradient are used as the inputs to the black box model but not in the form of universal approximators used in classical system identification. In contrast with the previous models, these models are dynamic. In the third category, the classical universal approximators are used as black box models with some additional inputs. For instance, the input voltage, input voltage rate and displacement gradients are the inputs to the black box models (Khan and Lagoudas, 2002). However, derivative and gradient-based inputs are not applicable at a practical level because of their sensitivity to the measurement noise. Therefore, Mohammadzaheri et al. (2012) used the first approach to improve black box models of piezoelectric actuators (Mohammadzaheri et al., 2012a). The results for this approach are shown in Table 5.1. In this table, the model has been validated by two validation approaches: the Simulation and OSP (see Section 4.1.1 for more explanation about these approaches) for three different output orders r_y. The first, second and third columns contain the model validation error respectively for the black box models, 'black box models including extremum values of the voltage' and, 'black box models including extremum values of the voltage and displacement'. Furthermore, they used Classical Nonlinear Auto-Regressive models with eXogenous inputs (NARX models) as the black box technique. As Table 5.1 shows, the model error decreases significantly when the extremum values of the voltage/displacement are introduced to the model. Overall, the result of introducing the new inputs to the black box models demonstrated a significant improvement in the models accuracies.

Table 5.1: Validation errors for the enhanced black box model.

Error	*Without extrema (μm)*	*With vext (μm)*	*With both vext & yext (μm)*
	Simulation/OSP	***Simulation/OSP***	***Simulation/OSP***
ry=1	2.2227/0.0837	0.2184/0.0222	0.2421/0.0290
ry=2	8.0331/0.0339	0.1145/0.0185	0.1866/0.0292
ry=3	1.2911/0.0362	0.1747/0.0194	0.1025/0.0259

Note: For all validation errors shown in Table 5.1, the simulation error is more than the OSP's due to error accumulation developed in the model error estimation through the Simulation approach (Mohammadzaheri et al., 2012a).

5.1.3. Enhanced Physics-based Models

The structure of the Preisach model, Eq. (5.1), inspires the enhancement for physics-based models by adding complementary terms/inputs to the models, similar to the modification for black box models explained in Section 5.1.2. To this purpose, the Voigt model, Eq. (4.8), is considered to be improved. Therefore, the new introduced model is presented as:

$$\dot{y} + \frac{y}{d(V)\cdot b} = \mathrm{sgn}(V)\cdot\left(\frac{|V|}{b}\right)^{P} + g\cdot\mathrm{sgn}(V)\cdot|V_{ext}|^{h} + e\cdot\mathrm{sgn}(y_{ext})\cdot|y_{ext}|^{f}. \tag{5.2}$$

In the discrete domain, Eq. (5.2) is written as:

$$y(k+1) = y(k) + \left(\mathrm{sgn}(V(k))\cdot\left(\frac{|V(k)|}{b}\right)^{P} - \frac{y(k)}{d(V(k))\cdot b} + g\cdot\mathrm{sgn}(V_{ext})\cdot|V_{ext}|^{h} + e.\cdot\mathrm{sgn}(y_{ext})\cdot|y_{ext}|^{f}\right)\cdot t_S. \tag{5.3}$$

where *g, h, e* and *f* are the model parameters presenting the contribution of the extremum values of the piezoelectric voltage and displacement in the model.

In short, the Voigt model is enhanced by adding terms containing extremum values of the displacement and voltage. This new model has nine independent parameters, five parameters of the Voigt model and four parameters of the extremum terms. To identify the parameters of this model, the same strategy of parameter identification presented in Chapter 4 is employed. This strategy is the global optimisation method by a GA.

Two reduced versions of the introduced model, only using the extremum of the piezoelectric voltage or displacement, are also presented in this thesis:

$$y(k+1) = y(k) + \left(\operatorname{sgn}(V(k)) \cdot \left(\frac{|V(k)|}{b} \right)^{P} - \frac{y(k)}{d(V(k)) \cdot b} + g \cdot \operatorname{sgn}(V_{ext}) \cdot |V_{ext}|^{h} \right) \cdot t_S . \tag{5.4}$$

$$y(k+1) = y(k) + \left(\operatorname{sgn}(V(k)) \cdot \left(\frac{|V(k)|}{b} \right)^{P} - \frac{y(k)}{d(V(k)) \cdot b} + e.\operatorname{sgn}(y_{ext}) \cdot |y_{ext}|^{f} \right) \cdot t_S . \tag{5.5}$$

In Eq. (5.4), the extremum values of the voltage are used as the model input; while in Eq. (5.5), the extremum values of the piezoelectric displacement are used as the model input. In both models, numbers of parameters is seven, requiring identification.

5.2. Simulation Results and Analysis

The parameters of three versions of the introduced model were identified based on minimising the model error obtained through the two approaches explained in Section 4.1.1: the OSP and Simulation. These parameters are shown in Table 5.2.

Table 5.2: Identified parameters for three versions of the new model made by two different approaches.

Model	*Eq. (5.4)*	*Eq. (5.5)*	*Eq. (5.3)*
OSP	$\alpha = 2414135 \mu m$ $\beta = 676.810\ V$ $\lambda = 0.00805\ V^{-1}$ $b = 31272727\ \Omega$ $P = 0.863$ $g = 14.21\ \Omega^{-1}$ $h = 0.628$	$\alpha = 2260.405\ \mu m$ $\beta = 863.929\ V$ $\lambda = 0.00622\ V^{-1}$ $b = 68909.09\ \Omega$ $P = 0.8445$ $e = 250.825 V\ \mu m^{-1}\Omega^{-1}$ $f = 1.252$	$\alpha = 1770.343\ \mu m$ $\beta = 563.636\ V$ $\lambda = 0.00950\ V^{-1}$ $b = 109511.730\ \Omega$ $P = 0.872$ $g = 60.428 \Omega^{-1}$ $h = 0.582$ $e = 736.694 V\ \mu m^{-1}\Omega^{-1}$ $f = 1.222$
Simulation	$\alpha = 2392473 \mu m$ $\beta = 672.336\ V$ $\lambda = 0.00959 V^{-1}$ $b = 88140762\ \Omega$ $P = 0.783$ $g = 61.69\ \Omega^{-1}$ $h = 0.061$	$\alpha = 1150.947\ \mu m$ $\beta = 958.553\ V$ $\lambda = 0.00600\ V^{-1}$ $b = 98211.144\ \Omega$ $P = 0.732$ $e = 449.560 V\ \mu m^{-1}\Omega^{-1}$ $f = 1.631$	$\alpha = 1790.724\ \mu m$ $\beta = 664.516\ V$ $\lambda = 0.00974\ V^{-1}$ $b = 130278.592\ \Omega$ $P = 0.763$ $g = 23.710\ \Omega^{-1}$ $h = 0.920$ $e = 525.753 V\ \mu m^{-1}\Omega^{-1}$ $f = 1.166$

Accuracy of the new model is verified by validating the model for arbitrary inputs. The validation errors for these models are presented in Tables 5.3 and 5.4. These tables present the two representatives of the model error: the mean of absolute error (MAE) and the maximum of absolute error (*MAX*).

Table 5.3: Validation errors for three models made by the OSP approach.

Model Structure	*Eq. (5.4)*		*Eq. (5.5)*		*Eq. (5.3)*	
Error Indicator	*MAE*	*MAX*	*MAE*	*MAX*	*MAE*	*MAX*
Error value (μm)	0.299	1.02	0.381	0.778	0.163	0.586

Table 5.4: Validation errors for three models made by the Simulation approach.

Model Structure	*Eq. (5.4)*		*Eq. (5.5)*		*Eq. (5.3)*	
Error Indicator	*MAE*	*MAX*	*MAE*	*MAE*	*MAE*	*MAX*
Error value (μm)	0.294	0.973	0.365	1.041	0.252	0.804

Table 5.5: Validation errors for the Voigt model made by the two approaches.

Minimized model error	*OSP*		*Simulation*	
Error Indicator	***MAE***	***MAX***	***MAE***	***MAX***
Error value(μm)	0.3324	0.9937	0.3357	0.9313

As seen in Table 5.3, the model Eq. (5.4) offers the best accuracy of the estimations while according to Table 5.5, the Voigt model resulted in the minimum MAE of 0.3324 μm . The model Eq. (5.4) decreases the estimation error to 0.299 μm implying that introducing extremum values of the voltage, in the form of the new terms, to the Voigt model boosts the model accuracy. However, the influence of adding extremum terms of the displacement, as presented by Eq. (5.5), did not meaningfully increase the accuracy, as shown in Tables 5.3 and 5.4, probably due to the displacement measurement noises. Nonetheless, the estimation accuracy increased considerably by adding the both terms including the extrema; as presented in the last columns of Tables 5.3 and 5.4. The estimated displacement through the enhanced model Eq. (5.3) showed a significant improvement for the model accuracy compared with the Voigt model. This accuracy is comparable with similar studies using black box models (Mohammadzaheri et al., 2012a).

Furthermore, the comparison between Table 5.3 and 5.4, i.e. Eq. (5.4) and Eq. (5.5), shows that there is not a meaningful difference between the two introduced modelling approaches: both OSP and Simulation approaches resulted in models with rather similar accuracies. However according to Tables 5.3 and 5.4, the model Eq. (5.3) made through the OSP approach shows the highest accuracy among the presented models. As the OSP approach is also less computationally demanding, it is recommended for modelling in similar research work.

Real and estimated displacement values of the piezoelectric actuators, generated through three different models, are illustrated in Figures (5.1)-(5.6). In these figures, the measured and simulated displacements made through the models are graphed using bold dashed and solid lines, respectively. The validation error for each model is demonstrated by narrow dashed lines.

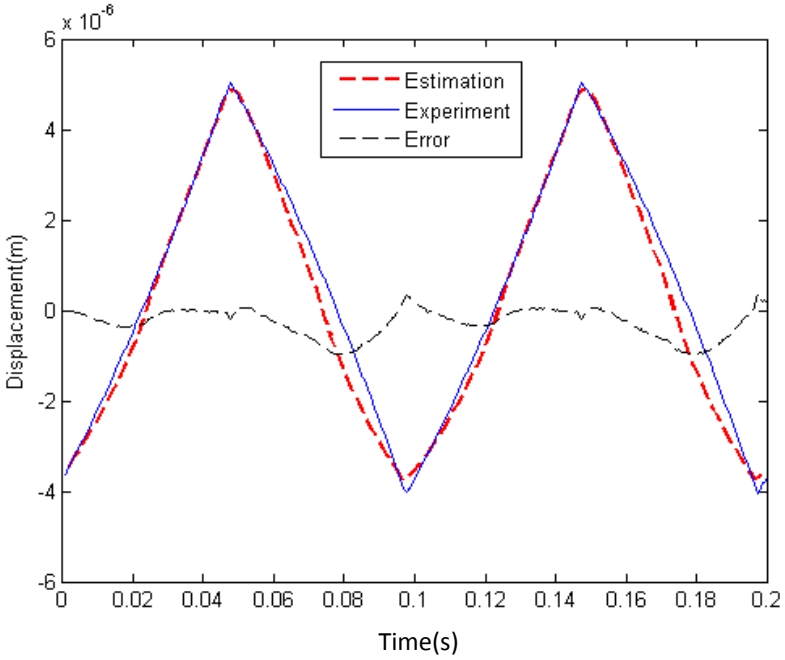

Figure 5.1: Real and estimated displacement values of the piezoelectric actuator made through Eq. (5.4) (Parameter tuning by the GA with minimal model error achieved through the OSP approach).

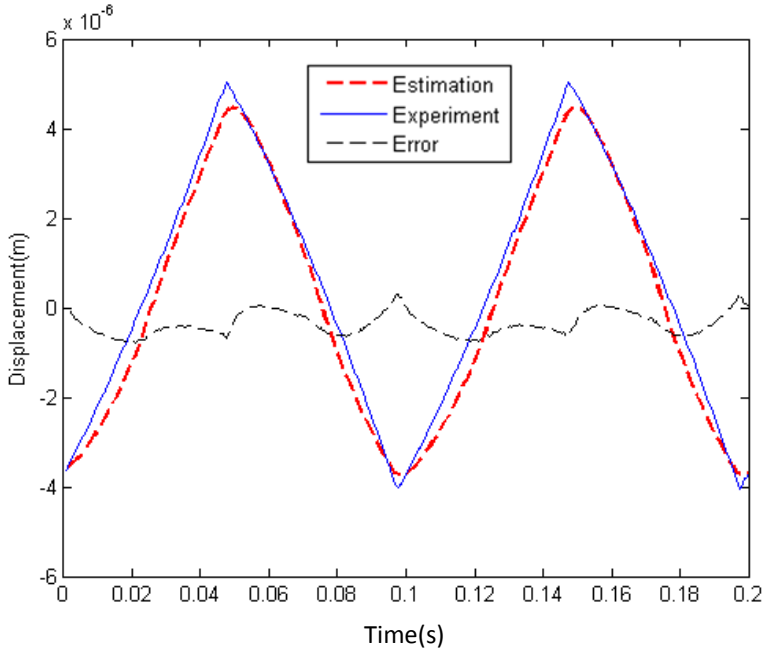

Figure 5.2: Real and estimated displacement values of the piezoelectric actuator made by Eq. (5.5) (Parameter tuning by the GA with minimal model error achieved through the OSP approach).

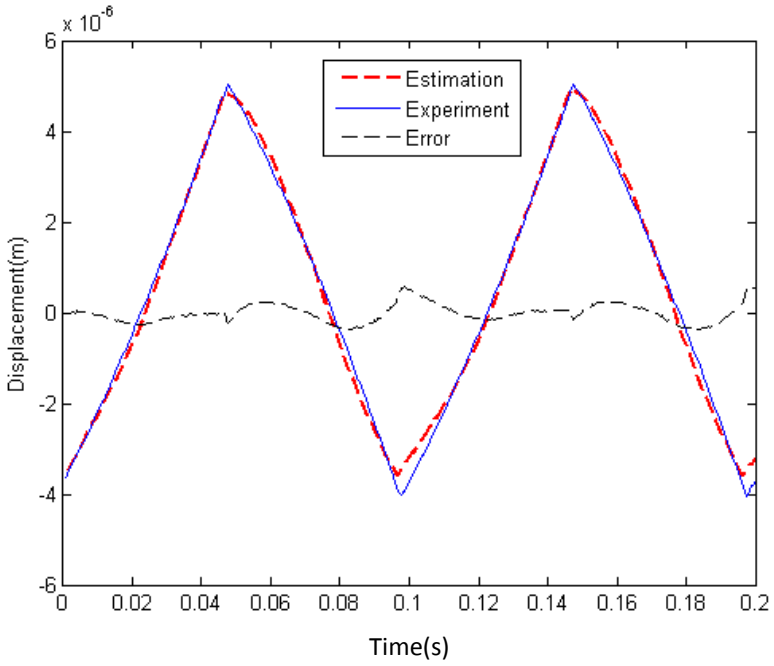

Figure 5.3: Real and estimated displacement values of the piezoelectric actuator made by Eq. (5.3) (Parameter tuning by the GA with minimal model error achieved through the OSP approach).

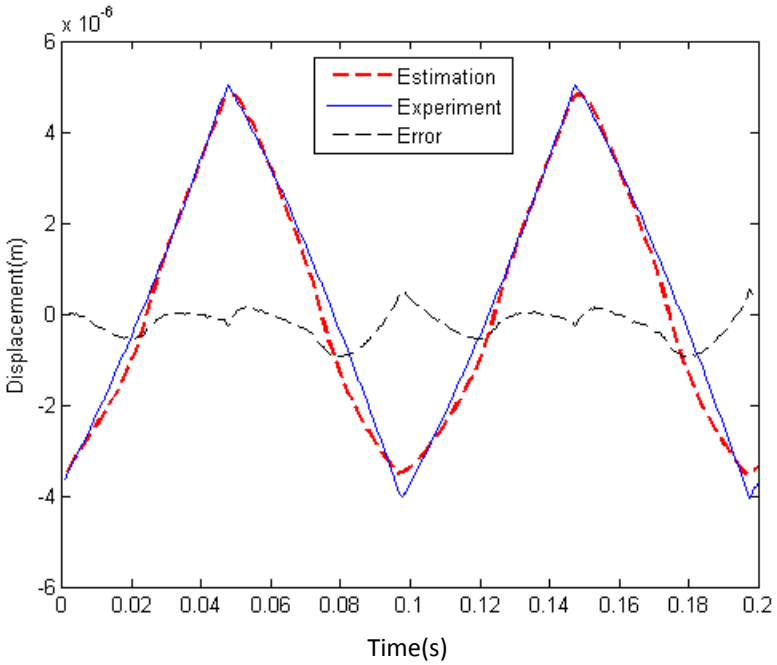

Figure 5.4: Real and estimated displacement values of the piezoelectric actuator made by Eq. (5.4) (Parameter tuning by the GA with minimal model error achieved through the Simulation approach).

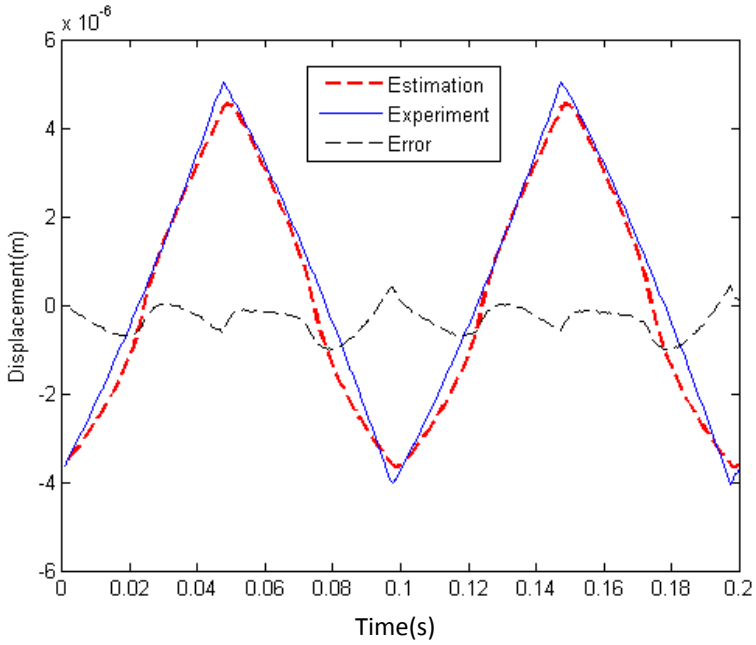

Figure 5.5: Real and estimated displacement values of the piezoelectric actuator made by Eq. (5.5) (Parameter tuning by the GA with minimal model error achieved through the Simulation approach).

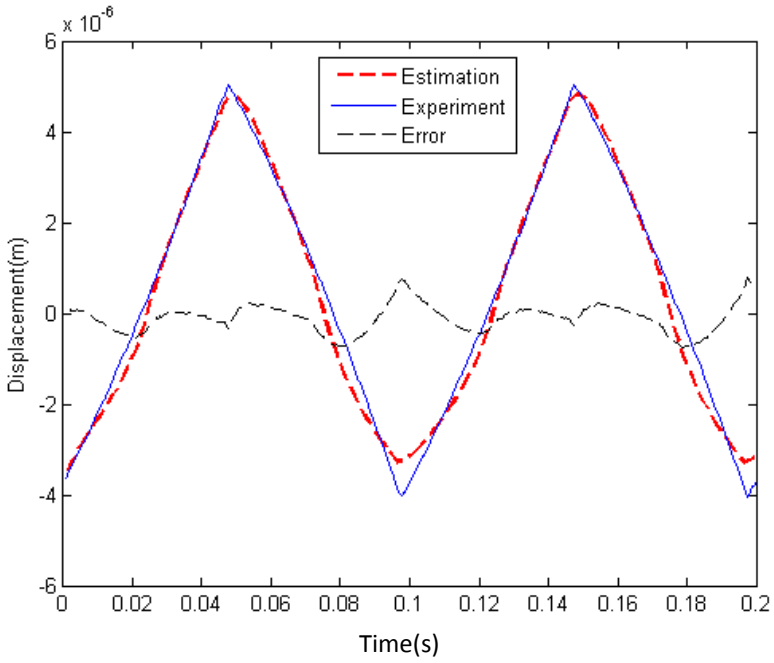

Figure 5.6: Real and estimated displacement values of the piezoelectric actuator made by Eq. (5.3) (Parameter tuning by the GA with minimal model error achieved through the Simulation approach).

5.3. Summary

In this chapter, improving the accuracy for a physics-based model of piezoelectric actuators was addressed. The model performance was enhanced through improving the sufficiency of the mathematical structure of the model, by modifying the model structure. The structural modification was performed by adding two terms, including four new parameters, inspired by another physics-based model. The new structure has a total of nine parameters. Subsequently, the parameters were identified through the optimisation method using a GA.

The models' errors were minimised through two approaches: 'One-Step-Prediction' and 'Simulation'. Both approaches and the new structure were assessed appropriately.

Modification of black box models by adding new inputs has been proven to increase the model accuracy. However, physics-based models are popular due to physically interpretable and a small number of parameters. Accordingly, this chapter aimed to enhance physics-based models. The enhanced model, on a rather similar basis with the black box models, doubled the estimation accuracy.

Chapter 6 - Conclusions and Future Work

Chapter 6 provides an overview of the research undertaken in this thesis, and it summarises the conclusions arising from the thesis. It also makes some suggestions for future research.

6.1. Conclusions

This thesis focused on pursuing physics-based and control-oriented models for piezoelectric actuators. The literature shows that an accurate model would be a valuable tool for the control of various nano-materials, design of nanopositioning and nano-manufacturing systems. Accordingly the aim of this research was to improve the models of piezoelectric actuators to develop accurate sensorless control systems for the actuators positioning. Such a model can eliminate limited applicable and/or expensive sensors from the control system. The model improvement was fulfilled through developing a global parameter identification method for the models and presenting an enhanced performance model.

The research was commenced with a literature review of various physics-based models of piezoelectric actuators. Each model was presented with its own specific advantages and limitations. The models are supposed to estimate the displacement of piezoelectric actuators using the voltage across the actuator; the closer the estimated displacement to the experimental displacement, the more accurate the model.

Current methods of parameter identification for physics-based models are not general or optimal treatments and they are solutions for particular problems. In this research, an optimal and global method is developed to identify the models' parameters (or, in general, modelling) using a GA. Consequently, parameter identification was defined as the process of identifying the model parameters so as to minimise the 'model error'.

An inadequate mathematical structure of the models was a reason for the relatively low accuracy of physics-based models due to the lack of any proof for their optimality. Therefore, in order to improve the models' accuracy, a model structure was modified by introducing two complementary terms inspired by the Preisach model. The new model contained nine parameters requiring identification.

From the range of physics-based models, the Voigt model was opted for this research due to its small number of parameters and other reported advantages. Under laboratory condition, the electrical voltage is applied to piezoelectric actuators and the displacements of the actuators are recorded.

In this research, the average absolute discrepancy for the estimated displacement by the model and real displacement was called the model error. Consequently, the model error was defined by the 'OSP' and 'Simulation' approaches. In each step of the calculations, the OSP approach uses the 'real' displacement of the previous step to estimate the current displacement while the Simulation approach employs the 'estimated' displacement of the previous step. According to the previous models of dynamic systems, the model error through the Simulation approach was higher than the OSP's due to the phenomenon of error accumulation in the Simulation approach. However, this research demonstrated that both approaches of minimising the model error resulted in almost the same model accuracy. Hence, it is recommended to employ the OSP approach for other similar research work as it is less computationally demanding.

Finally, high agreement between the measurements and simulations highlighted the appropriateness/sufficiency of the enhanced model. The proposed enhanced Voigt model presented significantly higher accuracy than the conventional Voigt model. The enhanced model's accuracy is also comparable with the accuracy of the black box models. In the literature, the enhanced black box models have been reported for the same actuator/modelling and validation data while they have around 25 times larger the number of parameters than the proposed physics-based model. This may result in the superiority of physics-based models over black box models.

6.2. Future Work

This research demonstrated that the model accuracy increases through the structural modification including adding extremum values of the actuator's voltage/displacement. Furthermore, the parameters of the models were identified through a global optimisation method. The presented ideas can be extended to other physics-based models of piezoelectric actuators or to other nonlinear systems.

The following suggestions are recommended for further research on the modelling of piezoelectric actuators in the future:

- Introducing complementary terms; including extremum values of the voltage/displacement, to the other physics-based models.
- Introducing complementary terms with higher orders (considering a greater number of the previous input/output) to the models.
- Assessing the reversibility of the enhanced model, the model ability to predict the induced voltage by loading the piezoelectric actuator, i.e. sensoriactuator model.
- Assessing the proposed model for nonlinear systems including other configurations of piezoelectric actuators such as piezoelectric tube.
- The global method of parameter identification may be further investigated and implemented for other physics-based models of piezoelectric actuators.
- Other global methods of parameter identification (e.g. Particle Swarm Optimisation or PSO) may be assessed for the models of piezoelectric actuators and their complexity level may be compared with the employed optimisation method.
- At this research, the model hasn't taken into account any load/temperature effect. Therefore, assessing the impact of force and/or temperature loading on the improved model could be performed in future.
- Assessing the effect of a weighted or exponentially weighted feedback to reduce the effect of 'error accumulation' phenomenon obtained through 'simulation' modelling approach.

NOTE:

This page is intentionally left blank.

References

ABRAMOVITCH, D. Y., ANDERSSON, S. B., PAO, L. Y. & SCHITTER, G. A tutorial on the mechanisms, dynamics, and control of atomic force microscopes. American Control Conference, 2007. IEEE, 3488-3502.

ADHIKARI, S. & WOODHOUSE, J. 2001. Identification of damping: part 1, viscous damping. *Journal of Sound and Vibration,* 243**,** 43-61.

ADRIAENS, H., DE KONING, W. & BANNING, R. 2000. Modeling piezoelectric actuators. *Mechatronics, IEEE/ASME Transactions on,* 5**,** 331-341.

AL JANAIDEH, M., CHUN-YI, S. & RAKHEJA, S. 2008. Development of the rate-dependent Prandtl-Ishlinskii model for smart actuators. *Smart Materials and Structures,* 17**,** 1-11.

AL JANAIDEH, M., RAKHEJA, S. & SU, C.-Y. 2011. An analytical generalized Prandtl–Ishlinskii model inversion for hysteresis compensation in micropositioning control. *IEEE/ASME Transactions on Mechatronics,* 16**,** 734-744.

ANG, W. T., KHOSLA, P. K. & RIVIERE, C. N. 2007. Feedforward controller with inverse rate-dependent model for piezoelectric actuators in trajectory-tracking applications. *Mechatronics, IEEE/ASME Transactions on,* 12**,** 134-142.

APHALE, S., FLEMING, A. & MOHEIMANI, S. 2007. High speed nano-scale positioning using a piezoelectric tube actuator with active shunt control. *Micro & Nano Letters, IET,* 2**,** 9-12.

BAZ, A. & POH, S. 1988. Performance of an active control system with piezoelectric actuators. *Journal of sound and vibration,* 126**,** 327-343.

BAZGHALEH, M., MOHAMMADZAHERI, M., GRAINGER, S., CAZZOLATO, B. & LU, T. F. 2013. A new hybrid method for sensorless control of piezoelectric actuators. *Sensors and Actuators A: Physical*.

BINNIG, G., QUATE, C. F. & GERBER, C. 1986. Atomic force microscope. *Physical review letters,* 56**,** 930-933.

BLACKWOOD, G. H. & EALEY, M. A. 1993. Electrostrictive behavior in lead magnesium niobate (PMN) actuators. I. Materials perspective. *Smart Materials and Structures,* 2**,** 124.

BOUKARI, A. 2010. *Piezoelectric actuators modeling for complex systems control.* Phd thesis, Arts et Métiers ParisTech, France.

BOUKARI, A. F., CARMONA, J. C., MORARU, G., MALBURET, F., CHAABA, A. & DOUIMI, M. 2011. Piezo-actuators modeling for smart applications. *Mechatronics,* 21**,** 339-349.

CAO, Y. & WU, Q. 1999. Teaching genetic algorithm using MATLAB. *International journal of electrical engineering education,* 36**,** 139-153.

CHANG, L., ZHOU, H., CHEN, L.-L., XIONG, X.-Z. & LIAO, C. 2013. The fine-grained parallel micro-genetic algorithm and its application to broadband conical corrugated-horn antenna. *Progress In Electromagnetics Research,* 138**,** 599-611.

CHEN, Z. & TAN, X. 2008. A Control-Oriented and Physics-Based Model for Ionic Polymer--Metal Composite Actuators. *IEEE/ASME Transactions on Mechatronics,* 13**,** 519-529.

CHIPPERFIELD, A. & FLEMING, P. 1995a. The MATLAB genetic algorithm toolbox. *Applied Control Techniques Using MATLAB, IEE Colloquium on.* IET.

CHIPPERFIELD, A. J. & FLEMING, P. J. 1995b. The MATLAB genetic algorithm toolbox. *IEE Colloquium on Applied Control Techniques Using MATLAB, ,* 10/1-10/4.

CHOPRA, I. 2002. Review of state of art of smart structures and integrated systems. *Aiaa Journal,* 40**,** 2145-2187.

COCA, D. & BILLINGS, S. 2001. Non-linear system identification using wavelet multiresolution models. *International Journal of Control,* 74**,** 1718-1736.

COELLO, C. A. C. & LAMONT, G. B. 2004. *Applications of multi-objective evolutionary algorithms*, World Scientific.

COLEMAN, B. D. & HODGDON, M. L. 1987. On a class of constitutive relations for ferromagnetic hysteresis. *Archive for Rational Mechanics and analysis,* 99**,** 375-396.

CROFT, D., SHEDD, G. & DEVASIA, S. Creep, hysteresis, and vibration compensation for piezoactuators: atomic force microscopy application. Proceedings of the American Control Conference 2000. 2123-2128.

DAHL, P. R. 1977. Measurement of solid friction parameters of ball bearings. DTIC Document.

DELLA TORRE, E., OTI, J. & KADAR, G. 1990. Preisach modeling and reversible magnetization. *IEEE Transactions on Magnetics,* 26**,** 3052-3058.

DENG, L. & TAN, Y. 2009. Modeling hysteresis in piezoelectric actuators using NARMAX models. *Sensors and Actuators A: Physical,* 149**,** 106-112.

DENG, M., JIANG, C., INOUE, A. & SU, C. Y. 2011. Operator-based robust control for nonlinear systems with Prandtl–Ishlinskii hysteresis. *International Journal of Systems Science,* 42**,** 643-652.

DEVOE, D. L. & PISANO, A. P. 1997. Modeling and optimal design of piezoelectric cantilever microactuators. *Journal of Microelectromechanical Systems* 6**,** 266-270.

DONG, R., TAN, Y., CHEN, H. & XIE, Y. 2008. A neural networks based model for rate-dependent hysteresis for piezoceramic actuators. *Sensors and Actuators A: Physical,* 143**,** 370-376.

DONOSO-BRAVO, A., MAILIER, J., MARTIN, C., RODRÍGUEZ, J., ACEVES-LARA, C. A. & WOUWER, A. V. 2011. Model selection, identification and validation in anaerobic digestion: A review. *Water Research,* 45**,** 5347-5364.

EATON, P. J. & WEST, P. 2010. *Atomic force microscopy*, Oxford University Press New York.

FAIRBAIRN, M. W., MOHEIMANI, S. O. R. & FLEMING, A. J. 2011. Q control of an atomic force microscope microcantilever: A sensorless approach. *Journal of Microelectromechanical Systems,* 20**,** 1372-1381.

FARSANGI, M. A. A. & SAIDI, A. 2012. Levy type solution for free vibration analysis of functionally graded rectangular plates with piezoelectric layers. *Smart Materials and Structures,* 21**,** 094017.

FIGUEIREDO, M. A., NOWAK, R. D. & WRIGHT, S. J. 2007. Gradient projection for sparse reconstruction: Application to compressed sensing and other inverse problems. *Selected Topics in Signal Processing, IEEE Journal of,* 1**,** 586-597.

FONTANA, R. E. 1995. Process complexity of magnetoresistive sensors: a review. *IEEE Transactions on Magnetics,* 31**,** 2579-2584.

FRASER, A. S. 1960. Simulation of genetic systems by automatic digital computers VI. epistasis. *Australian Journal of Biological Sciences,* 13**,** 150-162.

GEORGIOU, H. & BEN MRAD, R. 2006. Electromechanical modeling of piezoceramic actuators for dynamic loading applications. *Journal of dynamic systems, measurement, and control,* 128**,** 558-567.

GOLDFARB, M. & CELANOVIC, N. 1997. A lumped parameter electromechanical model for. *Journal of dynamic systems, measurement, and control,* 119**,** 479.

GUILLON, O., THIÉBAUD, F., DELOBELLE, P. & PERREUX, D. 2004. Compressive creep of PZT ceramics: experiments and modelling. *Journal of the European Ceramic Society,* 24**,** 2547-2552.

GUTELL, R. R. & JANSEN, R. K. 2006. Genetic algorithm approaches for the phylogenetic analysis of large biological sequence datasets under the maximum likelihood criterion.

HAGOOD, N. W. & VON FLOTOW, A. 1991. Damping of structural vibrations with piezoelectric materials and passive electrical networks. *Journal of sound and vibration,* 146**,** 243-268.

HALIM, D. & REZA MOHEIMANI, S. 2003. An optimization approach to optimal placement of collocated piezoelectric actuators and sensors on a thin plate. *Mechatronics,* 13**,** 27-47.

HAN, J. H., CHO, K. D., YOUN, S. H. & LEE, I. 1999. Vibration and actuation characteristics of composite structures with a bonded piezo-ceramic actuator. *Smart Materials and Structures,* 8**,** 136.

HASSANI, V. & TJAHJOWIDODO, T. Integrated Rate and Inertial dependent Prandtl-Ishlinskii model for piezoelectric actuator. 2nd International Conference on Instrumentation Control and Automation (ICA), , 2011. IEEE, , 35-40.

HAUPT, R. L. & HAUPT, S. E. 1998. The binary genetic algorithm. *Practical Genetic Algorithms, Second Edition***,** 27-50.

HEGEWALD, T., KALTENBACHER, B., KALTENBACHER, M. & LERCH, R. 2008. Efficient modeling of ferroelectric behavior for the analysis of piezoceramic actuators. *Journal of Intelligent Material Systems and Structures,* 19**,** 1117-1129.

HODGDON, M. L. 1988. Applications of a theory of ferromagnetic hysteresis. *IEEE Transactions on Magnetics,* 24**,** 218-221.

HOMAIFAR, A., QI, C. X. & LAI, S. H. 1994. Constrained optimization via genetic algorithms. *Simulation,* 62**,** 242-253.

HUANG, Y. C. & LIN, D. Y. 2008. Ultra fine tracking control on piezoelectric actuated motion stage using piezoelectric hysteresis model. *Asian Journal of Control,* 6**,** 208-216.

HUBER, J., FLECK, N. & ASHBY, M. 1997. The selection of mechanical actuators based on performance indices. *Proceedings of the Royal Society of London. Series A: Mathematical, Physical and Engineering Sciences,* 453**,** 2185-2205.

HUI, C., YONGHONG, T., XINGPENG, Z., RUILI, D. & YAHONG, Z. Identification of Dynamic Hysteresis Based on Duhem Model. International Conference on Intelligent Computation Technology and Automation (ICICTA), 2011. IEEE, 810-814.

HULHOVEN, X., WOUWER, A. V. & BOGAERTS, P. 2005. On a systematic procedure for the predetermination of macroscopic reaction schemes. *Bioprocess and biosystems engineering,* 27**,** 283-291.

IRSCHIK, H., KROMMER, M. & VETYUKOV, Y. 2010. On the use of piezoelectric sensors in structural mechanics: Some novel strategies. *Sensors,* 10**,** 5626-5641.

IZYUMSKAYA, N., ALIVOV, Y., CHO, S. J., MORKOC, H., LEE, H. & KANG, Y. S. 2007. Processing, structure, properties, and applications of PZT thin films. *Critical Reviews in Solid State and Materials Sciences,* 32**,** 111-202.

JIANG, H., JI, H., QIU, J. & CHEN, Y. 2010. A modified prandtl-ishlinskii model for modeling asymmetric hysteresis of piezoelectric actuators. *IEEE Transactions on Ultrasonics, Ferroelectrics and Frequency Control,* 57**,** 1200-1210.

JINHYOUNG, O. & BERNSTEIN, D. S. 2005. Semilinear Duhem model for rate-independent and rate-dependent hysteresis. *IEEE Transactions on Automatic Control,* 50**,** 631-45.

JUDITSKY, A., HJALMARSSON, H., BENVENISTE, A., DELYON, B., LJUNG, L., SJÖBERG, J. & ZHANG, Q. 1995. Nonlinear black-box models in system identification: Mathematical foundations. *Automatica,* 31**,** 1725-1750.

JUNG, H. & GWEON, D.-G. 2000. Creep characteristics of piezoelectric actuators. *Review of Scientific Instruments,* 71**,** 1896-1900.

KALTENBACHER, B. & KALTENBACHER, M. 2007. Modeling and iterative identification of hysteresis via preisach operators in pdes. *Lectures on advanced computational methods in mechanics,* 1**,** 1-45.

KARAM, R. 1999. Piezoelectric nanopositioner. Google Patents.

KERMANI, M., MOALLEM, M. & PATEL, R. V. Optimizing the performance of piezoelectric actuators for active vibration control. IEEE International Conference on Robotics and Automation, , 2002. IEEE, 2375-2380.

KHAN, M. M. & LAGOUDAS, D. C. 2002. Modeling of shape memory alloy pseudoelastic spring elements using Preisach model for passive vibration isolation. *SPIE's 9th Annual International Symposium on Smart Structures and Materials.* International Society for Optics and Photonics, 336-347.

KIM, S.-J., KIM, J. H. & LEE, C.-H. 2010. Domain switching and creep behavior of a poled PZT wafer under through-thickness electric fields at high temperatures. *Acta Materialia,* 58**,** 2237-2249.

KUHNEN, K. 2003. Modeling, identification and compensation of complex hysteretic nonlinearities: A modified Prandtl-Ishlinskii approach. *European Journal of Control,* 9**,** 407-418.

LAMPAERT, V., AL-BENDER, F. & SWEVERS, J. A generalized Maxwell-slip friction model appropriate for control purposes. International Conference on Physics and Control, 2003. IEEE, 1170-1177.

LEE, C. K. 1990. Theory of laminated piezoelectric plates for the design of distributed sensors/actuators. Part I: Governing equations and reciprocal relationships. *The Journal of the Acoustical Society of America,* 87**,** 1144-1158.

LIAW, H. C. & SHIRINZADEH, B. 2011. Robust adaptive constrained motion tracking control of piezo-actuated flexure-based mechanisms for micro/nano manipulation. *IEEE Transactions on Industrial Electronics,* 58**,** 1406-1415.

LJUNG, L. 1998. *System identification*, Springer.

MAKAVEEV, D., DUPRÉ, L., DE WULF, M. & MELKEBEEK, J. 2001. Modeling of quasistatic magnetic hysteresis with feed-forward neural networks. *Journal of Applied Physics,* 89**,** 6737-6739.

MAKAVEEV, D., DUPRÉ, L., DE WULF, M. & MELKEBEEK, J. 2002. Isotropic vector hysteresis modeling with feed-forward neural networks. *Journal of Applied Physics,* 91**,** 8322-8324.

MAYERGOYZ, I. & FRIEDMAN, G. 1988. Generalized Preisach model of hysteresis. *IEEE Transactions on Magnetics,* 24**,** 212-217.

MAYERGOYZ, I. D. 1986. Mathematical models of hysteresis. *IEEE Transactions on Industrial Electronics,* 22**,** 603-608.

MAYERGOYZ, I. D. 1991. *The Classical Preisach Model of Hysteresis*, Springer.

MEEKER, T. 1996. Publication and proposed revision of ANSI/IEEE standard 176-1987" ANSI/IEEE standard on piezoelectricity". *Ieee Transactions on Ultrasonics Ferroelectrics and Frequency Control.*

MICROMECHATRONICS, I. 2013. *NEC/TOKIN* [Online]. Available: http://www.mmech.com/tokin-actuators/nec-tokin-resin-coated.

MINASE, J., LU, T.-F., CAZZOLATO, B. & GRAINGER, S. 2010. A review, supported by experimental results, of voltage, charge and capacitor insertion method for driving piezoelectric actuators. *Precision Engineering,* 34**,** 692-700.

MIRI, N., MOHAMMADZAHERI, M. & CHEN, L. A comparative study of different physics-based approaches to modelling of piezoelectric actuators. ASME International Conference on Advanced Intelligent Mechatronics (AIM), 9-12 July 2013a Wollongong, Australia. IEEE, 1211-1216.

MIRI, N., MOHAMMADZAHERI, M., CHEN, L., GRAINGER, S. & BAZGHALEH, M. Physics-based modelling of a piezoelectric actuator using genetic algorithm. Symposium on Industrial Electronics and Applications (ISIEA), 22-25 Sept 2013b Kuching, Malaysia. IEEE 16-20.

MOHAMMADZAHERI, M. 2011. *New types of knowledge about system dynamics for intelligent control system design.* Phd thesis, The University of Adelaide, Australia.

MOHAMMADZAHERI, M., CHEN, L., GHAFFARI, A. & WILLISON, J. 2009. A combination of linear and nonlinear activation functions in neural networks for modeling a de-superheater. *Simulation Modelling Practice and Theory,* 17**,** 398-407.

MOHAMMADZAHERI, M., GRAINGER, S. & BAZGHALEH, M. 2012a. A comparative study on the use of black box modelling for piezoelectric actuators. *The International Journal of Advanced Manufacturing Technology,* 63**,** 1247-1255.

MOHAMMADZAHERI, M., GRAINGER, S. & BAZGHALEH, M. 2012b. Fuzzy modeling of a piezoelectric actuator. *International Journal of Precision Engineering and Manufacturing,* 13**,** 663-670.

MOHAMMADZAHERI, M., GRAINGER, S., BAZGHALEH, M. & YAGHMAEE, P. Intelligent modeling of a piezoelectric tube actuator. International Symposium on Innovations in Intelligent Systems and Applications (INISTA) 2012c. 1-6.

MÜLLER, T., NOYKOVA, N., GYLLENBERG, M. & TIMMER, J. 2002. Parameter identification in dynamical models of anaerobic waste water treatment. *Mathematical Biosciences,* 177**,** 147-160.

OH, J. & BERNSTEIN, D. S. Identification of rate-dependent hysteresis using the semilinear Duhem model. American Control Conference, 2004. IEEE, 4776-4781.

OZER, M. B. & ROYSTON, T. J. 2001. Modeling the effect of piezoceramic hysteresis in structural vibration control. 89-100.

PADTHE, A., DRINCIC, B., OH, J., RIZOS, D., FASSOIS, S. & BERNSTEIN, D. 2008. Duhem modeling of friction-induced hysteresis. *Control Systems, IEEE,* 28**,** 90-107.

PASQUERO, J. & HAYWARD, V. STRESS: A practical tactile display system with one millimeter spatial resolution and 700 Hz refresh rate. Proc. Eurohaptics, 2003. 94-110.

PHILTEC. 2013. *FIBEROPTIC SENSORS* [Online]. Available: http://www.philtec.com.

POPOV, A. 2005. Genetic Algorithms for optimization. *User Manual, Hamburg*.

QUANT, M., ELIZALDE, H., FLORES, A., RAMÍREZ, R., ORTA, P. & SONG, G. 2009. A comprehensive model for piezoceramic actuators: modelling, validation and application. *Smart Materials and Structures,* 18**,** 125011.

RAMTEKKAR, G. 2009. Free vibration analysis of delaminated beams using mixed finite element model. *Journal of Sound and Vibration,* 328**,** 428-440.

RICHTER, H., MISAWA, E. A., LUCCA, D. A. & LU, H. 2001. Modeling nonlinear behavior in a piezoelectric actuator. *Precision Engineering,* 25**,** 128-137.

ROBERT, G., DAMJANOVIC, D., SETTER, N. & TURIK, A. V. 2001. Preisach modeling of piezoelectric nonlinearity in ferroelectric ceramics. *Journal of Applied Physics,* 89**,** 5067-5074.

RONKANEN, P., KALLIO, P., VILKKO, M. & KOIVO, H. N. 2011. Displacement control of piezoelectric actuators using current and voltage. *IEEE/ASME Transactions on Mechatronics,* 16**,** 160-166.

RYOU, J. H. & OLDHAM, K. R. 2012. Model identification for impact dynamics of a piezoelectric microactuator. *Journal of Micromechanics and Microengineering,* 22**,** 115002.

SAKATA, M., WAKABAYASHI, S., GOTO, H., TOTANI, H., TAKEUCHI, M. & YADA, T. Sputtered high| d 31| coefficient PZT thin film for microactuators. Micro Electro Mechanical Systems, 11-15 Feb 1996. IEEE, 263-266.

SALAPAKA, S., SEBASTIAN, A., CLEVELAND, J. P. & SALAPAKA, M. V. 2002. High bandwidth nano-positioner: A robust control approach. *Review of scientific instruments,* 73**,** 3232-3241.

SHAYEGAN, M., KARRAI, K., SHKOLNIKOV, Y., VAKILI, K., DE POORTERE, E. & MANUS, S. 2003. Low-temperature, in situ tunable, uniaxial stress measurements in semiconductors using a piezoelectric actuator. *Applied physics letters,* 83**,** 5235-5237.

SHIMADA, E., THOMPSON, J., YAN, J., WOOD, R. & FEARING, R. Prototyping millirobots using dextrous microassembly and folding. Symposium on Microrobotics ASME Int. Mechanical Engineering Cong. and Exp, 2000. Proc. ASME IMECE/DSCD, 1-8.

SIROHI, J. & CHOPRA, I. 2000. Fundamental behavior of piezoceramic sheet actuators. *Journal of Intelligent Material Systems and Structures,* 11**,** 47-61.

SITTI, M., CAMPOLO, D., YAN, J. & FEARING, R. S. Development of PZT and PZN-PT based unimorph actuators for micromechanical flapping mechanisms. Robotics and Automation, 2001. IEEE, 3839-3846.

SIVANANDAM, S. & DEEPA, S. 2008. *Genetic Algorithm Optimization Problems*, Springer.

SIXDENIER, F., SCORRETTI, R., MARION, R. & MOREL, L. 2008. Quasistatic hysteresis modeling with feed-forward neural networks: Influence of the last but one extreme values. *Journal of Magnetism and Magnetic Materials,* 320**,** e992-e996.

SJÖBERG, J., ZHANG, Q., LJUNG, L., BENVENISTE, A., DELYON, B., GLORENNEC, P.-Y., HJALMARSSON, H. & JUDITSKY, A. 1995. Nonlinear black-box modeling in system identification: a unified overview. *Automatica,* 31**,** 1691-1724.

SODERKVIST, J. Using FEA to treat piezoelectric low-frequency resonators. Frequency Control Symposium, 1997. IEEE, 634-642.

SPREKELS, J. 1996. Differential models of hysteresis.(Applied Mathematical Sciences 111). *ZAMM - Journal of Applied Mathematics and Mechanics / Zeitschrift für Angewandte Mathematik und Mechanik,* 76**,** 144-144.

STEPANENKO, Y. & SU, C.-Y. Intelligent control of piezoelectric actuators. Decision and Control, 1998. IEEE, 4234-4239.

SWEVERS, J., AL-BENDER, F., GANSEMAN, C. G. & PROJOGO, T. 2000. An integrated friction model structure with improved presliding behavior for accurate friction compensation. *Automatic Control,* 45**,** 675-686.

TADIGADAPA, S. & MATETI, K. 2009. Piezoelectric MEMS sensors: state-of-the-art and perspectives. *Measurement Science & Technology,* 20**,** 1-30.

TAKAHASHI, S. 1985. Multilayer piezoelectric ceramic actuators and their applications. *Japanese Journal of Applied Physics Supplement,* 24**,** 41-45.

TAKAHASHI, S. 1989. Recent developments in multilayer piezoelectric ceramic actuators and their applications. *Ferroelectrics,* 91**,** 293-302.

TZOU, H. & TSENG, C. 1990. Distributed piezoelectric sensor/actuator design for dynamic measurement/control of distributed parameter systems: a piezoelectric finite element approach. *Journal of sound and vibration,* 138**,** 17-34.

VASANTHANATHAN, A. & RAAMACHANDRAN, J. 2008. Finite element modeling of warping in smart piezoelectric noncircular shaft. *The International Journal of Advanced Manufacturing Technology***,** 1-7.

VO-MINH, T., TJAHJOWIDODO, T., RAMON, H. & VAN BRUSSEL, H. 2011. A new approach to modeling hysteresis in a pneumatic artificial muscle using the Maxwell-slip model. *IEEE/ASME Transactions on Mechatronics,* 16**,** 177-186.

WANG, D., DONG, Z., JIAO, N., YUAN, S., ZHOU, L. & LI, W. J. An asymmetric PI hysteresis model for piezoceramics in nanoscale AFM imaging. Nano/Micro Engineered and Molecular Systems (NEMS), 2011. IEEE, 1075-1079.

WANG, Q. M. & CROSS, L. E. 1999. Constitutive equations of symmetrical triple layer piezoelectric benders. *Ultrasonics, Ferroelectrics and Frequency Control,* 46**,** 1343-1351.

WEINBERG, M. S. 1999. Working equations for piezoelectric actuators and sensors. *Journal of Microelectromechanical Systems,* 8**,** 529-533.

WEN, Y. K. 1976. Method for random vibration of hysteretic systems. *Journal of the Engineering Mechanics Division,* 102**,** 249-263.

WOLF, C., MCLOONE, S. & BONGARDS, M. 2008. Biogas plant optimization using genetic algorithms and particle swarm optimization.

WOLF, F., SUTOR, A., RUPITSCH, S. J. & LERCH, R. 2011. Modeling and measurement of creep-and rate-dependent hysteresis in ferroelectric actuators. *Sensors and Actuators A: Physical,* 172**,** 245-252.

WOOD, R. J., STELTZ, E. & FEARING, R. S. Nonlinear performance limits for high energy density piezoelectric bending actuators. Robotics and Automation (ICRA), 2005. IEEE, 3633-3640.

XIE, W. F., FU, J., YAO, H. & SU, C. 2009a. *Adaptive Control*, In Tech.

XIE, W. F., FU, J., YAO, H. & SU, C. Y. 2009b. Neural network based adaptive control of piezoelectric actuators with unknown hysteresis. *International Journal of Adaptive Control and Signal Processing,* 23**,** 30-54.

YANG, X., LI, W., WANG, Y. & YE, G. 2008. Modeling hysteresis in piezo actuator based on neural networks. *Advances in Computation and Intelligence.* Springer.

YEH, T. J., RUO-FENG, H. & SHIN-WEN, L. 2008. An integrated physical model that characterizes creep and hysteresis in piezoelectric actuators. *Simulation Modelling Practice and Theory,* 16**,** 93-110.

YING, H. 1998. General SISO Takagi-Sugeno fuzzy systems with linear rule consequent are universal approximators. *IEEE Transactions on Fuzzy Systems,* 6**,** 582-587.

YU, Y., NAGANATHAN, N. & DUKKIPATI, R. 2002. Preisach modeling of hysteresis for piezoceramic actuator system. *Mechanism and Machine Theory,* 37**,** 49-59.

ZELINKA, T., HEJDA, P. & KROPÁČEK, V. 1987. The vibrating-sample magnetometer and Preisach diagram. *Physics of the Earth and Planetary Interiors,* 46**,** 241-246.

ZHANG, M. & XU, J. 2011. Active control of fluctuating pressure induced by blade-vortex interaction. *Science China Technological Sciences,* 54**,** 862-868.

ZHANG, X., TAN, Y. & SU, M. 2009. Modeling of hysteresis in piezoelectric actuators using neural networks. *Mechanical Systems and Signal Processing,* 23**,** 2699-2711.

ZHOU, D. & KAMLAH, M. 2006. Room-temperature creep of soft PZT under static electrical and compressive stress loading. *Acta Materialia,* 54**,** 1389-1396.

Appendices

A. Black Box Models

Black box models are universal approximators used to model piezoelectric actuators. These models are composed of a large number of parameters requiring identification.

A.1. Model Structure

To identify the structure of the feedback/feedforward control system including a piezoelectric actuator, an appropriate model structure is required (Sjöberg et al., 1995). Considering prior knowledge and physical insight of the system, three 'colour coded' models are defined:

1- White-box models: The structure of a white-box model is perfectly defined by current knowledge and physical properties of the system.

2- Gray-box models: In a gray-box model, although some physical knowledge are available, there are some parameters need to be identified. Physic-based models are example of gray-box models.

3- Black-box models: A black box model is a model that is viewed by the system input and output without any knowledge about its internal working (Juditsky et al., 1995). No physical insights to the system is available but a flexible successful mathematical structure could be used to identify the system structure (Sjöberg et al., 1995).

A.2. Structure of Black Box Models

Black box models are divided into two categories: linear and nonlinear models. A linear structure has been successful in identifying the structure of the linear systems. However, nonlinear black box models cover more complicated structures and they identify a large

spectrum of systems (Mohammadzaheri et al., 2012a). The nonlinear behaviour of piezoelectric actuators sits in this area (Sjöberg et al., 1995).

If the inputs to the system are:

$$V = [V(1)\ V(2)\ V(3)\ ....,V(t)], \tag{A. 1}$$

and the system outputs are:

$$V = [V(1)\ V(2)\ V(3)\ ....,V(t)], \tag{A. 2}$$

a black box model would estimate the next instances' outputs by:

$$y(t) = g(V^{t-1},\ y^{t-1}) + \alpha(t), \tag{A. 3}$$

where $g(V^{t-1},\ y^{t-1})$ and $y(t)$ are system input and output, respectively, and $\alpha(t)$ is a term showing that the future data is not an exact function of the past data (Sjöberg et al., 1995).

The Eq. (A.3) is a general structure for both dynamic and static systems. Defining the function of $g(V^{t-1},\ y^{t-1})$ is the main task for black box models. In order to parameterize the function, the parameter vector of θ is added to structure parameters as:

$$g(V^{t-1},\ y^{t-1},\ \theta), \tag{A. 4}$$

θ is approximated by fitting the model and real system data according to:

$$\sum_{t=1}^{N} \left\| y(t) - g(V^{t-1},\ y^{t-1}, \theta) \right\|^2, \tag{A. 5}$$

The model structure of Eq. (A.4) is a general structure and it is divided into two concatenations:

1- Mapping the input values into the finite dimensional vector of $\varphi(t)$:

$$\varphi(t) = \varphi(V^{t-1},\ y^{t-1}). \tag{A. 6}$$

$\varphi(t)$ is called the regression vector and its components are called the repressors.

2- Mapping the $\varphi(t)$ values into the output space:

$$g(V^{t-1},\ y^{t-1},\ \theta) = g(\varphi(t),\ \theta) \tag{A. 7}$$

Identifying the two aforementioned concatenations would define the structure of the black box model. In other word, If Eq. (A.7) is identified, the model structure is defined. Some examples of the most popular model structures are Wavelet, Kernel estimators, Sigmoid

neural networks, partial least squares and fuzzy models. All these models are defined based on the function they present to model the variables but they are often explained by networks (Mohammadzaheri et al., 2012a). In all the model structures, the aim is to identify the model parameters so as the model fit Eq. (A.5) minimises; this is the optimisation process (Sjöberg et al., 1995).

A.3. Fuzzy Models

Fuzzy model is one of the most common black box models. The mapping role of the input variables to the output ones is performed by fuzzy interference systems. The fuzzy model uses fuzzy values (fuzzy sets) for variables rather than crisp values. It is composed of fuzzy sets, implication and aggregation and defuzzifier functions. The base of fuzzy models is fuzzy logic (Juditsky et al., 1995). According to the fuzzy logic, a variable statement could be partially true or false which is expressed by a probability range between 0 and 1 (Mohammadzaheri et al., 2012b, Ying, 1998).

Adaptive neuro fuzzy systems are usually used for fuzzy modelling. The parameters of these fuzzy models are often identified through a combined use of a derivative-based optimisation algorithm and the least square of error (LSE) using the modelling/training data (Mohammadzaheri et al., 2012e). Then, the model is validated by another set of data and the model accuracy is estimated.

B. Actuator Input-Output

Appendix B covers behaviour of the piezoelectric actuator for different excitation functions. The displacement of the actuator was measured for a variety excitation voltage functions. Triangular and sinusoidal voltage functions at three different frequencies of f= (1, 10 and 100) *Hz*, and amplitude range of A=±20V were employed to operate the piezoelectric actuator.

Figures (B.1)-(B.18) show the piezoelectric voltage and displacement at different functions and frequencies.

.

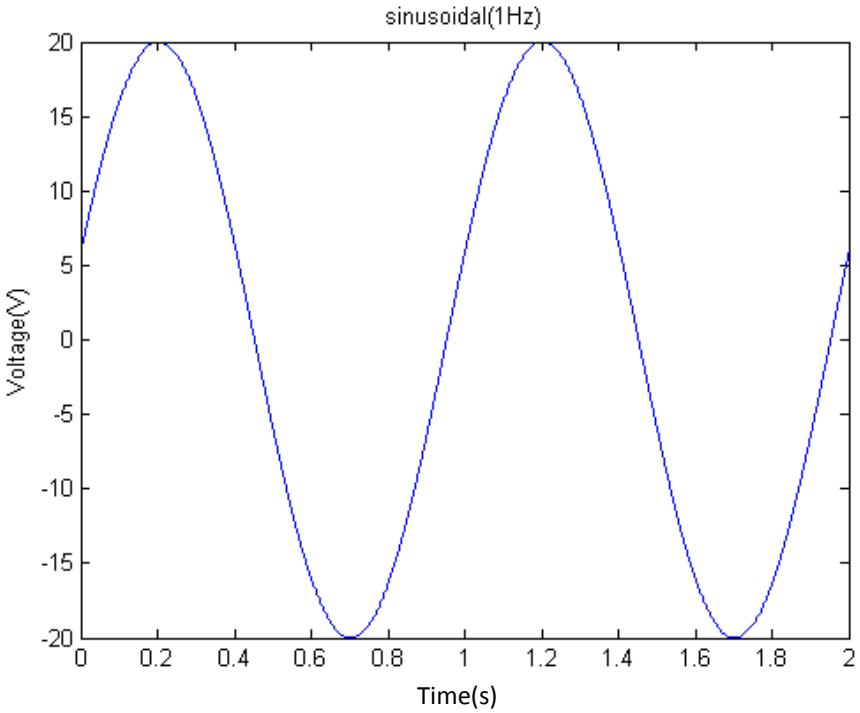

Figure B.1: Sinusoidal excitation voltage at a frequency of 1 *Hz*.

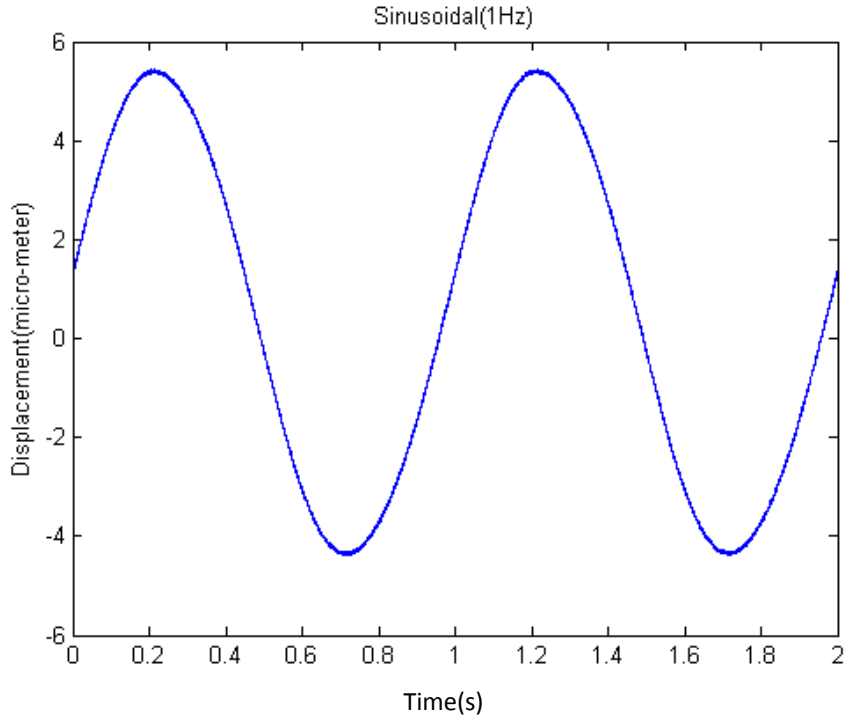

Figure B.2: Displacement vs time for the piezoelectric actuator excited through a sinusoidal voltage (*A*= ±20 V and *f*= 1 *Hz*).

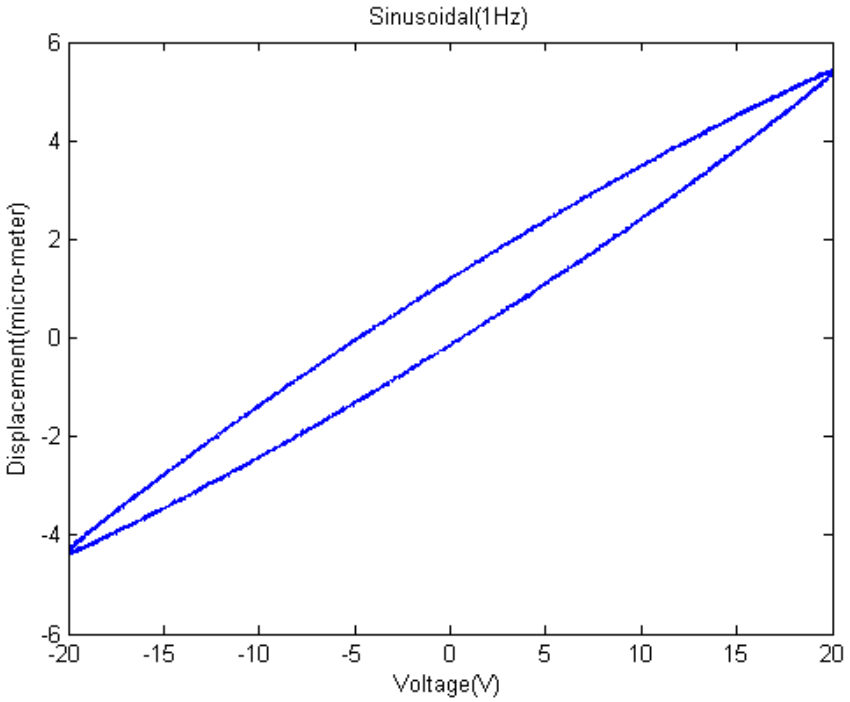

Figure B.3: Piezoelectric displacement versus voltage at a frequency of 1 *Hz*.

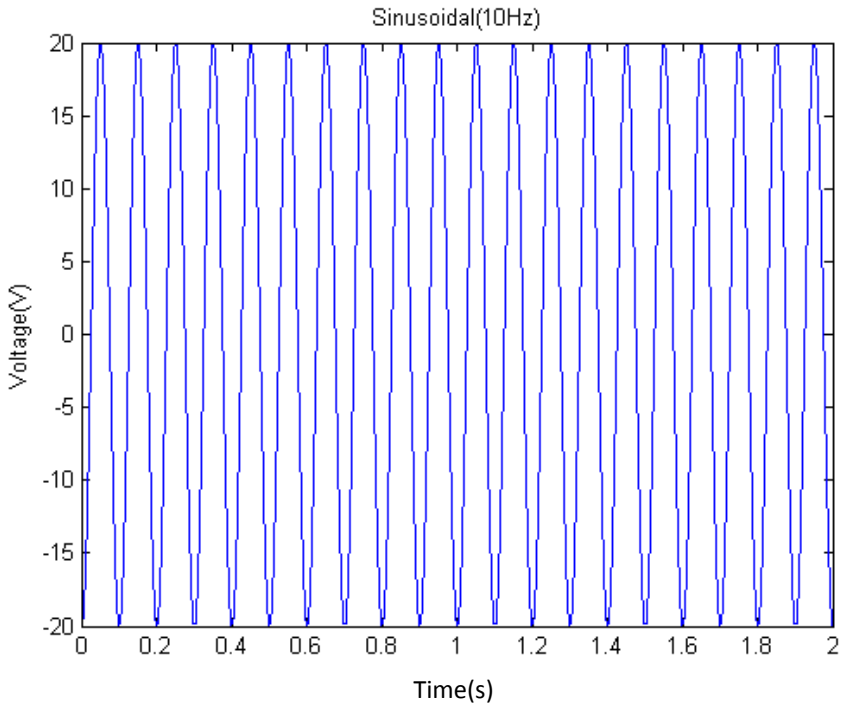

Figure B.4: Sinusoidal excitation voltage at a frequency of 10 *Hz*.

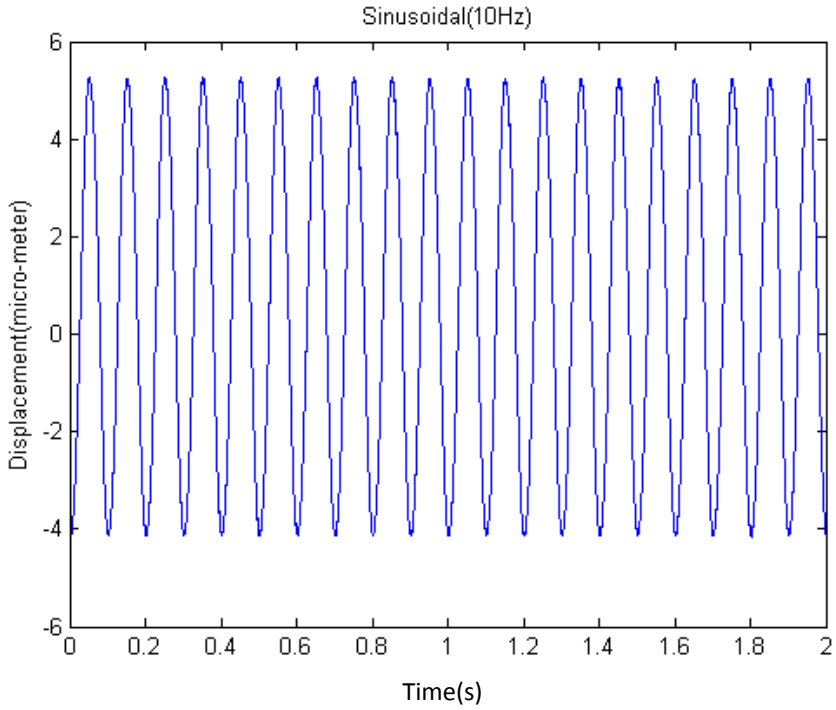

Figure B.5: Displacement vs time for the piezoelectric actuator excited through a sinusoidal voltage (*A*= ±20 V and *f*= 10 *Hz*).

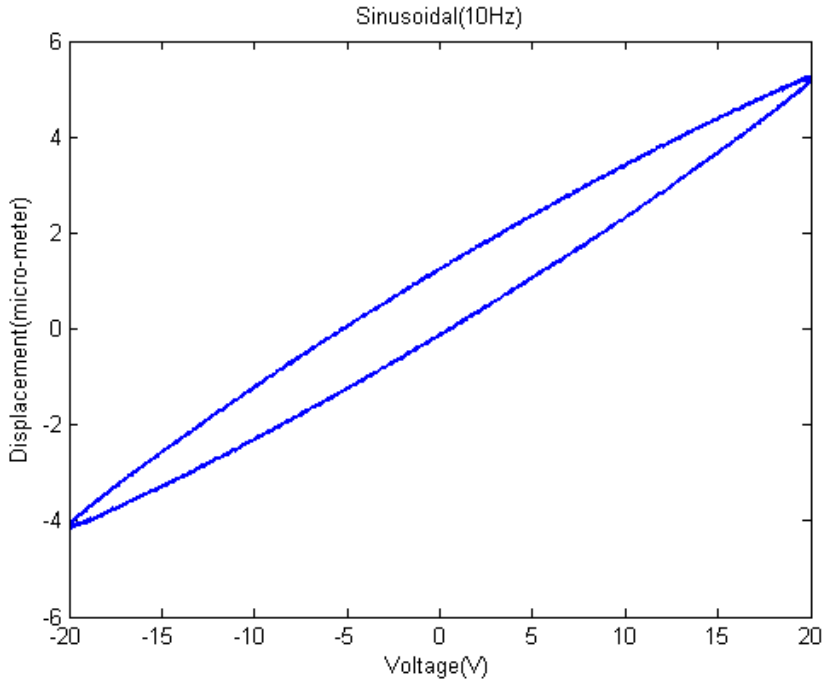

Figure B.6: Piezoelectric displacement versus voltage at a frequency of 10 *Hz*.

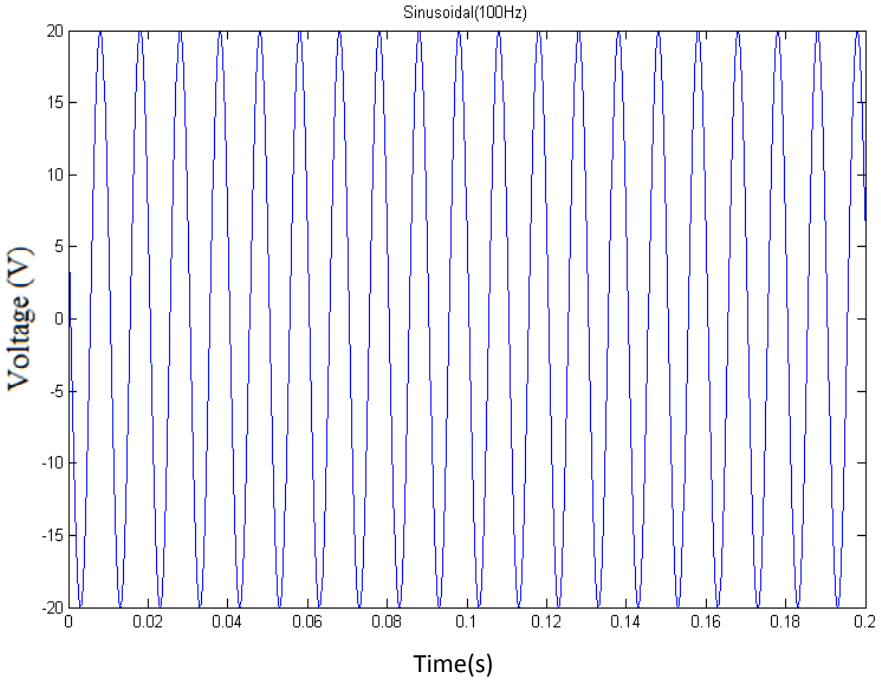

Figure B.7: Sinusoidal excitation voltage at a frequency of 100 *Hz*.

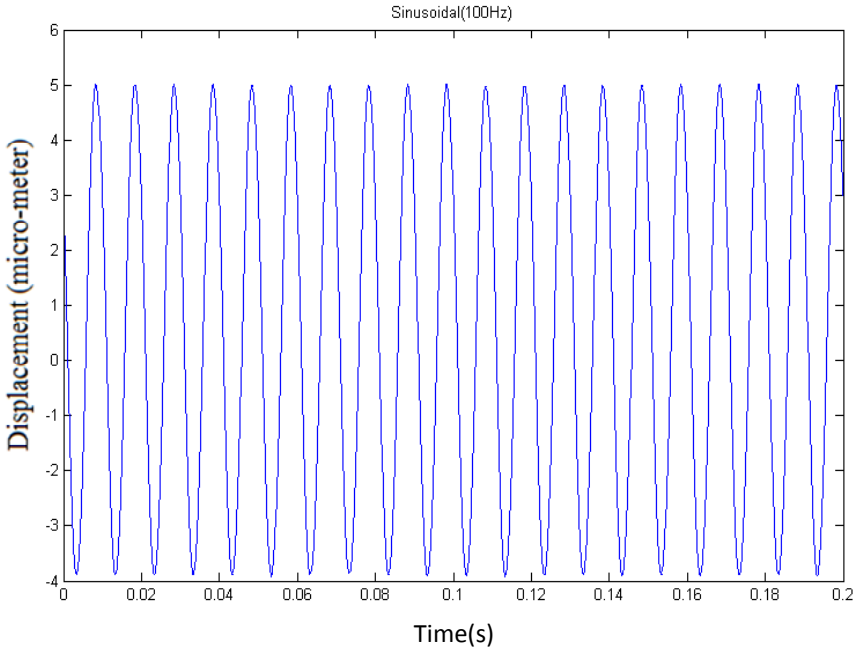

Figure B.8: Displacement vs time for the piezoelectric actuator excited through a sinusoidal voltage (*A*= ±20 V and *f*= 100 *Hz*).

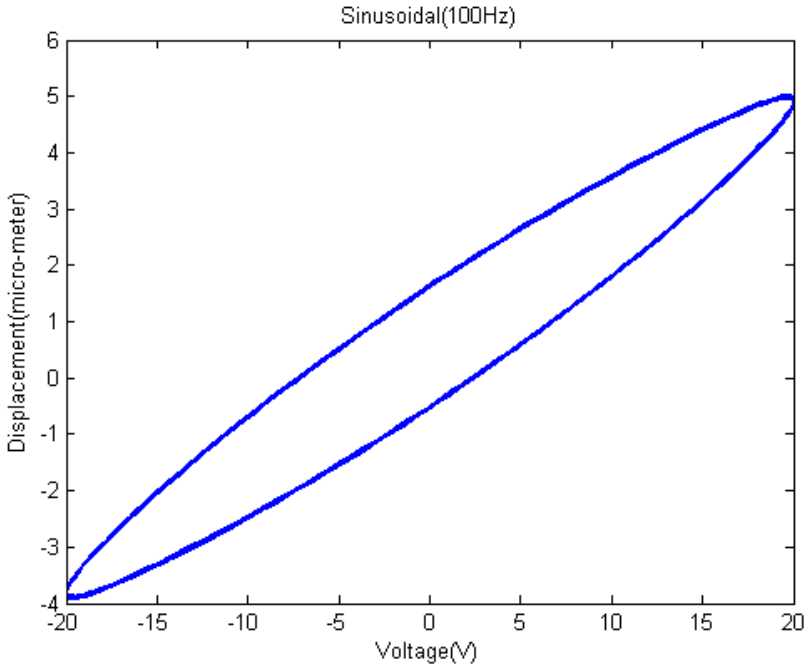

Figure B.9: Piezoelectric displacement versus voltage at a frequency of 100 *Hz*.

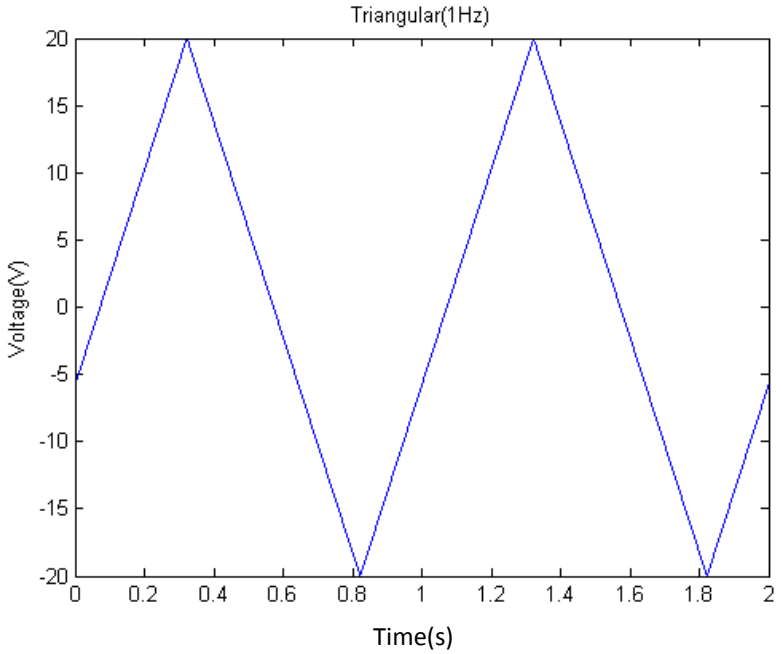

Figure B.10: Triangular excitation voltage at a frequency of 1 *Hz*.

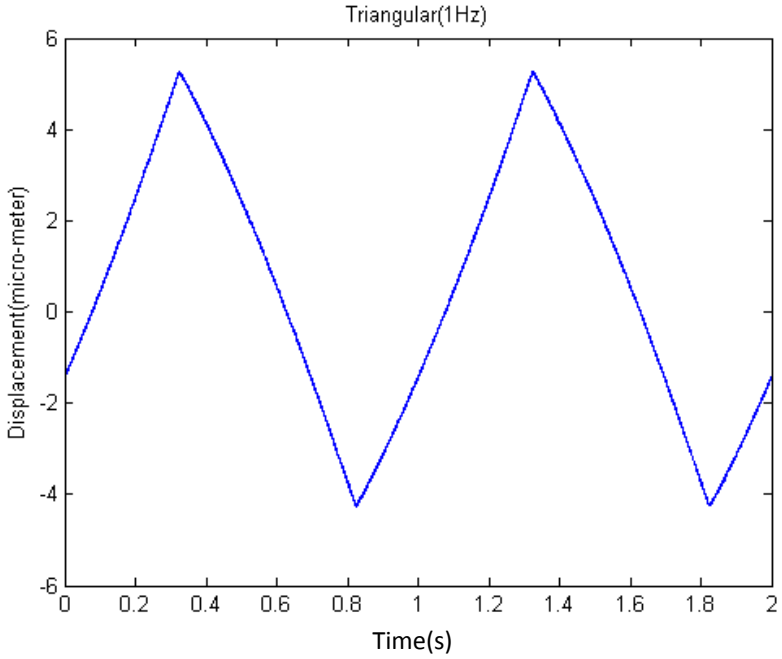

Figure B.11: Displacement vs time for the piezoelectric actuator excited through a triangular voltage (*A*= ±20 V and *f*= 1 *Hz*).

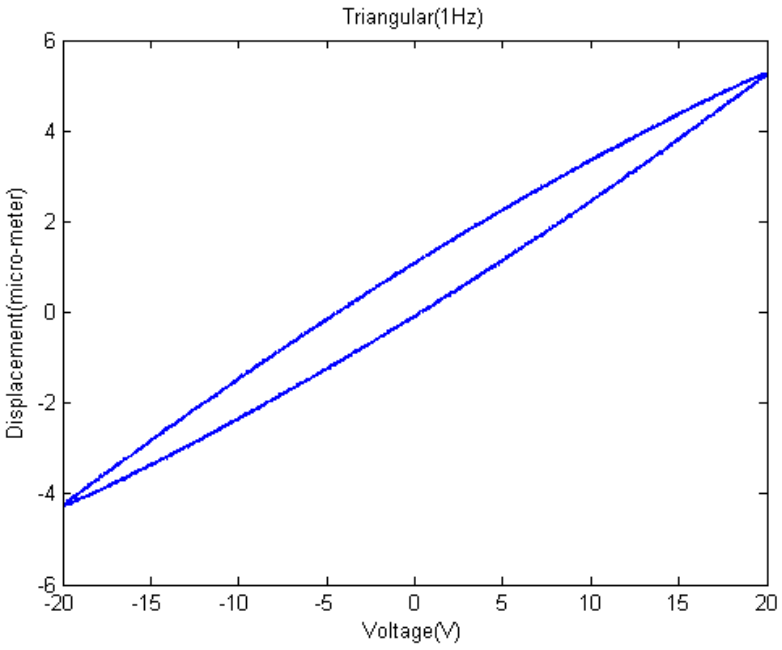

Figure B.12: Piezoelectric displacement versus voltage at a frequency of 1 *Hz*.

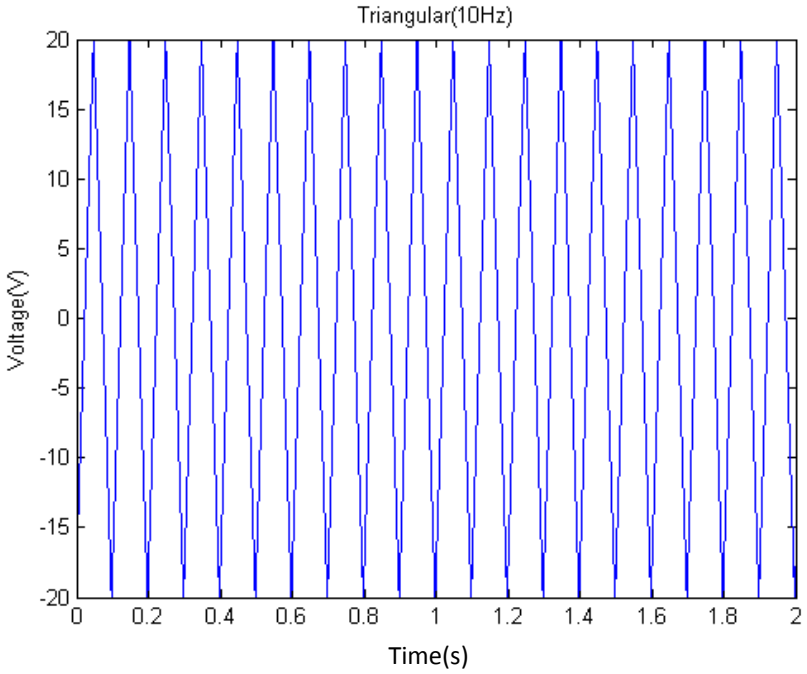

Figure B.13: Triangular excitation voltage at a frequency of 10 *Hz*.

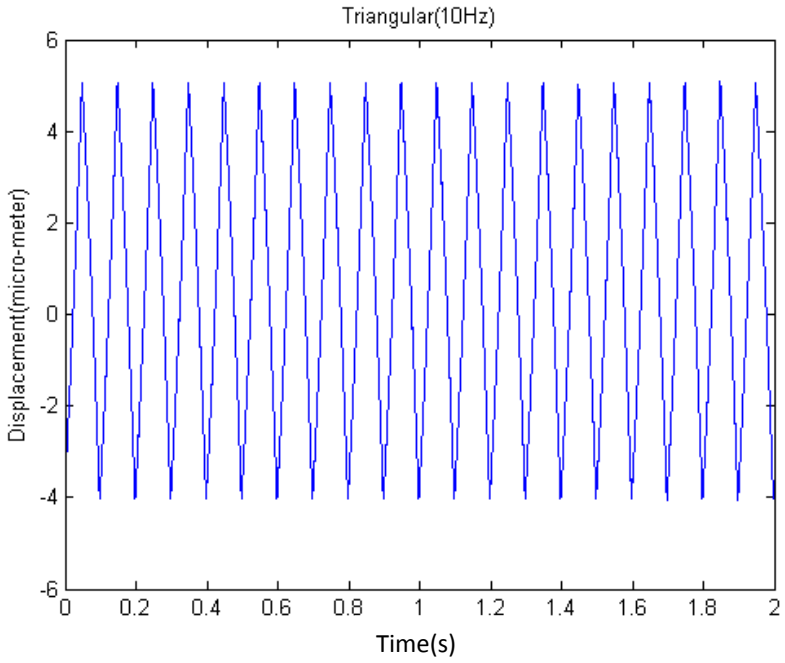

Figure B.14: Displacement vs time for the piezoelectric actuator excited through a triangular voltage (*A*= ±20 V and *f*= 10 *Hz*).

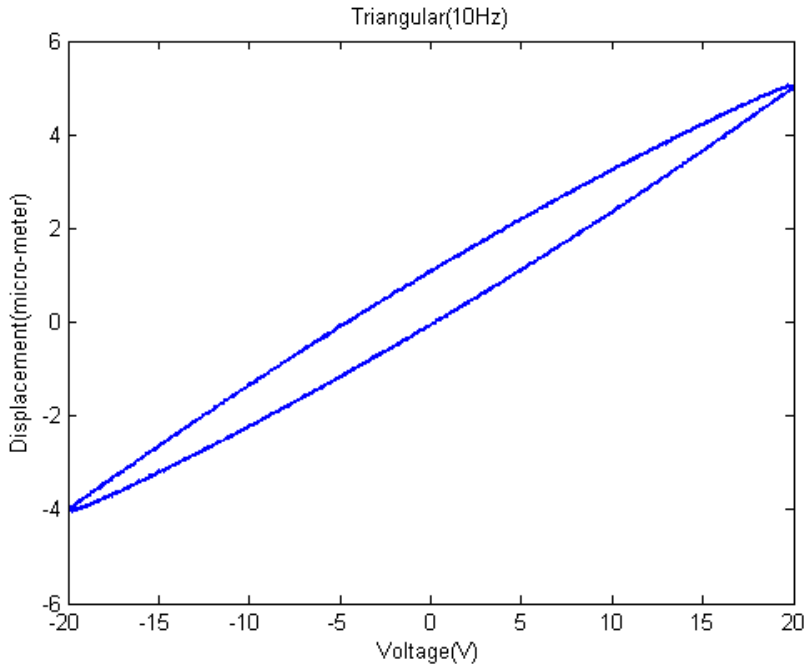

Figure B.15: Piezoelectric displacement versus voltage at a frequency of 10 *Hz*.

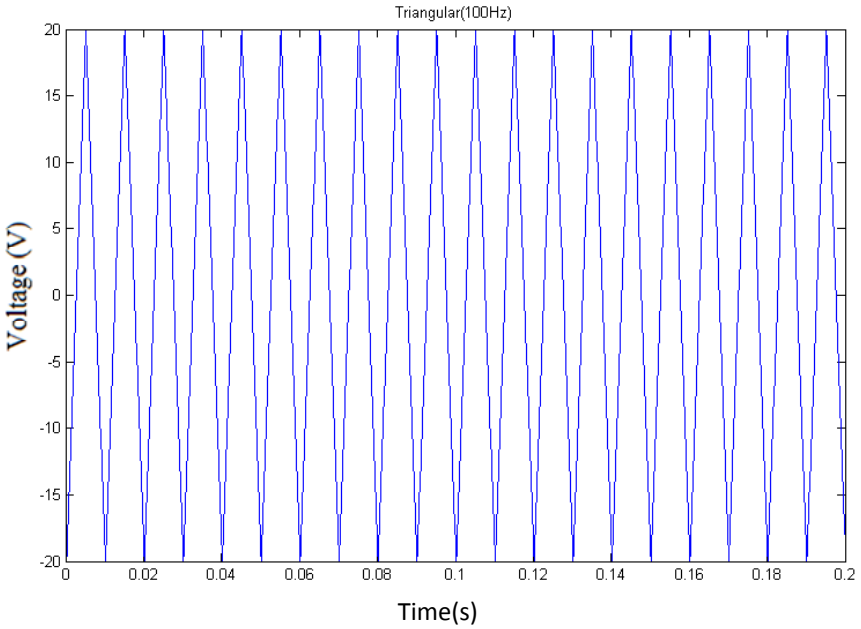

Figure B.16: Triangular excitation voltage at a frequency of 100 *Hz*.

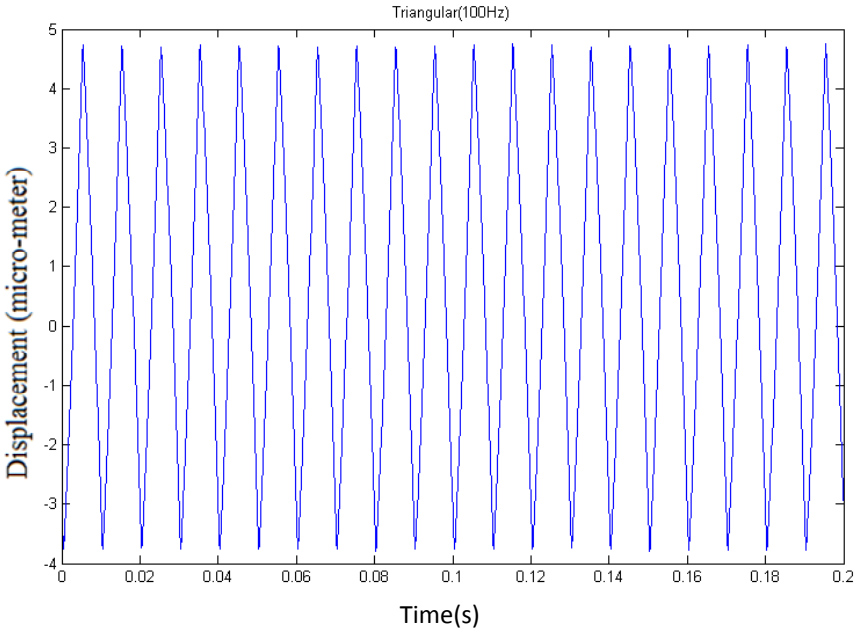

Figure B.17: Displacement vs time for the piezoelectric actuator excited through a triangular voltage (*A*= ±20 V and *f*= 100 *Hz*).

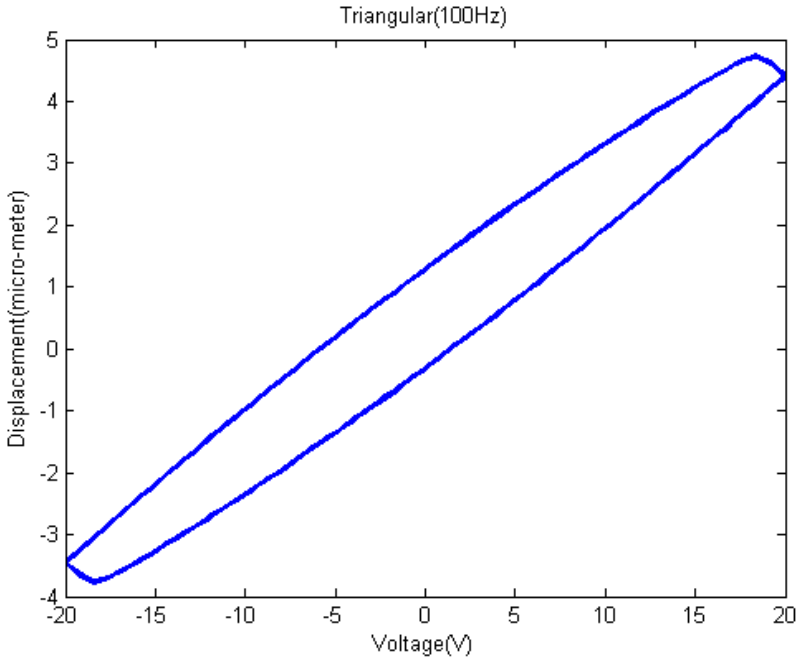

Figure B.18: Piezoelectric displacement versus piezoelectric voltage at a frequency of 100 *Hz*.

C. Genetic Algorithms

Initially, a random coded population (0 and 1) was created as detailed in section 4.1.2. Then the population, including the model parameters, is mapped into realistic values and the cost function for each set of parameter is determined. The experimental data (~5000#) are called to calculate the cost function of the model. The calculations are performed by the two methods, OSP and simulation methods. Then the population is evolved. The next section, first explains the *evolution* stages in the GA, and then presents a reasonable range for each parameter of the Voigt model addressed in Section 4.2.2.

C.1. Evolution

The *evolution* encompasses three major stages: Selection, Crossover and Mutation.

In the Selection stage, the chromosomes are selected to be mated and create a new generation. Roulette Wheels, Tournament, Boltzmann, Ranking and Steady State methods are different strategies for Selection (Cao and Wu, 1999). In all methods, the Selection deals with the chromosomes and their 'cost functions'. In this research a well-known method, the Roulette Wheel, is employed to select the parents. In this method, each chromosome is presented by a slice proportional to the chromosome's 'cost function' in which the least 'cost functions' are selected over a period of time (Cao and Wu, 1999).

Crossover is an important stage in which a new generation is created. The Crossover point is a random place in the string in which the values of two strings are replaced with each other in genes after that point. Different methods of Crossover include single-point, two-point, multi point, uniform and matrix methods. However, a significant discrepancy between the effectiveness of these methods has not been reported in the literature. In this research, the single-point method has been adopted for Crossover (Chipperfield and Fleming, 1995b).

At the Mutation stage, each bit in the string could mutate with a random low probability. A Mutation operator changes the bit code from '0' to '1' or vice-versa (Fraser, 1960).

For more details about different stages, see the program description in Appendix D defined by % at the beginning of the lines.

C.2. Parameter Ranges

In GAs, the initial population may fall outside the range of some parameters. Therefore, each parameter should be mapped within a correct range. The ranges should be identified before going through evolution stages. Moreover, selecting the number of bits for each parameter is a compromise between the computation time and accuracy. A greater number of bits per gene decreases MAC as defined in Section 4.1.2, so it may increase the accuracy. However, the number of bits is problem dependent initially generated by a random value (Cao and Wu, 1999). To find appropriate ranges and MACs, the GA was used with different arrangements according to Table C.1. Accordingly, the parameters of the model Eq. (4.8) were identified, as seen in Table C.2. As this table shows, the estimation accuracy increases by increasing the number of bits.

According to Table C.2, the values of the model parameters present a guideline to each parameter range. The resultant ranges have been demonstrated in Table 4.2.

Table C.1: Three different computational conditions.

No	*Population(#)*	*Bit(#)*
1	32	6
2	64	6
3	64	10

Table C.2: Identified parameters for the model (4.8) considering the conditions of Table C.1.

No	$\alpha(\mu)$	β	λ	b	P	*MAE* (μm)
1	1969.8	547.619	0.00586	8761.90	1.095	0.4008
2	308.0	553.275	0.00606	13571.8	0.799	0.4004
3	1392.7	753.666	0.00584	11648.1	0.865	0.3561

D. Genetic Algorithm Code in MATLAB

In Appendix D, the GA code, written for the Voigt model, is presented. In order to avoid repetition, the written codes for the three enhanced models are not presented here. Their structure is slightly different, although the algorithm is the same.

1- Body Code:

```
clc
clear all
% Genetic Algorithm (GA) is an Optimisation Program.
% The approach of data calling is One Step Prediction (OSP).
% It finds the model parameters of the performance function.
% The performance function is the Voigt function.
% Parameters are p11, p22, p33, p44 and p55.
% Experimental Displacement and Voltage are put into the equation.

%Initial condition
Npar=input('enter number of parameters=')
% Npar is the number of the model parameters; columns.
maxit=input('enter the maximum iteration=')
% The maximum number of evolution is called the iteration.
popsize=input('enter the population size, rows=')
% popsize is the number of rows; chromosomes.
nbit=input('enter the number of bits of each parameter=')
% nbit is the number of bits assigned to each parameter.
ts=input('enter sampling time=')
% ts is the sampling time of the gathered data.
mutrate=0.15;
% Sets mutration rate.
W=Npar*nbit;
% Total number of bits in each row; chromosome.

% Ranges of parameters.
varlo1=10^-6*290; varhi1=10^-6*2000;    varlo2=540; varhi2=780;
varlo3=0.0058; varhi3=0.0062;
varlo4=6500; varhi4=13000;   varlo5=0.799; varhi5=1.099;

% Data import
[am]=importdata('sin1.mat');
[bm]=importdata('sin10.mat');
[cm]=importdata('sin100.mat');
[dm]=importdata('tr100.mat');
[em]=importdata('tr1.mat');
[data]=[am bm cm dm em];

pop=round(rand(popsize,W));
% Creates the initial population by randomly selected '0' and '1''s.
[popsize,colu]=size (pop);
% It calls the 'popsize' and 'colu' to the number of rows and columns of
the 'pop' matrix, respectively.
```

```
finalpop=[];
% It is a gauge to put the selected population of each evolution.
finalcode=[];
% It is a gauge to put the selected code of each evolution.

myfhandle;
% This stage both maps the population data and calculates the model error,
then selects the genes with minimum cost function.

% Genetic algorithm (GA).
 for it=1:maxit;
% Increasing the generation counter incrementally before the maximum
iteration;maxit.

mytournamentmethod;
% Tournament selection differentiates lower cost functions.
mycrossover;
% Crossover stage produces children of each two chromosomes.
mymutation;
% Mutation stage mutates the codes of each gene.
myevaluation;
% It evaluates the created population and selects the genes with minimum
cost function.

% It compares the cost function of the initial population and created one,
then it selects the population of smaller cost function.
if aa<=a,
% aa is the cost function of the selected initial population a is the cos
function of the selected population from GA.
finalpop=[finalpop;pf(bb,:)];
% All selected rows in one matrix. Decimal values.
finalcode=[finalcode;popcoddd(bb,:)];
% All selected rows in one matrix. binary values.
else
finalpop=[finalpop;pff(b,:)];
% All selected rows in one matrix.
finalcode=[finalcode;popcoddd(b,:)];
% All selected rows in one matrix. binary values.
end
pop=popcoddd;
% Replacement of the generated population with the previous one.
it=it+1
% Increasing the iteration; evolution.
 end

[val,dd]=min(finalpop(:,6));
% It selects the minimum cost function of all rows.
selectedpop=finalpop(dd,:)
% It gives the selected row in the decimal format.
selectedcod=finalcode(dd,:)
% It gives the selected row in the binary format.
```

1-1- Myfhandle:

```
% This stage both maps parameters within the range and calculates the cost
function of each set of parameter.

 pf=[];                                                  % Population gauge.
 popcod=[];                                              % Code gauge.

for i=1:popsize;
st1=pop(i,1:nbit);                                       % First parameter.
st2=pop(i,nbit+1:2*nbit) ;                               % Second Parameter.
st3=pop(i,2*nbit+1:3*nbit) ;                             % Third parameter.
st4=pop(i,3*nbit+1:4*nbit) ;                             % Fourth parameter.
st5=pop(i,4*nbit+1:5*nbit);                              % Fifth parameter.
p1=bin2dec(num2str(st1));
% It attributes number to the string 1; st1.
p2=bin2dec(num2str(st2));
% It attributes number to the string 2; st2.
p3=bin2dec(num2str(st3));
% It attributes number to the string 3; st3.
p4=bin2dec(num2str(st4));
% It attributes number to the string 4; st4.
p5=bin2dec(num2str(st5));
% It attributes number to the string 5; st5.
p11=varlo1+(varhi1-varlo1)*p1/(2^nbit-1);
% It takes p1 and maps it within the available range.
p22=varlo2+(varhi2-varlo2)*p2/(2^nbit-1);
% It takes p2 and maps it within the available range.
p33=varlo3+(varhi3-varlo3)*p3/(2^nbit-1);
% It takes p3 and maps it within the available range.
p44=varlo4+(varhi4-varlo4)*p4/(2^nbit-1);
% It takes p4 and maps it within the available range.
p55=varlo5+(varhi5-varlo5)*p5/(2^nbit-1);
% It takes p5 and maps it within the available range.
p=[p11 p22 p33 p44 p55];
% p includes the values of parameters.

% Model evaluation
functv3;                                                 %M-file

% Attribution of a mean cost function to each set of parameters.
pf=[pf;p mean1] ;
% It gives the values of each set of population and the value of the cost
function.
popcod=[popcod;pop(i,:)];
% It gives the code of each set of population.
[aa,bb]=min(pf(:,6));
% It gives the minimum cost of all rows. aa is the value of that cost
function and bb is the row number of that cost function.
end
```

1-1-1

A) Funcv3 (OSP approach):

```
% Model error by OSP approach. The experimental inputs are from five
functions with different frequencies; sin1 Hz, sin 10 Hz, sin100 Hz, tr100
Hz and tr1 Hz.

fs=1/ts;      % Experimental sampling Frequency.
ss=ts/0.0001; % Step of data sample reading.

% Sin 1 Hz.
cost1=[];     % Gauge for cost functions.
    for   j=1:ss:20000,    % Loop for data reading.
 aaa=j+ss;                 % Next step.
 D=10^-6*data(3,aaa);      % Experimental displacement of the next step.
 m=10^-6*data(3,j);        % Experimental displacement of the current step.
 v=data(2,j);              % Input voltage of the current step.

subfm                      % Calculating the cost function of the model.
cost1=[cost1;func];        % Cost functions in a gauge.

end
x1=mean(cost1);            % Mean value of the cost function matrix.

% Sin10 Hz.
cost2=[];    % Gauge for cost functions.
    for j=20002:ss:40001,  % Loop for data reading.
 bbb=j+ss;                 % Next step.
 D=10^-6*data(3,bbb);      % Experimental displacement of the next step.
 m=10^-6*data(3,j);        % Experimental displacement of the current step.
 v=data(2,j);              % Input voltage of the current step.

subfm                      % Calculating the cost function of the model.
cost2=[cost2;func];        % Cost functions in a gauge.

end
 x2=mean(cost2);           % Mean value of the cost function matrix.

%Sin100 Hz.
cost3=[];   % Gauge for cost functions.
    for j=40003:ss:60002,  % Loop for data reading.
 ccc=j+ss;                 % Next step.
 D=10^-6*data(3,ccc);      % Experimental displacement of the next step.
 m=10^-6*data(3,j);        % Experimental displacement of the current step.
 v=data(2,j);              % Input voltage of the current step.

subfm                     % Calculating the cost function of the model.
cost3=[cost3;func];       % Cost functions in a gauge.

end
 x3=mean(cost3);          % Mean value of the cost function matrix.

%tr100 Hz.
cost4=[];   % Gauge for cost functions.
    for j=60004:ss:80003, % Loop for data reading.
 ddd=j+ss;                % Next step.
```

```
 D=10^-6*data(3,ddd);     % Experimental displacement of the next step.
 m=10^-6*data(3,j) ;      % Experimental displacement of the current step.
 v=data(2,j);             % Input voltage of the current step.

subfm                     % Calculating the cost function of the model.
cost4=[cost4;func];       % Cost functions in a gauge.

end
 x4=mean(cost4);          % Mean value of the cost function matrix.

%tr1 Hz.
 cost5=[]; % Gauge for cost functions.
    for j=80005:ss:100004,% Loop for data reading.
eee=j+ss;                 % Next step.
D=10^-6*data(3,eee);      % Experimental displacement of the next step.
m=10^-6*data(3,j);        % Experimental displacement of the current step.
v=data(2,j);              % Input voltage of the current step.

subfm                     % Calculating the cost function of the model.
cost5=[cost5;func];       % Cost functions in a gauge.

 end
 x5=mean(cost5);          % Mean value of the cost function matrix.


cost=[x1 x2 x3 x4 x5];    % Achieved cost functions in one matrix.
mean1=mean(cost);         % Mean value of the cost functions.
```

- **Subfm:**

```
% calculating the cost functions of the model.

f=inline('(sign(v).*(abs(v)/p44).^p55)/fs-(m.*(1+exp(-p33.*(v-
p22))).^2./(fs*p44*p11*p33*exp(-p33.*(v-
p22))))+m','m','fs','p33','v','p22','p44','p11','p55');
%Objective function from the Voigt model.
functi=f(m,fs,p33,v,p22,p44,p11,p55);
% It replaces the values of(m,fs,p33,v,p22,p44,p11,p55) in the function.
dif=functi-D;
% It subtracts the experimental displacement from estimated one.
func=abs(dif);
% absolute value of (D(experimental)-D(theoretical)).
```

B) Funcv3 (Simulation approach):

```
% Model error by Simulation approach. The experimental iputs are from five
functions
% with different frequencies; sin1 Hz, sin 10 Hz, sin100 Hz, tr100 Hz and
tr1 Hz.

fs=1/ts;      % Experimental sampling Frequency.
```

```
ss=ts/0.0001; % Step of data sample reading.

dis=[];       % A gauge for experimental displacement.
DIS=[];       % A gauge for theoretical displacement.


%sin1 Hz.
m=10^-6.*[data(3,1)];     % Initial experimental displacement.
v=[data(2,1)];            % Initial voltage.
fisrtdisplacement;
% Estimation of the second displacement. M-file.
cost1=[abs(D-(10^-6.*data(3,1+ss)))];
% Cost function of the first estimation by the model.
m=10^-6.*data(3,1+2*ss);  % Next experimental displacement.
    for   j=1+2*ss:ss:20001-ss,  % Loop for data reading.
 DD=10^-6.*data(3,j+ss);  % Experimental displacement of the next step.
 dis=[dis;DD];
% Experimental displacement of the next steps in a gauge.
 v=data(2,j);             % Input voltage of the current step.
 subfm                    % Calculating the cost function of the model.
 cost1=[cost1;func];      % Cost functions in a gauge.

    end
x1=mean(cost1);           % Mean value of the cost function matrix.


%sin10 Hz.
m=10^-6.*[data(3,20002)];    % Initial experimental displacement.
v=[data(2,20002)];           % Initial voltage.
fisrtdisplacement;
% Estimation of the second displacement. M-file.
cost2=[abs(D-(10^-6.*data(3,20002+ss)))];
% Cost function of the first estimation by the model.
m=10^-6.*data(3,20002+2*ss); % Next experimental displacement.
    for j=20002+2*ss:ss:40002-ss,  % Loop for data reading.
DD=10^-6.*data(3,j+ss);
% Experimental displacement of the next step.
dis=[dis;DD];
% Experimental displacement of the next steps in a gauge.
v=data(2,j);                 % Input voltage of the current step.
subfm
% Calculating the cost function of the model.
cost2=[cost2;func];          % Cost functions in a gauge.
    end
x2=mean(cost2);              % Mean value of the cost function matrix.


%sin100 Hz.
m=10^-6.*[data(3,40003)];    % Initial experimental displacement.
v=[data(2,40003)];           % Initial voltage.
fisrtdisplacement;
% Estimation of the second displacement. M-file.
cost3=[abs(D-(10^-6.*data(3,40003+ss)))];
% Cost function of the first estimation by the model.
m=10^-6.*data(3,40003+2*ss); % Next experimental displacement.
    for j=40003+2*ss:ss:60003-ss,    % Loop for data reading.
 DD=10^-6.*data(3,j+ss);
% Experimental displacement of the next step.
 dis=[dis;DD];
% Experimental displacement of the next steps in a gauge.
```

```
 v=data(2,j);                % Input voltage of the current step.
 subfm
% Calculating the cost function of the model.
 cost3=[cost3;func];         % Cost functions in a gauge.

    end
x3=mean(cost3);              % Mean value of the cost function matrix.


%tr100 Hz.
m=10^-6.*[data(3,60004)];    % Initial experimental displacement.
v=[data(2,60004)];           % Initial voltage.
fisrtdisplacement;
% Estimation of the second displacement. M-file.
cost4=[abs(D-(10^-6.*data(3,60004+ss)))];
% Cost function of the first estimation by the model.
m=10^-6.*data(3,60004+2*ss); % Next experimental displacement.
    for j=60004+2*ss:ss:80004-ss, % Loop for data reading.
 DD=10^-6.*data(3,j+ss);
% Experimental displacement of the next step.
 dis=[dis;DD];
% Experimental displacement of the next steps in a gauge.
 v=data(2,j);                % Input voltage of the current step.
 subfm
% Calculating the cost function of the model.
 cost4=[cost4;func];         % Cost functions in a gauge.

    end
x4=mean(cost4);              % Mean value of the cost function matrix.


%tr1 Hz.
m=10^-6.*[data(3,80005)];   % Initial experimental displacement.
v=[data(2,80005)];          % Initial voltage.
fisrtdisplacement;
% Estimation of the second displacement. M-file.
cost5=[abs(D-(10^-6.*data(3,80005+ss)))];
% Cost function of the first estimation by the model.
m=10^-6.*data(3,80005+2*ss);% Next experimental displacement.
    for j=80005+2*ss:ss:100005-ss, % Loop for data reading.
 DD=10^-6.*data(3,j+ss);
% Experimental displacement of the next step.
 dis=[dis;DD];
% Experimental displacement of the next steps in a gauge.
 v=data(2,j);                % Input voltage of the current step.
 subfm                       % Calculating the cost function of the model.
 cost5=[cost5;func];         % Cost functions in a gauge.

    end
x5=mean(cost5);              % Mean value of the cost function matrix.


cost=[x1 x2 x3 x4 x5];       % Achieved cost functions in one matrix.
mean1=mean(cost);            % Mean value of the cost functions.
```

- **Firstdisplacement (Simulation approach):**

```
f=inline('(sign(v).*(abs(v)/p44).^p55)/fs-(m.*(1+exp(-p33.*(v-
p22))).^2./(fs*p44*p11*p33*exp(-p33.*(v-
p22))))+m','m','fs','p33','v','p22','p44','p11','p55');
% Objective function from the Voigt model.
D=f(m,fs,p33,v,p22,p44,p11,p55);
% It replaces the values of(m,fs,p33,v,p22,p44,p11,p55) in the function.
```

- **Subfm (Simulation approach):**

```
% Calculating the cost functions of the model.

f=inline('(sign(v)*(abs(v)/p44)^p55)/fs-(m*(1+exp(-p33*(v-
p22)))^2/(fs*p44*p11*p33*exp(-p33*(v-
p22))))+m','m','fs','p33','v','p22','p44','p11','p55');
%Objective function from the Voigt model.
functi=f(m,fs,p33,v,p22,p44,p11,p55);
% It replaces the values of(m,fs,p33,v,p22,p44,p11,p55) in the function.
DIS=[DIS;functi];
% It puts the estimated displacement in a gauge.
dif=functi-DD;
% It subtracts the experimental displacement from estimated one.
func=abs(dif);
% absolute value of (D(experimental)-D(theoretical)).
m=functi;
% It replaces the previous estimated displacement as the input displacement
for the next step.
```

1-2- Mytournamentmethod:

```
% Pairing by tournament method: Selecting parents. It differentiates lower
cost functions each time in loop, two rows are randomly selected and their
costs are compared.

popcodd=[];                    % The parent gauge in the binary format.
popul=[];                      % The parent gauge in the decimal format.

for n=1:popsize;               % Loop number to scan all rows, popsizes.

% Choosing two random numbers between 1 and popsize. It randomly selects
numbers, counter of two rows, from the population.

n1=max(1, round(rand*popsize));
% a random number between 1 and popsize;For selecting the first parent.
n2=max(1, round(rand*popsize));
% a random number between 1 and popsize;For selecting the second parent.
```

```
%finding the relevant cost of the chromosomes; each selected row.
co1=pf(n1,6);                   % Selects the cost of the n1 row./Mate1.
co2=pf(n2,6);                   % Selects the cost of the n2 row./Mate2.

% It re-arrange selected rows based on the value of the cost function.
if co1<co2;
% If co1 is smaller, it is selected as parent and co2 is removed.
    popul=[popul;pf(n1,:)];
% Puting the row of n1 in popul gauge; in digit format.
    popcodd=[popcodd;popcod(n1,:)];
% Puting the row of n1 in popcodd gauge; in binary format.

else
% If co1 is not smaller, co2 is selected as parent and co1 is removed.
    popul=[popul;pf(n2,:)];
% Puting the row of n2 in popul gauge; in digit format.
    popcodd=[popcodd;popcod(n2,:)];
 % Puting the row of n1 in popcodd gauge; in binary format.
end                                     % If end.

end                                     % For end.
```

1-3- Mycrossover:

```
% Crossover stage produces children of each two chromosomes.

n1=max(1, round(rand*Npar*nbit));
% A random number between 1 and N*nbit.
popn=[];

for i=1:2:popsize-1                 % i is the counter of rows.
    for j=1:W          % j is the counter of culomns.'0' and '1' digits.
    if j<=n1
% It selects codes from the parent1 before selected point(n1).
ch1(j)=popcodd(i,j);                % Selection of the parameters of ch1.
ch2(j)=popcodd(i+1,j);              % Selection of the parameters of ch2.
    else

% It selects codes from the parent2 for points after (n1).
ch1(j)=popcodd(i+1,j);              % Selection of the parameters of ch1.
ch2(j)=popcodd(i,j);                % Selection of the parameters of ch2.
    end
    end
    popn=[popn;ch1;ch2] ;           % popn is the codded population after
crossover. This population is in binary form.

end
```

1-4- Mymutation:

```
% Mutation stage mutates the codes of each chromosome; children.
```

```
nmut=ceil(mutrate*Npar*nbit*(popsize-1));  % Total number of mutation.

for mi=1:nmut
% Counting is carried on to the number of mutation.
i=ceil(popsize*rand) ;
% Random selection of population elements, row, to mutate.
j=ceil(Npar*nbit*rand);
 % Random selection of population elements, column , to mutate.
a=1-popn(i,j);
% Changing the selected element. '1' to '0' or '0' to '1'.
popn(i,j)=a;
% Substitution of the new element in the population.

end
popn;
% This is the population after all mutations.
```

1-5- Myevaluation:

```
% Myevaluation evaluates the created population and calculates the cost
function of each set of genes.

popu=popn;      % Calling the created population, popu.
pff=[];         % Population gauge.
popcoddd=[];    % Code gauge.

for i=1:popsize;
st1=popu(i,1:nbit);                         % First parameter.
st2=popu(i,nbit+1:2*nbit) ;                 % Second Parameter.
st3=popu(i,2*nbit+1:3*nbit) ;               % Third parameter.
st4=popu(i,3*nbit+1:4*nbit) ;               % Fourth parameter.
st5=popu(i,4*nbit+1:5*nbit);                % Fifth parameter.
p1=bin2dec(num2str(st1));
% It attributes number to the string 1; st1.
p2=bin2dec(num2str(st2));
% It attributes number to the string 2; st2.
p3=bin2dec(num2str(st3));
% It attributes number to the string 3; st3.
p4=bin2dec(num2str(st4));
% It attributes number to the string 4; st4.
p5=bin2dec(num2str(st5));
% It attributes number to the string 5; st5.
p11=varlo1+(varhi1-varlo1)*p1/(2^nbit-1);
% It takes p1 and maps it within the available range.
p22=varlo2+(varhi2-varlo2)*p2/(2^nbit-1);
% It takes p2 and maps it within the available range.
p33=varlo3+(varhi3-varlo3)*p3/(2^nbit-1);
% It takes p3 and maps it within the available range.
p44=varlo4+(varhi4-varlo4)*p4/(2^nbit-1);
% It takes p4 and maps it within the available range.
p55=varlo5+(varhi5-varlo5)*p5/(2^nbit-1);
 % It takes p5 and maps it within the available range.
p=[p11 p22 p33 p44 p55];     % P includes the values of the parameters.

% Model evaluation
```

```
functv3;  %M-file

% Attribution of a mean cost function to each set of parameters.
po=[p mean1];
pff=[pff;po] ;                                          % It gives the
values of each population pack and the value of the cost function.
popcoddd=[popcoddd;popu(i,:)] ;                         % It gives the code
of each chromosome.
[a,b]=min(pff(:,6));                                    % It gives the
minimum cost of all rows.

end
```

2- Voigt model validation:

```
% Validation of the Voigt Model.
clc
clear all
[data]=importdata('tr10.mat');  % It takes the input data.

ts=5*1e-4; fs=0.2*1e4;
% Sampling time and frequency.
% Selected population.
P=1.0e+04 *[0.000000160045455   0.074293255131965   0.000000608269795
1.277761485826002   0.000087905865103   0.000000000074163];
y=1; x=1; %y is row number.
p11=P(y,x);p22=P(y,x+1);p33=P(y,x+2);p44=P(y,x+3);p55=P(y,x+4);
% Matrix elements in the row.

t=[];   % Time gauge.
d=[];   % Experimental displacement gauge.
v=[];   % Experimental voltage gauge.
DIS=[]; % Estimated displacement matrix.
ddd=10^-6.*[data(3,1)];% Initial experimental displacement.
vvv=[data(2,1)];% Initial experimental voltage.
ss=ts/0.0001;   % Number of steps.

% First estimation of the displacement.
f=inline('(sign(vvv).*(abs(vvv)/p44).^p55)/fs-(ddd.*(1+exp(-p33.*(vvv-
p22))).^2./(fs*p44*p11*p33*exp(-p33.*(vvv-
p22))))+ddd','ddd','fs','p33','vvv','p22','p44','p11','p55');
% Objective function by the Voigt model.
D=f(ddd,fs,p33,vvv,p22,p44,p11,p55);
% It replaces the values of(m,fs,p33,v,p22,p44,p11,p55) in the function.
initid=D;
% Estimation of the second displacement.
ddd=10^-6.*[data(3,1+2*ss)];          % Next experimental displacement.

for i=1+2*ss:ss:19991  % Loop for data reading.

ttt=data(1,i);
% Reading experimental times and putting them into a matrix.
t=[t;ttt];

vvv=data(2,i);
% Reading experimental voltages and putting them into a matrix.
v=[v;vvv];
```

```
ja=10^-6.*data(3,i);
% Reading experimental displacements and putting them into a matrix.
d=[d;ja];

f=inline('(sign(vvv).*(abs(vvv)/p44).^p55)/fs-(ddd.*(1+exp(-p33.*(vvv-
p22))).^2./(fs*p44*p11*p33*exp(-p33.*(vvv-
p22))))+ddd','ddd','fs','p33','vvv','p22','p44','p11','p55');
% Objective function by the Voigt model.
D=f(ddd,fs,p33,vvv,p22,p44,p11,p55);
% It replaces the values of(m,fs,p33,v,p22,p44,p11,p55) in the function.
ddd=D;
% It considers the estimated displacement as the input displacement for the
next step.
DIS=[DIS;D];     % Estimated displacements.

end

t=[data(1,1+ss);t];% Experimental time without the first one.
[x,xx]=size(t);

v=[data(2,1+ss);v];% Experimental voltage without the first one.
[y,yy]=size(v);

d=[10^-6.*data(3,1+ss);10^-6.*data(3,1+2*ss);d(2:3997,1)];
% Experimental displacement without the first one.
[z,zz]=size(d);

[w,ww]=size(DIS);
www=w-1;
DIS=[initid;10^-6.*data(3,1+2*ss);DIS(1:www,1)];
% All estimated displacements.

a=DIS-d;
% It subtracts the experimental displacements from estimated ones.
plot(t(1:400),DIS(1:400),'--','LineWidth',2,'Color','red')
hold on
plot(t(1:400),d(1:400))
hold on
plot(t(1:400),a(1:400),'--','LineWidth',1,'Color','black')

max(abs(a))
% Maximum of the absolute value of (D(experimental)-D(theoretical)).
mae(a)
% Mean of the absolute value of (D(experimental)-D(theoretical)).

%plot(v,DIS,'r')
%hold on
%plot(v,d)
```

NOTE:

This page is intentionally left blank.